



The development of TiO_2 based catalyst for poisoning organic molecules removal

Suchadee Sribenja

A Thesis Submitted in Partial Fulfillment of Requirements for
degree of Doctor of Philosophy in Chemistry

July 2023

Copyright of Maharakham University

การพัฒนาตัวเร่งปฏิกิริยาที่มีไทเทเนียมไดออกไซด์เป็นองค์ประกอบหลักเพื่อใช้ในการกำจัด
โมเลกุลของสารอินทรีย์ที่เป็นพิษ

วิทยานิพนธ์
ของ
สุชาติ ศรีเบญจา

เสนอต่อมหาวิทยาลัยมหาสารคาม เพื่อเป็นส่วนหนึ่งของการศึกษาตามหลักสูตร
ปริญญาปรัชญาดุษฎีบัณฑิต สาขาวิชาเคมี
กรกฎาคม 2566
ลิขสิทธิ์เป็นของมหาวิทยาลัยมหาสารคาม

The development of TiO₂ based catalyst for poisoning organic molecules removal

Suchadee Sribenja

A Thesis Submitted in Partial Fulfillment of Requirements
for Doctor of Philosophy (Chemistry)

July 2023

Copyright of Mahasarakham University



The examining committee has unanimously approved this Thesis, submitted by Miss Suchadee Sribenja , as a partial fulfillment of the requirements for the Doctor of Philosophy Chemistry at Maharakham University

Examining Committee

.....Chairman
(Asst. Prof. Viyada Harnchana ,
Ph.D.)

.....Advisor
(Assoc. Prof. Ratchaneekorn
Wanchanthuek , Ph.D.)

.....Committee
(Assoc. Prof. Uthai Sakee , Ph.D.)

.....Committee
(Asst. Prof. Widchaya
Radchatawedchakoon , Ph.D.)

.....Committee
(Asst. Prof. Senee Kruanetr , Ph.D.)

Maharakham University has granted approval to accept this Thesis as a partial fulfillment of the requirements for the Doctor of Philosophy Chemistry

.....
(Prof. Pairot Pramual , Ph.D.)
Dean of The Faculty of Science

.....
(Assoc. Prof. Krit Chaimoon , Ph.D.)
Dean of Graduate School

TITLE	The development of TiO ₂ based catalyst for poisoning organic molecules removal		
AUTHOR	Suchadee Sribenja		
ADVISORS	Associate Professor Ratchaneekorn Wanchanthuek , Ph.D.		
DEGREE	Doctor of Philosophy	MAJOR	Chemistry
UNIVERSITY	Maharakham University	YEAR	2023

ABSTRACT

This research aims to study a synthesis of the Titanium dioxide (TiO₂) as a photocatalyst which is loading onto a pineapple leaf fiber (TiO₂/PF) by using hydrolysis method and heating with autoclave, and using succinic acid as a crosslink molecules. The researchers conduct the experiment to compare to use and non-use sodium hydrogen phosphite (NaH₂PO₂) as a catalyst support. Afterwards, we verifies the attribute and property of the catalyst which has been through the x-ray diffraction (XRD), the Fourier transform infrared spectroscopy (FTIR), scanning electrons microscopy (SEM) the thermal gravimetric analysis (TGA) and determination of TiO₂ deposited on PF. Determination pf Ti on catalyst using Inductively coupled plasma atomic emission spectroscopy (ICP-OES). The activity of the catalyst could experiment by testing the degradation of a methylene blue using UV-vis spectrophotometer under UV irradiation at 664 nm. The study demonstrate that the catalyst TiO₂/PF which uses Succinic acid as a crosslink molecule and using NaH₂PO₂ as a catalyst support could provide the degradation of a methylene blue to be the most efficient way rather than non-using the catalyst.

Keyword : Photodegradation, Titaniumdioxide, Methyleneblue degradation, Succinic acid

ACKNOWLEDGEMENTS

The author would like to gratefully acknowledge the Science achievement scholarship of thailand (sast) and the grant for graduate students, fiscal year 2015, for partial financial support. I am grateful to the Department of Chemistry, Faculty of Science, Mahasarakham University, for providing chemicals, instrumental support and all other facilities.

I wish to express my deepest and sincere gratitude to my advisor, Assoc. Prof. Dr. Ratchaneekorn Wanchanthuek who gave me valuable instructions, excellent suggestions and kindness which are more than I can describe here, that have enable me to pass through this course successfully.

I was very fortunate to have many friends both within and outside the Faculty of Accountancy and Management during my doctoral life. I thank them all for their being very supportive.

I wish to express my sincere appreciation to all of my friends for their excellent assistance, encouragement, sincerity and impression friendship. Everything will always be in my mind.

Most of all, I wish to express my heartfelt gratitude here to my family; my beloved parents for their tender love, care, sacrifice, inculcation and encouragement that found me to be a fortitude person.

Suchadee Sribenja

Suchadee Sribenja

TABLE OF CONTENTS

	Page
ABSTRACT	D
ACKNOWLEDGEMENTS	E
TABLE OF CONTENTS	F
LIST OF TABLES	J
LIST OF FIGURES	K
CHAPTER 1	1
1.1 Background.....	1
1.2 Research objectives.....	2
1.3 Expected results obtained from the research	2
1.4 Scopes of research.....	3
1.5 Research Place	3
CHAPTER 2	4
2.1 The environmental problem.....	4
2.2 Persistent organic pollutants	5
2.3 Photocatalyst	12
2.4 Semiconductors.....	12
2.5 Mechanism and fundamentals of photocatalytic reactions	14
2.6 Factors affecting the photocatalytic process	15
2.6.1 Operational parameters	16
2.6.2 TiO ₂ structural and morphological properties	18
2.7 Titanium dioxide photocatalyst (TiO ₂)	19
2.7.1 TiO ₂ application.....	21
2.7.2 Methods for loading TiO ₂ onto various supports	24
2.8 Supporting materials	28
2.8.1 Cellulose fibers support	28

2.8.2 Pineapple leaf fibers	29
2.9 Effect of cross-link to graft nano TiO ₂ on fibers	30
2.9.1 Applications.....	31
2.9.2 Coating process.....	32
CHAPTER 3	33
3.1 Chemicals and materials	33
3.1.1 Chemicals	33
Sodium chloride (NaCl).....	33
3.1.2 Materials	34
3.2 Instrument	34
3.3 Experimental.....	35
3.3.1 Preparation of TiO ₂ powder.....	35
3.3.2 Preparation of pineapple leaf fibers (PF).....	36
3.3.3 Preparation of TiO ₂ deposited on pineapple fibers.....	36
3.3.4 Preparation of crosslink on pineapple fibers.....	36
3.3.5 Calibration curve	37
3.4 Activity test.....	37
3.4.1 Paraquad degradation activity.....	37
3.4.2 Methylene blue degradation activity.....	37
3.5 Analytical methods	38
3.6 Characterization of catalyst.....	38
3.6.1 Fourier transform infrared spectroscopy (FTIR)	38
3.6.2 Scanning electron microscopy (SEM)	38
3.6.3 BET Surface area analyzsis (BET)	38
3.6.4 X-ray diffraction spectroscopy (XRD)	39
3.6.5 Diffuse reflectance UV-vis spectroscopy	39
3.6.6 Thermogravimetric analysis (TGA).....	39
3.6.7 Inductively Coupled Plasma-Optical Emission Spectrometer (ICP-OES).....	39
3.7 Data analysis	39

CHAPTER 4	40
4.1 TiO ₂ catalyst preparation	40
4.1.1 Characterizations	40
4.1.1.1 X-Ray diffraction analysis.....	40
4.1.1.2 Surface morphological analysis.....	42
4.1.1.3 Surface area analysis	43
4.1.1.4 Functional group analysis.....	44
4.1.1.5 Ban gab energy analysis	45
4.1.1.6 XPS analysis.....	46
4.1.2 Catalytic activity	48
4.1.2.1 Paraquat degradation	48
4.1.2.3 Methylene blue degradation	50
4.1.2.5 Methyl orange degradation.....	51
4.1.2.7 Photo degradation.....	53
4.2 Application of TiO ₂ deposited on pineapple fibers (PF).....	55
4.2.1 Characterizations	55
4.2.1.1 X-Ray diffraction analysis.....	55
4.2.1.2 Surface morphological analysis.....	56
4.2.1.3 SEM EDX analysis.....	58
4.2.1.4 Surface area analysis	59
4.2.1.5 Functional group analysis.....	61
4.2.1.6 Ban gab energy analysis	62
4.2.1.7 Thermogravimetric analysis	63
4.2.2 Catalytic activity	64
4.2.2.1 Methylene blue removal.....	64
4.2.2.2 Methylene blue adsorption study	65
4.2.2.3 Methylene blue photodegradation study	66
4.3 Application of crosslink molecule on TiO ₂ composite on pineapple fibers	67
4.3.1 Characterizations	67

4.3.1.1 X-Ray diffraction analysis.....	67
4.3.1.2 Surface morphological analysis.....	68
4.3.1.3 Functional group analysis.....	69
4.3.1.4 Thermogravimetric analysis	70
4.3.1.4 XPS analysis.....	72
4.3.2 Catalytic activity	74
4.3.2.1 Methylene blue removal.....	74
4.3.2.2 Methylene blue adsorption study	75
4.3.2.3 Methylene blue photo degradation	76
4.3.1.4 XPS analysis and Activity of catalyst	77
4.3.2.4 Recycle ability	78
4.3.2.5 Determination of TiO ₂ deposited on catalyst analysis	80
4.3.2.6 Connection of succinic acid to cellulose and TiO ₂	81
CHAPTER 5	82
REFERENCES	83
BIOGRAPHY	94

LIST OF TABLES

	Page
Table 1 Band gap energies of various semiconductors at relevant wavelengths [32].	13
Table 2 Some factors affecting the efficiency of photocatalytic processes.	22
Table 3 The chemicals used in this research.....	33
Table 4 The detail of instruments used in this research.....	34
Table 5 Physicochemical properties of catalysts.	59
Table 6 Results of Ti incatalyst analyses by ICP-OES.....	80

LIST OF FIGURES

	Page
Figure 1 Water withdrawal by sector in the regions of the world (2000) [24].	5
Figure 2 Reaction mechanism of TiO ₂ photocatalysis [38].	15
Figure 3 Crystalline Phases of TiO ₂ .	20
Figure 4 Schematic of adsorb and shuttle process [66].	24
Figure 5 Pineapple leaf fibers after alkali treatment.	29
Figure 6 Chemical structure of cellulose.	30
Figure 7 Connection of succinic acid to cotton and TiO ₂ through using the cross-link method [93].	30
Figure 8 XRD pattern of TiO ₂ powder used in geometries calcined at 450°C for 2 h. which contains both anatase and rutile phase.	40
Figure 9 The XRD pattern of P25 and TiO ₂ with different 4 methods.	41
Figure 10 The surface morphological of various TiO ₂ powder prepare from 4 different methods, (a) method 1, (b) method 2, (c) method 3 and (d) method 4.	42
Figure 11 Nitrogen adsorption-desorption isotherm of P25 and TiO ₂ with 4 different methods.	43
Figure 12 The FTIR spectra of P25 and TiO ₂ over prepared from different methods.	44
Figure 13 a) UV-vis diffuse reflectance spectrum b) spectrum curves of Kubelka-Munk function as the vertical axis and plotted against the photo energy of TiO ₂ synthesized from method 4.	45
Figure 14 XPS spectra of Ti element on various TiO ₂ powder prepare from different methods, (a) P25, (b) method 1, (c) method 3, (d) method 4 and (e) and (f) intensity of Ti ⁴⁺ and Ti ⁰ in various materials, respectively.	46
Figure 15 (a) Effect of maximum intensity of Ti ⁴⁺ on PQ photoactivity, (b) Effect of maximum intensity of Ti ⁰ on PQ photoactivity, (c) Effect of surface area on PQ photoactivity and (d) The photo PQ degradation under UV irradiation using various TiO ₂ powder prepare from different 4 methods.	48
Figure 16 (a) Effect of maximum intensity of Ti ⁴⁺ on MB photoactivity, (a) Effect of maximum intensity of Ti ⁰ on MB photoactivity, (c) Effect of surface area on MB	

photoactivity and (d) The photo MB degradation under UV irradiation using various TiO ₂ powder prepare from different 4 methods.....	50
Figure 17 (a) Effect of maximum intensity of Ti ⁴⁺ on MO photoactivity, (b) Effect of maximum intensity of Ti ⁰ on MO photoactivity, (c) Effect of surface area on MB photoactivity and (d) The photo MO degradation under UV irradiation using various TiO ₂ powder prepare from different 4 methods.....	51
Figure 18 (a) Effect of maximum intensity of Ti ⁴⁺ on photoactivity, (b) Effect of maximum intensity of Ti ⁰ on photoactivity, (c) Effect of surface area on photoactivity and (d) The photo degradation under UV irradiation using various TiO ₂ powder prepare from different 4 methods.	53
Figure 19 The XRD pattern of pure TiO ₂ and TiO ₂ :PF with difference ratio.	55
Figure 20 The SEM image of a) virgin fiber, b) fibers after calcination and c) pure TiO ₂	56
Figure 21 The SEM image of TiO ₂ :PF with different ratio a) 1:10, b) 1:5, c) 1:1, d) 2:1.	57
Figure 22 SEM-EDX of 2:1 TiO ₂ :PF.....	58
Figure 23 Nitrogen adsorption-desorption isotherm of pure TiO ₂ and TiO ₂ :PF with different ratio.	60
Figure 24 The FTIR of pure FB, pure TiO ₂ and TiO ₂ :PF with different ratio.....	61
Figure 25 UV-vis diffuse reflectance spectra of pure TiO ₂ and 2:1 TiO ₂ :PF.....	62
Figure 26 DTG and TG curves of pure FB and TiO ₂ :PF with different ratio.....	63
Figure 27 The total MB removal under UV irradiation using pure TiO ₂ and different ratio of TiO ₂ :PF.....	64
Figure 28 MB adsorption under dark reaction for 60 minute using pure TiO ₂ and different ratio of TiO ₂ :PF.....	65
Figure 29 MB degradation under UV irradiation for 2 hour using pure TiO ₂ and different ratio of TiO ₂ :PF.....	66
Figure 30 XRD pattern of various TiO ₂ :PF.	67
Figure 31 The SEM image of a) TiO ₂ :PF, b) TiO ₂ :PF+SA, c) TiO ₂ :PF+SA+Na	68
Figure 32 ATR-FTIR spectrum of various TiO ₂ :PF.....	69
Figure 33 DTG and TG curves of various materials.....	70
Figure 34 DTG and TG curves of various materials.....	71

Figure 35 XPS spectra of Ti element on various TiO ₂ , (a) pure TiO ₂ , (b) TiO ₂ :PF, (c) TiO ₂ :PF+SA (d) TiO ₂ :PF+SA+Na and (e) intensity of Ti ⁴⁺ in various materials.	72
Figure 36 Effect of total MB removal (first hr. in dark and another hrs. under UV irradiation) using various TiO ₂ :PF.....	74
Figure 37 MB adsorption under dark reaction for 60 minute using various TiO ₂ :PF.	75
Figure 38 Effect of MB degradation under UV irradiation of various TiO ₂ :PF.....	76
Figure 39 Effect of maximum intensity of Ti ⁴⁺ on photo-activity using various TiO ₂ materials.....	77
Figure 40 Effect of recycling on the photocatalytic degradation with 3 cycle using TiO ₂ :PF+SA+Na.....	78
Figure 41 Effect of recycling on the photocatalytic degradation with 3 cycle using TiO ₂ :PF+SA+Na.....	79

CHAPTER 1

INTRODUCTION

1.1 Background

Pesticides (herbicides, fungicides or insecticides) are environmental pollutants often found in soil, water, atmosphere, and agricultural products, and may exist in harmful levels, posing an environmental threat. Even low levels of contaminants can cause adverse effects on humans, plants, animals and ecosystems [1]. In recent years, more attentions is paid to the application of semiconductors like ZnO, Fe₂O₃, and CdS as photocatalysts to degrade organic contaminations. As a popular photocatalyst, TiO₂ has been widely used because of its various merits, such as optical and electronic properties, low cost, high photocatalytic activity, chemical stability and non-toxicity [2,3]. This process is performed by activation of photocatalyst using ultraviolet or visible light to produce primarily hydroxyl and superoxide radicals which are the active sites on TiO₂ surfaces for oxidizing organic compounds and antibacterial to water vapour and carbon dioxide [4]. Some particle characters affecting photocatalytic activity are particle size, crystal structure, hydroxylated level, absolute crystallinity, intensity of light irradiation, surface absorption of contaminants, pH of the solution, and the preparation method. Typically, porous structure has been considered as an effective way to enhance the light adsorption capacity due to the increased surface area and multiple interparticle scattering, leading to the enhancement of photocatalytic reactions [5–7]. Up to date, some strategies have been adopted to prepare porous TiO₂, such as solgel process [8], hydrothermal process [9], ultrasonic process [10], template assisted method [11], and et al. When TiO₂ particles' size is reduced to nano scale, photocatalytic activity increases firstly as a result of expansion of light band-gap for quantum size and secondly due to enhancement of effective surface area [12–16]. However, TiO₂ powders used for industry are difficult for separation and removal from air or water. Therefore, many studies have shown that TiO₂ film coated on many kinds of substrates such as [17], stainless steel [18] and polymer [19] in order to separate them

more easily. And many studies have shown that TiO₂ coated on glass and tiles for purification, antibacterial [20,21] and self-cleaning [22] under UV-light in living area.

Cellulose is the most abundant and widespread biopolymer on earth. Owing to its abundance, biodegradability, and specific properties, cellulose is a very important renewable resource for the development of environment friendly, biocompatible, and functional materials, quite apart from its traditional and massive use in papermaking and cotton textiles. Cellulose fibres present a polar surface associated to the hydroxylated nature of the constituting anhydroglucose units. Such feature is responsible for the high hydrophilicity of cellulose, enabling the establishment of strong hydrogen bonding between fibres and the formation of three dimensional fibre-based structures. On the other hand, the presence of these hydrophilic groups can promote the nucleation and growth of inorganic phases, such as TiO₂, at the cellulose fibre surfaces and thus allowing production of nanocomposites [23]. One way to graft nano TiO₂ on cotton fabrics is achieved using cross-link method.

In this study, effect of TiO₂ preparation was studied. Then, the optimum method was used to deposit TiO₂ to pineapple fibers. The activity of the obtained catalyst in MB removal was studied. Finally, the effect of crosslink molecule in TiO₂ over pineapple molecules was studied. The succinic acid was used as crosslink molecule.

1.2 Research objectives

- 1.2.1 To study the optimum method for synthesizing the TiO₂ photocatalyst.
- 1.2.2 To study the preparation method of the TiO₂ deposition over the natural fibers.
- 1.2.3 To study the effect of crosslink addition to TiO₂ deposited over natural fibers.
- 1.2.4 To study the possibility of using the catalyst in photocatalysis reaction.

1.3 Expected results obtained from the research

- 1.3.1 The optimum method in synthesizing the TiO₂ photocatalyst was obtained.
- 1.3.2 The effect of TiO₂ deposition over the natural fibers was illustrated.

1.3.3 The effect of cross-linked part in TiO₂ over natural fibers was studied.

1.3.4 The catalyst possible for using in photocatalysis reaction.

1.4 Scopes of research

1.4.1 The preparation of TiO₂ was carried out by different 4 methods.

1.4.2 The ratio of TiO₂: fibers was investigated; 1:10, 1:5, 1:2, 1:1 and 2:1 by using the optimum preparation method from previous study.

1.4.3 The addition of crosslinked molecule between TiO₂ and fiber by using succinic acid was established.

1.4.4 The synthesized photocatalyst was tested the photo activity in MB degradation.

1.4.5 The catalyst samples were characterized by FTIR, SEM and EDS, BET, XRD, XPS and UV-vis diffuse reflectance.

1.5 Research Place

Department of Chemistry, Faculty of Science, Mahasarakham University.

CHAPTER 2

LITERATURE REVIEW

2.1 The environmental problem

Environmental protection and the correction of environmental problems are major questions for an effective improvement of life quality and for a sustainable development. Water is present in multiple human activities being used for very diverse purposes like in domestic use, agriculture, industry and energy production. Until a recent past, water demand increased with the slow population growth. The industrial revolution brought an improvement on people's quality of life and consequently a large increase in life expectancy. The exponential growth of human population and the intensification of agricultural and industrial activities led to a continuous increase in the demand for earth's limited supply of freshwater. Protection of natural water resources and development of new technologies for water and wastewater treatment became key environmental issues of the 21st century. Globally, domestic use only represents 15% of the total water consumption, while 25% is used in industrial activities and 60% in agriculture (Fig. 1). Associated to each of these activities are distinct types of pollution and pollutant compounds. In the Iberian region, main wastewater producing industrial processes include petrochemical, chemical synthesis, textile, pharmaceutical, agrochemical, paper and food.

Recently, the European Union Commission Services proposed a new Directive, amending Directive 2000/60/EC, where new Environmental Quality Standards (EQS) for hazardous priority substances have been defined within Europe. In particular pesticides and phenols are referred, with admissible thresholds lower than 0.5 microgram per liter in water. Thus, adequate treatment of contaminated waters is of primary concern in order to preserve the natural ecosystem. The biological processes are more natural and easy to implement but they have a major drawback, which is the production of sludge proportionally to the volume of treated water. When the volume to treat is huge, recycling is essential. Nevertheless, used water always requires some treatment prior to reuse, with or without addition of freshwater. The extent of the

treatment depends either on the degree of contamination, or on the requirements of the next use. Chemical treatments provide adequate response to a number of specific cases, because with them the pollutant is not being transferred, rather converted, or in the ideal case mineralized.

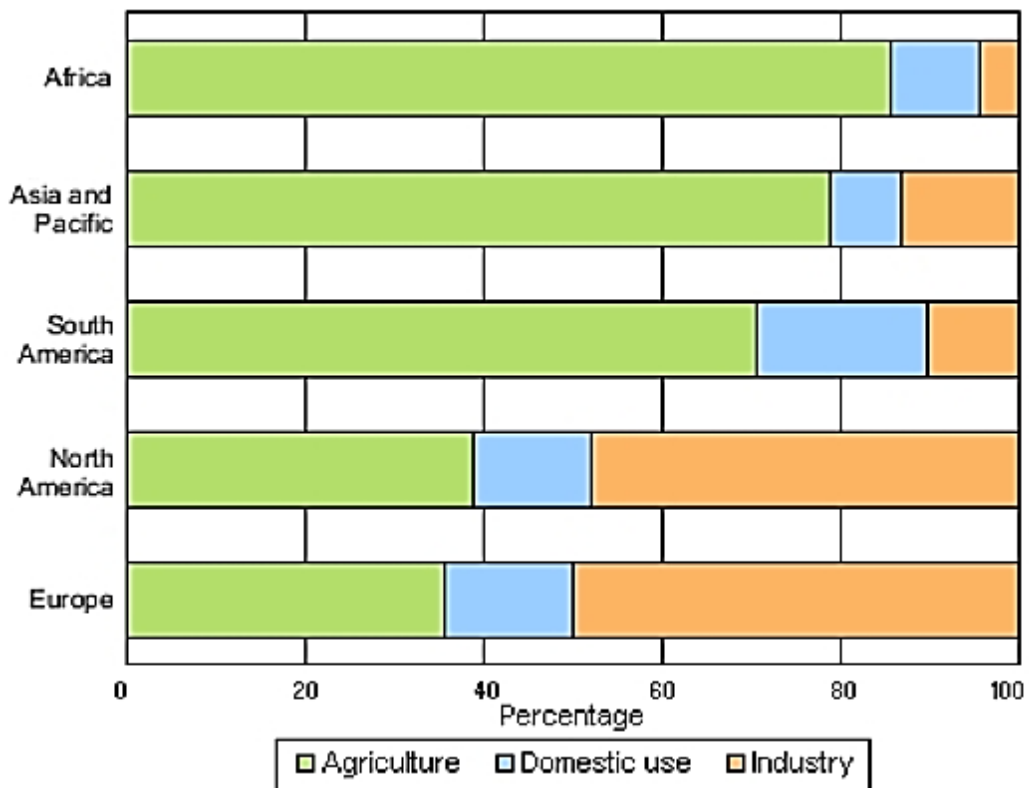


Figure 1 Water withdrawal by sector in the regions of the world (2000) [24].

2.2 Persistent organic pollutants

Persistent organic pollutants (POPs) are chemicals of global concern due to their potential for long-range transport, persistence in the environment, ability to bio-magnify and bio-accumulate in ecosystems, as well as their significant negative effects on human health and the environment. Humans are exposed to these chemicals in a variety of ways: mainly through the food we eat, but also through the air we breathe, in the outdoors, indoors and at the workplace. Many products used in our daily lives may contain POPs, which have been added to improve product characteristics, such as flame retardants or surfactants. As a result, POPs can be found virtually everywhere on our planet in measurable concentrations.

The most commonly encountered POPs are organochlorine pesticides, such as DDT, industrial chemicals, most notably polychlorinated biphenyls (PCB), as well as unintentional by-products of many industrial processes, especially polychlorinated dibenzo-p-dioxins (PCDD) and dibenzofurans (PCDF), commonly known as 'dioxins'. POPs bio-magnify throughout the food chain and bio-accumulate in organisms. The highest concentrations of POPs are thus found in organisms at the top of the food chain. Consequently, background levels of POPs can be found in the human body. Human exposure - for some compounds and scenarios, even to low levels of POPs - can lead, among others, to increased cancer risk, reproductive disorders, alteration of the immune system, neurobehavioural impairment, endocrine disruption, genotoxicity and increased birth defects. The effect of POPs on human and environmental health was discussed, with intention to eliminate or severely restrict their production, by the international community at the Stockholm Convention on Persistent Organic Pollutants in 2001 [24].

Stockholm Convention on Persistent Organic Pollutants

The Stockholm Convention was adopted and put into practice by the United Nations Environment Programme (UNEP) on May 22, 2001. The UNEP decided that POP regulation needed to be addressed globally for the future. The purpose statement of the agreement is "to protect human health and the environment from persistent organic pollutants." As of 2014, there are 179 countries in compliance with the Stockholm convention. The convention and its participants have recognized the potential human and environmental toxicity of POPs. They recognize that POPs have the potential for long range transport and bioaccumulation and biomagnification. The convention seeks to study and then judge whether or not a number of chemicals that have been developed with advances in technology and science can be categorized as POPs or not. The initial meeting in 2001 made a preliminary list, termed the "dirty dozen," of chemicals that are classified as POPs. As of 2014, the United States of America has signed the Stockholm Convention but has not ratified it. There are a handful of other countries that have not ratified the convention but most countries in the world have ratified the convention [24].

In May 1995, the United Nations Environment Programme Governing Council investigated POPs. Initially the Convention recognized only twelve POPs for their adverse effects on human health and the environment, placing a global ban on these particularly harmful and toxic compounds and requiring its parties to take measures to eliminate or reduce the release of POPs in the environment [29-31].

1. **Aldrin**, an insecticide used in soils to kill termites, grasshoppers, Western corn rootworm, and others, is also known to kill birds, fish, and humans. Humans are primarily exposed to aldrin through dairy products and animal meats.
2. **Chlordane**, an insecticide used to control termites and on a range of agricultural crops, is known to be lethal in various species of birds, including mallard ducks, bobwhite quail, and pink shrimp; it is a chemical that remains in the soil with a reported half-life of one year. Chlordane has been postulated to affect the human immune system and is classified as a possible human carcinogen. Chlordane air pollution is believed the primary route of humane exposure.
3. **Dieldrin**, a pesticide used to control termites, textile pests, insect-borne diseases and insects living in agricultural soils. In soil and insects, aldrin can be oxidized, resulting in rapid conversion to dieldrin. Dieldrin's half-life is approximately five years. Dieldrin is highly toxic to fish and other aquatic animals, particularly frogs, whose embryos can develop spinal deformities after exposure to low levels. Dieldrin has been linked to Parkinson's disease, breast cancer, and classified as immunotoxic, neurotoxic, with endocrine disrupting capacity. Dieldrin residues have been found in air, water, soil, fish, birds, and mammals. Human exposure to dieldrin primarily derives from food.
4. **Endrin**, an insecticide sprayed on the leaves of crops, and used to control rodents. Animals can metabolize endrin, so fatty tissue accumulation is not an issue, however the chemical has a long half-life in soil for up to 12 years. Endrin is highly toxic to aquatic animals and humans as a neurotoxin. Human exposure results primarily through food.
5. **Heptachlor**, a pesticide primarily used to kill soil insects and termites, along with cotton insects, grasshoppers, other crop pests, and malaria-carrying mosquitoes. Heptachlor, even at every low doses has been associated with the

decline of several wild bird populations – Canada geese and American kestrels. In laboratory tests have shown high-dose heptachlor as lethal, with adverse behavioral changes and reduced reproductive success at low-doses, and is classified as a possible human carcinogen. Human exposure primarily results from food.

6. **Hexachlorobenzene (HCB)**, was first introduced in 1945–59 to treat seeds because it can kill fungi on food crops. HCB-treated seed grain consumption is associated with photosensitive skin lesions, colic, debilitation, and a metabolic disorder called porphyria turcica, which can be lethal. Mothers who pass HCB to their infants through the placenta and breast milk had limited reproductive success including infant death. Human exposure is primarily from food.
7. **Mirex**, an insecticide used against ants and termites or as a flame retardant in plastics, rubber, and electrical goods. Mirex is one of the most stable and persistent pesticides, with a half-life of up to 10 years. Mirex is toxic to several plant, fish and crustacean species, with suggested carcinogenic capacity in humans. Humans are exposed primarily through animal meat, fish, and wild game.
8. **Toxaphene**, an insecticide used on cotton, cereal, grain, fruits, nuts, and vegetables, as well as for tick and mite control in livestock. Widespread toxaphene use in the US and chemical persistence, with a half-life of up to 12 years in soil, results in residual toxaphene in the environment. Toxaphene is highly toxic to fish, inducing dramatic weight loss and reduced egg viability. Human exposure primarily results from food. While human toxicity to direct toxaphene exposure is low, the compound is classified as a possible human carcinogen.
9. **Polychlorinated biphenyls (PCBs)**, used as heat exchange fluids, in electrical transformers, and capacitors, and as additives in paint, carbonless copy paper, and plastics. Persistence varies with degree of halogenation, an estimated half-life of 10 years. PCBs are toxic to fish at high doses, and associated with spawning failure at low doses. Human exposure occurs through food, and is associated with reproductive failure and immune suppression. Immediate

effects of PCB exposure include pigmentation of nails and mucous membranes and swelling of the eyelids, along with fatigue, nausea, and vomiting. Effects are transgenerational, as the chemical can persist in a mother's body for up to 7 years, resulting in developmental delays and behavioral problems in her children. Food contamination has led to large scale PCB exposure.

10. **Dichlorodiphenyltrichloroethane (DDT)** is probably the most infamous POP. It was widely used as insecticide during WWII to protect against malaria and typhus. After the war, DDT was used as an agricultural insecticide. In 1962, the American biologist Rachel Carson published *Silent Spring*, describing the impact of DDT spraying on the US environment and human health. DDT's persistence in the soil for up to 10–15 years after application has resulted in widespread and persistent DDT residues throughout the world including the arctic, even though it has been banned or severely restricted in most of the world. DDT is toxic to many organisms including birds where it is detrimental to reproduction due to eggshell thinning. DDT can be detected in foods from all over the world and food-borne DDT remains the greatest source of human exposure. Short-term acute effects of DDT on humans are limited, however long-term exposure has been associated with chronic health effects including increased risk of cancer and diabetes, reduced reproductive success, and neurological disease.
11. **Dioxins** are unintentional by-products of high-temperature processes, such as incomplete combustion and pesticide production. Dioxins are typically emitted from the burning of hospital waste, municipal waste, and hazardous waste, along with automobile emissions, peat, coal, and wood. Dioxins have been associated with several adverse effects in humans, including immune and enzyme disorders, chloracne, and are classified as a possible human carcinogen. In laboratory studies of dioxin effects an increase in birth defects and stillbirths, and lethal exposure have been associated with the substances. Food, particularly from animals, is the principal source of human exposure to dioxins.
12. **Polychlorinated dibenzofurans** are by-products of high-temperature processes, such as incomplete combustion after waste incineration or in

automobiles, pesticide production, and polychlorinated biphenyl production. Structurally similar to dioxins, the two compounds share toxic effects. Furans persist in the environment and classified as possible human carcinogens. Human exposure to furans primarily results from food, particularly animal products.

Since 2001, this list has been expanded to include some polycyclic aromatic hydrocarbons (PAHs), brominated flame retardants, and other compounds. Additions to the initial 2001 Stockholm Convention list are as following POPs:

13. **Chlordecone**, a synthetic chlorinated organic compound, is primarily used as an agricultural pesticide, related to DDT and Mirex. Chlordecone is toxic to aquatic organisms, and classified as a possible human carcinogen. Many countries have banned chlordecone sale and use, or intend to phase out stockpiles and wastes.
14. **α -Hexachlorocyclohexane (α -HCH)** and **β -Hexachlorocyclohexane (β -HCH)** are insecticides as well as by-products in the production of lindane. Large stockpiles of HCH isomers exist in the environment. α -HCH and β -HCH are highly persistent in the water of colder regions. α -HCH and β -HCH has been linked Parkinson's and Alzheimer's disease.
15. **Hexabromodiphenylether (hexaBDE)** and **heptabromodiphenyl ether (heptaBDE)** are main components of commercial octabromodiphenyl ether (octaBDE). Commercial octaBDE is highly persistent in the environment, whose only degradation pathway is through debromination and the production of bromodiphenyl ethers, which can increase toxicity.
16. **Lindane (γ -hexachlorocyclohexane)**, a pesticide used as a broad spectrum insecticide for seed, soil, leaf, tree and wood treatment, and against ectoparasites in animals and humans (head lice and scabies). Lindane rapidly bioconcentrates. It is immunotoxic, neurotoxic, carcinogenic, linked to liver and kidney damage as well as adverse reproductive and developmental effects in laboratory animals and aquatic organisms. Production of lindane unintentionally produces two other POPs α -HCH and β -HCH.^[citation needed]
17. **Pentachlorobenzene (PeCB)**, is a pesticide and unintentional byproduct. PeCB has also been used in PCB products, dyestuff carriers, as a fungicide, a flame

retardant, and a chemical intermediate. PeCB is moderately toxic to humans, while highly toxic to aquatic organisms.

18. **Tetrabromodiphenyl ether** (tetraBDE) and pentabromodiphenyl ether (pentaBDE) are industrial chemicals and the main components of commercial pentabromodiphenyl ether (pentaBDE). PentaBDE has been detected in humans in all regions of the world.
19. **Perfluorooctanesulfonic acid** (PFOS) and its salts are used in the production of fluoropolymers. PFOS and related compounds are extremely persistent, bioaccumulating and biomagnifying. The negative effects of trace levels of PFOS have not been established.
20. **Endosulfans** are insecticides to control pests on crops such as coffee, cotton, rice and sorghum and soybeans, tsetse flies, ectoparasites of cattle. They are used as a wood preservative. Global use and manufacturing of endosulfan has been banned under the Stockholm convention in 2011, although many countries had previously banned or introduced phase-outs of the chemical when the ban was announced. Toxic to humans and aquatic and terrestrial organisms, linked to congenital physical disorders, mental retardation, and death. Endosulfans' negative health effects are primarily linked to its endocrine disrupting capacity acting as an antiandrogen.
21. **Hexabromocyclododecane** (HBCD) is a brominated flame retardant primarily used in thermal insulation in the building industry. HBCD is persistent, toxic and ecotoxic, with bioaccumulative and long-range transport properties.

Current studies aimed at minimizing POPs in the environment are investigating their behavior in photocatalytic oxidation reactions. POPs that are found in humans and in aquatic environments the most are the main subjects of these experiments. Aromatic and aliphatic degradation products have been identified in these reactions. Photochemical degradation is negligible compared to photocatalytic degradation. A method of removal of POPs from marine environments that has been explored is adsorption. It occurs when an absorbable solute comes into contact with a solid with a porous surface structure. Current efforts are more focused on banning the use and production of POPs worldwide rather than removal of POPs [24].

2.3 Photocatalyst

A photocatalyst is defined as a substance which is activated by adsorbing a photon and is capable of accelerating a reaction without being consumed (25). In photogenerated catalysis, the photocatalytic activity depends on the ability of the catalyst to create electron-hole pairs, which generate free radicals (e.g. hydroxyl radicals: $\bullet\text{OH}$) able to undergo secondary reactions. Therefore, a suitable bandgap energy together with chemical and physical stability, nontoxic nature, availability, and low cost are important requirements to be taken into account to choose a solid photocatalyst. These substances are invariably semiconductors. Semiconducting oxide photocatalysts have been increasingly focused in recent years due to their potential applications in solar energy conversion and environmental purification. Semiconductor heterogeneous photocatalysis has enormous potential to treat organic contaminants in water and air. This process is known as advanced oxidation process (AOP) are a set of chemical treatment procedures designed to remove organic (and sometimes inorganic) materials in water and wastewater by oxidation through reactions with hydroxyl radicals ($\cdot\text{OH}$). In real-world applications of wastewater treatment, however, this term usually refers more specifically to a subset of such chemical processes that employ ozone (O_3), hydrogen peroxide (H_2O_2) and/or UV light. One such type of process is called in situ chemical oxidation. Among AOPs, Developed in the 1970s, heterogeneous photocatalytic oxidation has been given considerable attention and in the past two decades numerous studies have been carried out on the application of heterogeneous photocatalytic oxidation process with a view to decompose and mineralize recalcitrant organic compounds. It involves the acceleration of photoreaction in the presence of a semiconductor catalyst [26].

2.4 Semiconductors

Semiconductor materials are materials whose valence band and conduction band are separated by an energy gap or band-gap. When a semiconductor molecule absorbs photons with energy equal or greater than its band-gap, electrons in the valence band can be excited and jump up into the conduction band, and thus charge carriers are

generated. In order to have a photocatalyzed reaction, the e^-h^+ recombination, subsequent to the initial charge separation, must be prevented as much as possible [27,28]. Several semiconductors (such as TiO_2 , ZnO , Fe_2O_3 , CdS , and ZnS) can act as sensitizers for light-induced redox-processes due to the electronic structure of the metal atoms in chemical combination, which is characterized by a filled valence band, and an empty conduction band [29]. Metal oxide semiconductors are considered to be the most suitable photocatalysts due to their photo corrosion resistance and wide band gap energies. Table 1. provides the band gap energies at corresponding wavelength for well-known semiconductors. TiO_2 stands out as the most effective photocatalyst and has been extensively used in water and wastewater treatment studies [30,31].

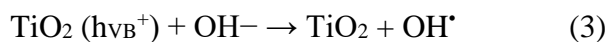
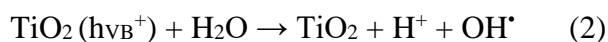
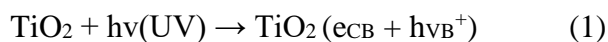
Table 1 Band gap energies of various semiconductors at relevant wavelengths [32].

Semiconductor	Band gap energy (eV)	Wavelength
TiO_2 (rutile)	3.0	413
TiO_2 (anatase)	3.2	388
ZnO	3.2	388
ZnS	3.6	335
CdS	2.4	516
Fe_2O_3	2.3	539

Among all these semiconductors, TiO_2 has been most commonly studied due to its ability to break down organic pollutants and even achieve complete mineralization. Photocatalytic and hydrophilic properties of TiO_2 makes it close to an ideal catalyst due to its high reactivity, reduced toxicity, chemical stability and lower costs [33]. Fujishima and Honda [34] pioneered the concept of titania photocatalysis (also known as “Honda-Fujishima effect”). Though TiO_2 has the disadvantage of not being activated by visible light, but by ultraviolet (UV) light, it is advantageous over the others in that it is chemically and biologically inert, photocatalytically stable, relatively easy to produce and to use, able to efficiently catalyze reactions, cheap and without risks to environment or humans [(35,36)].

2.5 Mechanism and fundamentals of photocatalytic reactions

Photocatalysis may be termed as a photo induced reaction which is accelerated by the presence of a catalyst [30]. These types of reactions are activated by absorption of a photon with sufficient energy (equals or higher than the band-gap energy (E_{bg}) of the catalyst) [35]. The absorption leads to a charge separation due to promotion of an electron (e^-) from the valence band of the semiconductor catalyst to the conduction band, thus generating a hole (h^+) in the valence band (the schematic diagram of the process is presented in Figure 2 [26]). The recombination of the electron and the hole must be prevented as much as possible if a photocatalyzed reaction must be favored. The ultimate goal of the process is to have a reaction between the activated electrons with an oxidant to produce a reduced product, and also a reaction between the generated holes with a reductant to produce an oxidized product. The photogenerated electrons could reduce the dye or react with electron acceptors such as O_2 adsorbed on the $Ti(III)^-$ surface or dissolved in water, reducing it to superoxide radical anion (O_2^-) \cdot . The photo generated holes can oxidize the organic molecule to form R^+ , or react with OH^- or H_2O oxidizing them into OH^\cdot radicals. Together with other highly oxidant species (peroxide radicals) they are reported to be responsible for the heterogeneous TiO_2 photodecomposition of organic substrates as dyes. The resulting $\cdot OH$ radical, being a very strong oxidizing agent (standard redox potential +2.8 V) can oxidize most azo dyes to the mineral end-products. According to this, the relevant reactions at the semiconductor surface causing the degradation of dyes can be expressed as follows:



where $h\nu$ is photon energy required to excite the semiconductor electron from the valence band (VB) region to conduction band (CB) region and R represents the organic compound. [37].

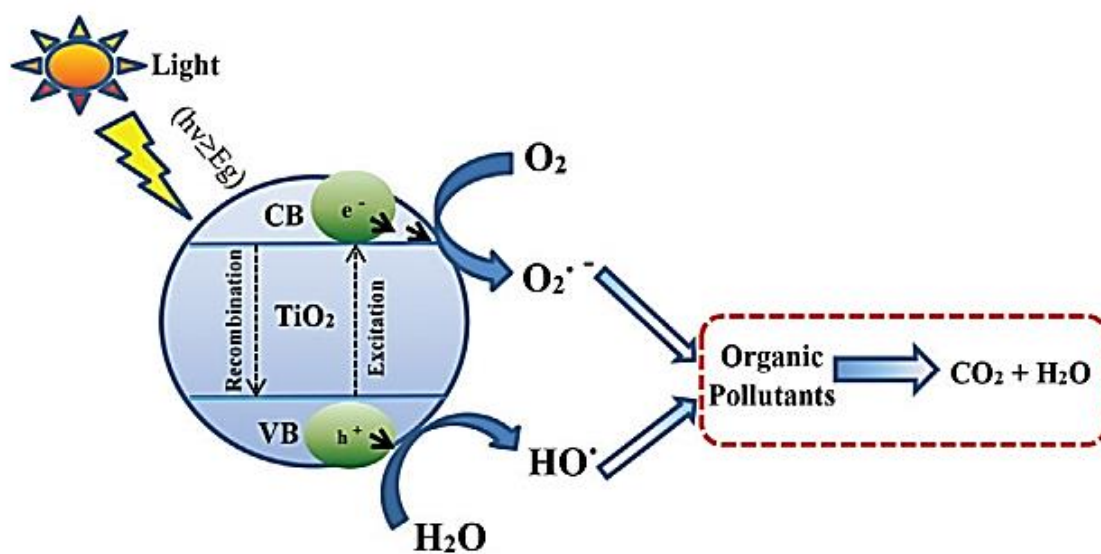


Figure 2 Reaction mechanism of TiO₂ photocatalysis [38].

2.6 Factors affecting the photocatalytic process

As showed earlier, photocatalytic reactions are extremely complex processes involving many participants namely water, organic substrate, catalyst, light and oxygen. Therefore, it is obvious that operational parameters related to each of these agents may affect the efficiency of the photocatalytic process. Photocatalytic reaction rates are known to be affected by several operation conditions including pH of the medium, catalyst loading, substrate concentration, light intensity (photonic flux), temperature and oxygen pressure. Also, physical and chemical intrinsic properties of the photocatalyst may affect its photoefficiency. TiO₂ crystal composition, surface area, crystallite dimensions and presence of surface hydroxyl groups are known to be important parameters that influence the efficiency of the catalyst in photocatalytic

reactions. Since these themes will be the subject of some of the studies presented in this research work, they will be discussed in detail in the chapters dedicated to results. However, a brief description of the effect caused by each operational parameter in the efficiency of the photocatalytic process is described in the following.

2.6.1 Operational parameters

Catalyst loading

In photocatalytic processes, the initial rates of reaction are found to be proportional to the mass of catalyst. However, above a certain amount, the reaction rate becomes independent of the mass of catalyst. This limit corresponds to the maximum amount of TiO₂ at which all particles are totally illuminated. Generally, in any given photocatalytic application, the optimum catalysts loading must be determined, in order to avoid excess catalyst and ensure total absorption of efficient photons [39].

Substrate concentration

In photocatalytic degradation reactions, the observed rate constant decreases with the increase of initial organic pollutant concentration. The main steps of the photocatalytic reaction occur on the surface of the catalyst, and therefore, a high adsorption capacity is associated with reaction favoring. It is assumed that most of the reactions follow a Langmuir-Hinshelwood kinetic rate model, meaning that for high initial concentration all catalytic sites are occupied. A further increase of the concentration does not affect the actual catalyst surface concentration, and therefore, this may result in a decrease of the observed rate constant. Intermediates generated during the photocatalytic process also affect the rate constant of their parent compounds. A high initial concentration of the initial pollutant means higher concentrations of adsorbed reaction intermediates, which will negatively affect the overall rate [38].

pH of the medium

The acid-basic properties of the reaction medium play an important role in the photocatalytic reaction taking place at the surface of the semiconductor. The variation of pH affects TiO₂ surface speciation due to the amphoteric (point of zero

charge at pH~6.5) nature of titania particles. Under acidic or alkaline conditions the surface of titania can be protonated or deprotonated, respectively. Also, the electronic state of the substrate molecule in the reaction media will depend on its acidic properties, namely pKa. The effect of the pH on the reaction rate can be interpreted in terms of electrostatic interactions between charged TiO₂ particles and the substrate. This in turn affects the adsorption process, important since the photocatalytic reactions are believed to be surface processes. For photocatalytic reactions using TiO₂ slurries, pH conditions has also been reported to have an influence on the dispersion of the semiconductor particles in suspension, and therefore on the photodegradation rate [40].

Temperature

The overall process of photocatalytic degradation is not too sensitive to temperature. The degradation rate dependency on temperature is reflected by the low activation energy (5–20 kJ mol⁻¹) compared with ordinary thermal reactions [41]. Due to photonic activation, the photocatalytic systems do not require heating and can operate at room temperature. This absence of heating is very attractive for processes carried out in aqueous medium, especially for water purification, because there is no need to waste energy in heating water, which has a high heat capacity.

Oxygen pressure

In liquid phase reactions, it becomes difficult to study the influence of oxygen partial pressure because the reaction is polyphasic. It is generally assumed that oxygen adsorbs on titania from the liquid phase, where it is dissolved following Henry's law [7]. If oxygen is regularly supplied, it can be assumed that its coverage at the surface of TiO₂ is constant and its contribution can be integrated in the apparent rate constant. Dissolved oxygen is strongly electrophilic and thus an increase of its content probably reduces unfavorable electron/hole recombination routes. However, higher concentrations lead to a downturn of the reaction rate, which can be attributed to the fact that the TiO₂ surface becomes highly hydroxylated inhibiting the adsorption of the pollutant at the active sites [42].

Photon flux

The radiant flux (ϕ), which is proportional to the light intensity, constitutes a very important parameter in the design of the reactor and in the choosing of the light source. Photocatalytic degradation rates have been found to follow two distinct regimes with respect to the radiant flux: a first-order regime for low photon flux and a half-order regime for high intensities [43]. In the former regime, the electron/hole pairs are consumed more rapidly by chemical reactions than by recombination reactions, whereas in the half-order regime, the electron/hole recombination is the dominant process.

2.6.2 TiO₂ structural and morphological properties

TiO₂ crystal structure

Titanium dioxide in the anatase form is generally accepted to be the most active polymorph. This better efficiency is attributed to a higher degree of hydroxylation of anatase when compared with rutile phase. Also, the higher surface area of anatase TiO₂ is pointed as one of the properties that contribute to its superior efficiency. Even though, some studies have revealed that pure anatase not always lead to the best photocatalytic performance [31]. These findings were discussed in terms of the presence of rutile phase may introduce mesoporosity and a wider pore size distribution to the resultant catalyst. The catalytic activity may be a combined effect of the pore size, the pore size distribution and the appropriate crystal plane on which adsorption takes place.

Surface area

The surface area of a solid catalyst is directly related to the concentration of active sites for adsorption and reaction. A large surface area can be a determining factor in certain photodegradation reactions, since the adsorption of large amounts of substrate and oxygen promotes the reaction rate. However, powders with high surface areas are usually associated with large amounts of crystal lattice defects, facilitating the recombination of the photo-generated electron/hole pairs, leading to a poor photocatalytic activity [44]. It has been reported that the photocatalytic activity of amorphous titania is negligible indicating that crystallinity is an important requirement

[10]. Therefore, a balance between surface area and crystallinity must be found in order to obtain the maximum photoactivity.

Particle dimensions

Particle size and ultimately, crystallite dimensions play an important role in the photoactivity of the semiconductor, since the electron/hole recombination process was showed to be particle size dependent [44]. It is known that in nanometer-size range, the physical and chemical properties of the semiconductors are modified, when compared to bulk size dimensions [45]. Small variations in particle size leads to great modifications in surface/bulk ratio, thus modifying the significance of volume and surface electron/hole recombination processes. Generally it is assumed that the smaller is the particle (in a nanometer range), the higher is the efficiency of the photocatalytic process. However, if the TiO₂ crystallite size is extremely reduced, in the range of a few nanometers, lattice defects can lead to an increase in the electron/hole recombination.

Additionally, particle size is an important parameter for heterogeneous catalysis in general since it directly impacts the specific surface area of a catalyst. With a smaller particle size, the number of active surface sites increases, and so does the surface charge carrier transfer rate in photocatalysis. Some studies revealed that the photocatalytic efficiency does not monotonically increase with decreasing particle size, and there exists an optimal particle size of a few nanometers (3–10 nm) for pure nanocrystalline TiO₂ photocatalyst [46]. Nevertheless, as for other properties, an optimum value may be discussed only in the context of the used catalyst, organic compound and process parameters.

2.7 Titanium dioxide photocatalyst (TiO₂)

Titanium dioxide (TiO₂) or titania is a very well-known and well researched material due to the stability of its chemical structure, biocompatibility, physical, optical and electrical properties. It exists in four mineral forms, anatase, rutile, brookite and titanium dioxide or TiO₂ as shown in fig 3.

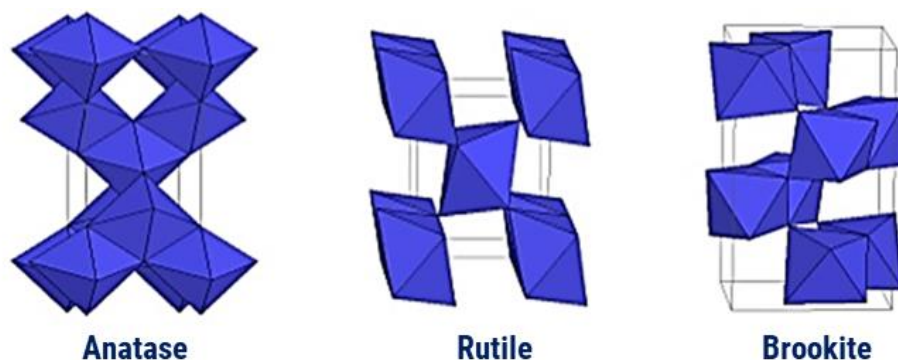


Figure 3 Crystalline Phases of TiO₂.

Anatase type TiO₂ has a crystalline structure that corresponds to the tetragonal system (with dipyramidal habit) and is used mainly as a photocatalyst under UV irradiation. Rutile type TiO₂ also has a tetragonal crystal structure (with prismatic habit). This type of titania is mainly used as white pigment in paint. Rutile is the thermodynamically most stable modification (ca. 1.2–2.8 kcal mol⁻¹ more stable than anatase). Rutile to anatase transformation occurs in the temperature range 700–1000 °C depending on the crystallite size and impurity content. The band gap energies for anatase and rutile have been estimated to be 3.2 and 3.0 eV, respectively. The smaller band gap of rutile however implies that a higher fraction of the solar radiation can induce band gap excitation (three-fold increase in photocurrents). Anatase is the low-temperature stable form (appears in the form of pyramid-like crystals) and rutile (needlelike) is the dominant form in high temperature preparations, including single crystals. The reduced density of anatase as compared to rutile (3.89 g cm⁻³ versus 4.26 g cm⁻³) leads to significant differences in many physical properties. Rutile has non-negligible absorption in the near-UV region (350 - 400 nm), ca. 4% of the incident solar radiation. The anatase form of titanium dioxide has the desirable properties of being chemically stable, readily available and active as a photocatalyst for oxidation processes. Brookite type TiO₂ has an orthorhombic crystalline structure. TiO₂ is a monoclinic mineral and is a relatively newcomer to the titania family. TiO₂, therefore is a versatile material that has applications in various products such as paint pigments, sunscreen lotions, electrochemical electrodes, capacitors, solar cells and even as a food coloring agent and in toothpastes [47].

The possible application for this material as a photocatalyst in a commercial scale water treatment facility is due to several factors:

(a) Photocatalytic reaction takes place at room temperature.

(b) Photocatalytic reactions do not suffer the drawbacks of photolysis reactions in terms of the production of intermediate products because organic pollutants are usually completely mineralized to non-toxic substances such as CO₂, HCl and water [65–68].

(c) The photocatalyst is inexpensive and can be supported on various substrates such as, glass, fibers, stainless steel, inorganic materials, sand, activated carbons (ACs), allowing continuous reuse.

(d) Photogenerated holes are extremely oxidizing and photogenerated electrons reduce sufficiently to produce superoxides from dioxygens [48].

2.7.1 TiO₂ application

After Fujishima and Honda's discovery in 1972 of water splitting using TiO₂ [49], photocatalysis became significantly attractive for researchers in the fields of energy and the environment. Photocatalysis using TiO₂ has since been the subject of numerous studies, with an aim to improve its performance and investigate its advantages over other semiconductors [50,51]. Upon the absorption of light, electrons in the valence band of TiO₂ become excited and move to an unoccupied conduction band and generate positive electron vacancies in the valence band. The photo generated electrons and holes can either recombine or react with electron donors or acceptors near the surface of the photocatalyst. OH groups on the TiO₂ surface and O₂ in the environment limit electron-hole recombination by reacting with holes and electrons to produce OH[•] and O₂^{•-} radicals respectively. Subsequently, these radicals can take part in various reactions to produce other radicals depending on the reaction environment, or they can directly degrade organic pollutants in close proximity to the surface [52,53]. During the adsorption of pollutants onto the TiO₂ surface the pollutant molecules have to move from the bulk environment closer to the photocatalytic TiO₂ sites where they encounter layers of water molecules near the TiO₂ surface. Certain pollutants can form hydrogen bonds with these water molecules, however to move further, the mentioned

pollutant molecules need to break the hydrogen bonds and disorganize the water layers. This is difficult as close to the surface of TiO_2 the water molecules form a rigid network and hence the adsorption of pollutants on TiO_2 may be hindered. Additionally, the rigid water molecule network renders the produced OH^\bullet radicals less mobile compared to ones that are produced in the bulk by homogenous photocatalysis. It has been suggested that these issues arising from the water layers near the surface of TiO_2 may be overcome by the addition of an adsorbent which has greater preference for certain pollutants. Although heterogeneous photocatalysis is a promising method for pollutant removal in a sustainable way, its actual application is limited. Various factors can improve the efficiency of TiO_2 photocatalysis while there are also factors which reduce its efficiency. Some of these parameters are discussed in Table 2.

Table 2 Some factors affecting the efficiency of photocatalytic processes.

Factor Studied	Key findings
Crystalline Phase	Anatase phase has shown higher activity compared to the rutile phase. Rutile's high temperature heat treatment is detrimental to activity. A mixture of anatase and rutile phases can result in enhanced activity.
Particle Size	A reduction in size will generally improve photocatalytic activity.
Excitation Wavelength	Doping of TiO_2 photocatalyst with metal and non-metal deposits and ions can aid its visible light activation.
Affinity for organic pollutants	Generally TiO_2 has a low tendency to adsorb organic molecules. Addition of surfactants can increase its adsorption capability; however, oxidation of surfactant groups during photocatalysis can occur. Loading TiO_2 on an adsorbent support can increase the concentration of pollutants near the TiO_2 surface.

Photocatalyst particle separation post reaction	Separation of TiO ₂ particles from the bulk can be improved by fixing them on a large size support.
---	--

As can be seen from Table 2, in addition to TiO₂'s properties that influence its performance, the shortcomings of this semiconductor can also be improved using various strategies. Firstly, TiO₂'s narrow excitation region (< 400) and absorption of only 5% of the solar spectrum limits its applications under solar illumination. The second issue is TiO₂'s poor affinity for hydrophobic organic substances which makes the adsorption of organic pollutants on its surface relatively low. Finally, the practical application of fine nanosized TiO₂ particles is difficult due to the issue of separating such fine materials from bulk media. Agglomerated nanoparticles have lower efficiencies as, in such systems, light cannot reach all of the particles. Therefore, many studies have shown that TiO₂ film on many kinds of substrates such as stainless steel, fiber and polymer. Loading TiO₂ on inert, adsorptive domains, through the so-called "adsorb and shuttle" approach [54–59], can be a very good strategy to increase the concentration of pollutants near the photocatalytic sites and thus improve the overall performance of photocatalytic systems. This is schematically described in Figure 4.

The above-mentioned "adsorb and shuttle" approach to improve photocatalytic reaction rates involves attaching photocatalyst particles to highly adsorbing domains to produce composite TiO₂/adsorbent materials. They can be prepared using various methods and the final properties of the composites can be tailored depending on their final application. As mentioned earlier, such composites can also be used in a way where photocatalysis can act as an alternative regeneration method for adsorbent materials [42,60–65].

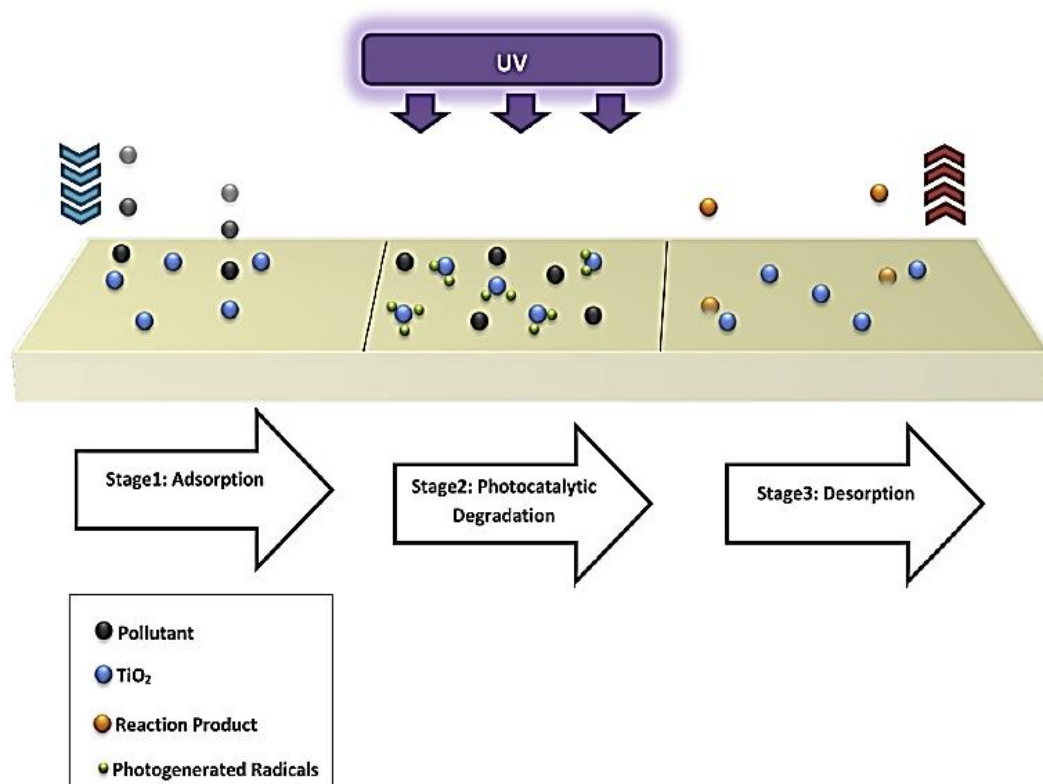


Figure 4 Schematic of adsorb and shuttle process [66].

2.7.2 Methods for loading TiO₂ onto various supports

As mentioned earlier, application of an adsorbent support may be one strategy to overcome TiO₂'s limitations and improve reaction efficiencies. The synthesis methods of TiO₂/adsorbent photocatalytic composites are significant in determining their final properties. The properties of the TiO₂ component of a composite TiO₂/adsorbent system such as its size, crystalline phase and dispersion will influence its photocatalytic efficiency, while characteristics of the adsorbent such as pore size and surface chemistry will affect its adsorption capability. Hence by choosing the appropriate synthesis method, within its given limitations and possibilities, and considering the resulting properties of both the TiO₂ component and the adsorbent component, the final properties of the composite TiO₂/adsorbent photocatalysts can be tailored. This section will briefly outline various loading methods which can be used to load TiO₂ on an adsorptive support and the parameters of each of the methods which can be used to tailor the final photocatalyst/adsorbent properties [67,68].

The methods for loading TiO₂ onto various supports can be classified according to whether TiO₂ powder is added to the surface of a support or the TiO₂ is deposited in-situ onto the surface of the support. There are many ways to prepare it, including some physical methods. More commonly-used methods are hydrothermal, solvothermal, impregnation, precipitation, hydrolysis and sol-gel methods [69].

Hydrothermal

Hydrothermal synthesis is normally conducted in steel pressure vessels called autoclaves with or without Teflon liners under controlled temperature or pressure with the reaction in aqueous solutions. The temperature can be elevated above the boiling point of water, reaching the pressure of vapor saturation. The temperature and the amount of solution added to the autoclave largely determine the internal pressure produced. It is a method that is widely used for the production of small particles in the ceramics industry. TiO₂ nanoparticles can be obtained by hydrothermal treatment of peptized precipitates of a titanium precursor with water. The precipitates were prepared by adding an isopropanol solution of titanium solution into deionized water, and then they were peptized at 70 °C for 1 h. Besides TiO₂ nanoparticles. In a typical preparation procedure, 2 g P25 TiO₂ white power was placed into a Teflon-lined autoclave. After the autoclave was naturally cooled to room temperature, the obtained sample was filtered, washed with distilled water for several times. Then, the obtained products were collected and washed with HCl aqueous solution (pH 1.6) for 24 h, and washed with distilled water for several times until the pH value turned to 7. At last, the products were annealed in air for 2 h. [69–71].

Solvothermal

The solvothermal method is almost identical to the hydrothermal method except that the solvent used here is nonaqueous. However, the temperature can be elevated much higher than that in hydrothermal method, since a variety of organic solvents with high boiling points can be chosen. The solvothermal method normally has better control than hydrothermal methods of the size and shape distributions and the crystallinity of the TiO₂ nanoparticles. The solvothermal method has been found to be a versatile method for the synthesis of a variety of nanoparticles with narrow size

distribution and dispersity. The solvothermal method has been employed to synthesize TiO₂ nanoparticles [72,73].

Impregnation

Impregnation is the simplest method to preparing supported catalysts. Impregnation is related to ion-exchange/adsorption processes and the interaction with the support is dominant. (Water) solution containing the metal precursors is contacted with a porous support. Dry impregnation (pore volume impregnation) the exact amount of liquid to fill the pore volume of the support is used and wet impregnation the amount of liquid is only “controlled” by the solubility of the metal precursor. The impregnation method has been used by many researchers as a convenient means of loading photocatalytic TiO₂ onto various supports [44,45,74,75].

Precipitation

Precipitation is in principle a crystallization process and can occur in the bulk of the liquid or on a relatively inert surface. The support particles act as crystallization nuclei for the active site precursor, when the hydrothermal solution was changed from an ammonium solution to water, the particles were smaller and more uniform as the nucleation and growth rates were slower in water. Prepare dilute solution of titanium tetrachloride. First add 10 mL hydrochloric acid in the beaker with 40 mL de-ionized water and put the beaker in the ice-water bath. Then placed it on the magnetic stirrer, add 6 mL pure solution of titanium tetrachloride drop by drop while stirring and prepare the expected solution. Keep the temperature of the solution of titanium tetrachloride under 10 °C, add excessive H₂O₂ into it, in the process the solution will turn dark red first, then it will get darker and finally it turn to black liquid. Under the effect of magnetic stirring, add ammonia gradually in the above-mentioned solution and adjust the pH to 10. When adding ammonia, a white sediment is obtained, but it dissolved with the stirring. A dense yellow particulate materials at pH is 8 is formed. With the increase of ammonia, the materials dissolve when pH is close to 10, the solution become bright milky yellow semi solid. Heat it to 50 °C and keep the temperature for 0.5 h and left for 18 h. Wash the sediment properly. After the seasoning, several layers are formed in the solution. The lower layer is light yellow cottonshaped sediment. Inhale the clear solution from the upper part of the beaker by the straw. Pour

the rest of the solution into the microburette to centrifugate it for 5 min. Pour out the solution from the microburette, add de-ionized water and use ultrasonic dispersion, centrifugate it again, repeat the action for three times. Put the sediment into the 60 °C drying box for 0.5 h and the white powder is formed. Heat it in the 500 °C muffle for 2 h and white anatase titanium dioxide will be produced [76–78].

Hydrolysis

Prepare the dilute solution of titanium tetrachloride. The method is most similar to the above-mentioned experiment, we can produce liquid A. Dissolve ammonium sulphate in the de-ionized water and add hydrochloric acid into it, which produce liquid B. Pour B into A (keep the temperature under 15 °C), B appears to be oily and gradually dissolves in A. The solution becomes clear and is heated to be 95 °C. In the process when the temperature is about 60 °C, the color gradually gets darken, it turns turbid at 95 °C. Add ammonia until pH is 6, the solution turns milky white and become pure white sediment after seasoning it for 12 h. After pouring out the clear solution in the upper part, add a certain amount of de-ionized water into it. Then pour it into a microburette to centrifugate for 5 min. Then pour out the water in the microburette, add de-ionized water again. Put it in ultrasonic washer, centrifugate it after mixing thoroughly, repeat the action for three times. Put the white sediment which has been washed in the 80 °C drying box, dry it for 24 h and the sample becomes a dark solid mass. Place the sample in the 550 °C muffle to bake for 2 h to get nano powder of titanium dioxide [53,79].

Sol-gel

The sol–gel process is a method for producing solid materials from small molecules. The method is used for the fabrication of metal oxides, especially the oxides of silicon and titanium. The process involves conversion of monomers into a colloidal solution (sol) that acts as the precursor for an integrated network (or gel) of either discrete particles or network polymers. Typical precursors are metal alkoxides. The sol-gel method is one of the most widely applied methods for loading TiO₂ onto a support. The main objective during the sol-gel loading procedure is to control the hydrolysis rate and slow it down as much as possible, to achieve a good dispersion of TiO₂ over the support. The nanocrystalline titanium dioxide sol–gel formulations were prepared by

hydrolysis and condensation reaction of 5% titanium tetra-isopropoxide in acidic aqueous containing 5% acetic acid and 1.4% hydrochloric acid. The solutions were heated at 60 °C under vigorous stirring for 2 h. Porphyrize the product and put it to bake for 2 h in the 550 °C muffle and obtain the sample after cooling it. [79–82].

2.8 Supporting materials

TiO₂ powders, which represents a high photoactivity and a significant quantum effect is commonly in nanometer size, and there are also problems of separation and recovery of photocatalyst from the reaction media, supported TiO₂ is one of the choice

for the field application of the photocatalyst. Therefore, much recent work has been devoted to immobilize TiO₂ photocatalyst on porous supporting matrices, such as silica, alumina, zeolites, activated carbon (AC) and activated carbon fiber (ACF). It has been reported that some natural biological materials, such as cellulose fiber felts, naturally grown wood (such as rattan and pine), and corrugated cardboard structures and different ash-forming biological materials, such as gills of mushrooms, cotton wool, spider silk, dog's hair, and human hair [23,65,83] were also used in recent years as biological templates to prepare various materials with different structures. Natural biological templates have received so much attention due to their advantages such as that they are cheap, abundant, pollution-free, and renewable.

2.8.1 Cellulose fibers support

Cellulose is the most abundant and widespread biopolymer on the Earth. Owing to its abundance, biodegradability and some physical properties (high moisture adsorption, softness, high strength, etc.), cellulose is a very important renewable resource for the development of environment friendly, biocompatible and functional materials, quite apart from its traditional and massive use in papermaking and cotton textiles. Cellulose fibers present a polar surface associated with the hydroxylated nature of the constituting anhydroglucose units. Such a feature is responsible for the high hydrophilicity of cellulose, enabling the establishment of strong hydrogen bonding between fibers and the formation of three-dimensional fiber-based structures. On the other hand, the presence of these hydrophilic groups can promote the nucleation and growth of inorganic phases, such as TiO₂ and ZnO, at the cellulose fiber surfaces, thus

allowing the production of nanocomposites with antimicrobial, UV blocking and novel infrared radiation properties [15,23,82,84–86]. Several studies have reported that TiO₂ coating of cotton textiles could be performed using different pretreatments and techniques such as RF-plasma, MW-plasma, UV-irradiation, dip-pad–dry-cure and dip-coating [87,88].

2.8.2 Pineapple leaf fibers

Thailand is one of the major countries in the world for pineapple production. Tons of pineapple leaf have become agricultural wastes after harvesting which have been interested for value adding. Pineapple leaf fiber (PALF) consists of cellulose about 70-80 %wt giving its high specific modulus and strength. It can be an efficient reinforcement for different polymers after its surface improvement with coupling agent. Compatibility of the components within the composites especially at the interfacial region, where stress transfer occurred, plays an important role for mechanical properties of the composite materials [24,86,89,90].

Alkaline treatment is widely used chemical process to remove hemicellulose and lignin components from natural fiber resulting in better-purified cellulose [91,92]. In this studies have reported that TiO₂ coating on Pineapple leaf fibers.

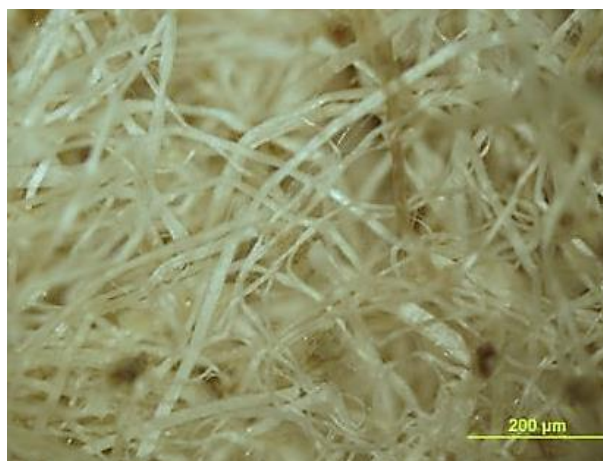


Figure 5 Pineapple leaf fibers after alkali treatment.

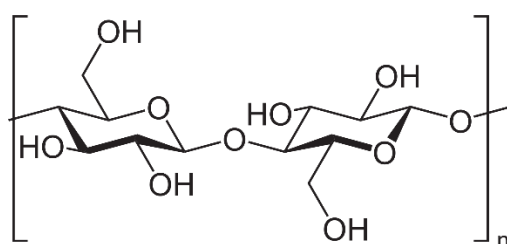


Figure 6 Chemical structure of cellulose.

2.9 Effect of cross-link to graft nano TiO₂ on fibers

One way to graft nano TiO₂ on cotton fabrics is achieved using cross-link method. This spacer needs to have at least two free carboxylic groups to be able to bind both the cotton and the TiO₂. The spacer should also have an acceptable chemical and thermal stability. Cotton-cellulose is a polysaccharide with many free hydroxyl groups on the surface. The spacer will be introduced by formation of a covalent ester-bond. This indicates esterification of a spacer carboxylic group through cellulose carboxylic group. This implies esterification of one carboxylic group of the spacer by a hydroxyl group of cellulose. The second spacer carboxylic group is meant to anchor TiO₂ by electrostatic interaction. Previous work shows that TiO₂ presents a strong electrostatic interaction with carboxylic groups (Figure 7) [23,85,87]. In this study, succinic acid was used as a cross-link agent to attach TiO₂ to the cotton. The amount of loaded titania particles to cotton fabrics and the thermal behavior of cured samples.

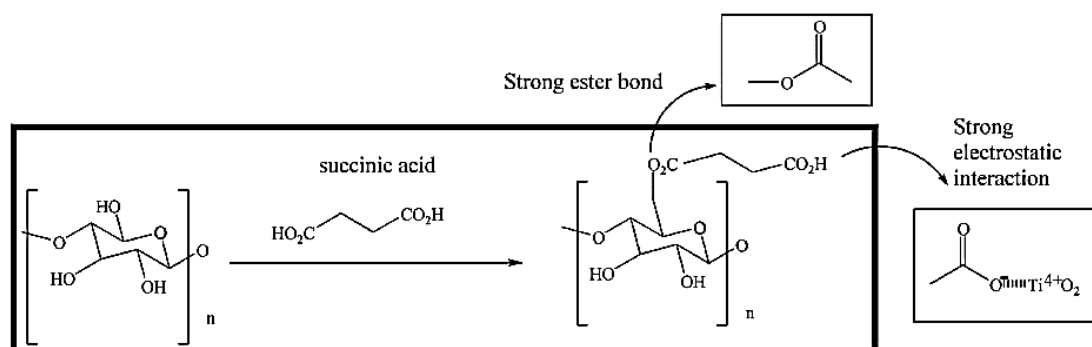


Figure 7 Connection of succinic acid to cotton and TiO₂ through using the cross-link method [93].

2.9.1 Applications

In recent years, the use of nano titanium dioxide photo-catalyst to cover textile and improve their surface has expanded which is because of their ability to absorb ultra-violet irradiation. In addition, the coat of nano TiO_2 particles on fabrics will not affect their breathability or hand feel. Several methods could be used to apply finishing materials onto fabrics, including spraying, transfer printing, foaming, and padding among which padding is the most commonly used method. At the same time, various poly carboxylic acids were investigated as cross-linkers for durable press finishing of cotton. Formaldehyde free formation of ester linkages, improved tensile and abrasion strength are among the advantages of these compounds. Poly carboxylic acids as citric acid (CA) and 1,2,3,4-butane tetra carboxylic acid (BTCA) are cotton cross-linking agents that are environment-friendly and can be suitable substitutes for methylols which contain cross-linkers. Cross-linking of BTCA and CA with cotton fabrics has been proposed to be catalyzed by sodium hypophosphite in acidic conditions. The mechanism of cross-linking is suggested to include cyclic anhydrides as reactive intermediates which are trapped by hydroxyl groups of fabrics. CA with cotton fabrics has been proposed to be catalyzed by sodium hypophosphite in acidic conditions. The mechanism of cross-linking is suggested to include cyclic anhydrides as reactive intermediates which are trapped by hydroxyl groups of fabrics. The use of nano TiO_2 as photo-catalyst in the presence of maleic anhydride (MA) as cross-linker to improve the crease recovery properties of the silk fabrics has been reported. Chen and Wang have reported the application of four different carboxylic acids, named, BTCA, MA, CA and succinic acid (SUA) as cross-linking agents to treat cotton fabrics in the presence of nanometer titanium dioxide as catalyst under UV irradiation and electronic field. It has been suggested that the dry crease recovery angle (DCRA) and wet crease recovery angle (WCRA) values of treated fabrics were in the rank of $\text{BTCA} > \text{MA} > \text{CA} > \text{SUA}$ and the tensile strength retention values were as $\text{BTCA} < \text{MA} < \text{CA} < \text{SUA}$ [(94)].

In this study, succinic acid was used as a cross-link agent to attach TiO_2 to the cotton. The amount of loaded titania particles to cotton fabrics and the thermal behavior of cured samples.

2.9.2 Coating process

Two methods of using cross-link were used to coat cotton with titania. Cross-link method was performed in 7 stages as follows:

1. Cotton fabric was washed with distilled water at 80°C for an hour to remove wax and extra materials.
2. Samples of washed cotton were immersed in an aqueous solution with succinic acid as cross-link agent (6%, w/w) in the presence of sodium hypo-phosphate as catalyst (4%, w/w) for 1 h.
3. Cured cotton in stage 2 was dried in an oven at 85°C for 3 minutes and then curing process was applied for 2 minutes at 180°C.
4. A TiO₂ suspension was sonicated for 30 min.
5. The cotton with loaded compound succinic acid from stage 3 were immersed into this aqueous suspensions of TiO₂ and heated for 1 h at 75 °C.
6. Resultant fabric from stage 5 was put in an oven at 100°C until nano dioxide titanium particles got fixed over the cotton fabric.
7. Cured cotton was ultrasonically washed for 10 minutes in order to remove titania particles having no bonding reaction with cotton & investigation stability of the TiO₂ coatings.

Methods with and without cross-link are the same, the only difference is elimination of stages 2 and 3 in the latter. Different titania weight percents are chosen for these two methods. Distilled water was used as consumed water at all stages [93].

CHAPTER 3

RESEARCH METHODOLOGY

3.1 Chemicals and materials

3.1.1 Chemicals

The chemicals used in this research were listed in Table 3.

Table 3 The chemicals used in this research.

Chemicals	Grade	Brand
Titanium (IV) n butoxide (TBOT) 99%	AR	Acros Organics
Ethanol absolute	AR	Carlo Erba Reagent
Acetic acid (glacial)	AR	Acros Organics
Ammonia solution 25%	AR	Sigma Aldrich
Tetraethyl orthosilicate (TEOS) 98%	AR	Acros Organics
Hydrochloric acid (HCl) 37%	AR	Sigma Aldrich
Ammonium Acetate	AR	Sigma Aldrich
Titanium(IV) Isopropoxide (TTIP) 98%	AR	Acros Organics
Isopropanol	AR	Sigma Aldrich
Sodium hydroxide (NaOH)	AR	Ajax Finechem
Succinic acid	AR	Ajax Finechem
Sodium chloride (NaCl)	AR	Ajax Finechem
Potassium dihydrogen phosphate (KH ₂ PO ₄)	AR	Ajax Finechem
Sodium hypophosphite hydrate (NaH ₂ PO ₂)	AR	Ajax Finechem
Sodium dihydrogen phosphate (Na ₂ HPO ₄)	AR	Ajax Finechem
Potassium chloride (KCl)	AR	Ajax Finechem
Methylene Blue	AR	Sigma Aldrich
Methyl Orange	AR	Sigma Aldrich
Paraquat dichloride hydrate 99.99%	AR	Sigma Aldrich
Paraquat dichloride solution 24% GMZ	COM	Syngenta

3.1.2 Materials

The materials used in this research was pineapple leaf. The pineapple leaf was collected from Na Chueak Sub-district of Na Chueak District in Mahasarakham Province. The pineapple leaf fibers were extracted by alkaline hydrolysis.

3.2 Instrument

The main items of instruments used in this research were listed in Table 4.

Table 4 The detail of instruments used in this research.

Instruments	Model	Company
Spectrophotometer	Thermo Scientific 4001/4	Thermo Electron
Fourier transform infrared spectroscopy (FTIR)	SENSOR 27	Bruker
Scanning electron microscope (SEM)	OL JSM-6460 LV	JEOL
pH meter	CONSORT C-830	Metrohm Siam
Voltammeter	Heto SBD 50	Scientific Promotion
UV-Vis spectrophotometer	UV-3101PC	Shimadzu
X-Ray Diffractometer (XRD)	D8 Advance	Bruker
Surface Area and Pore Size Analyzer (BET and BJH)	Autosorb-1	Quanta chrome
Thermogravimetric analyzer (TGA)	SDT Q600	TA Instruments
Furnace	CWF 1200	Carbolite
Incubators	ED 23	Binder
Centifuge	X3	Thermo Scientific
Stirring Hotplate	Fisher Scientific hot	Fisher Scientific
Uv light Box	F20T-BLB	GE GE
Inductively Coupled Plasma-Optical Emission Spectrometer (ICP-OES)	Optima 7300DV	Perkin Elmer

3.3 Experimental

3.3.1 Preparation of TiO₂ powder

Preparation of TiO₂ nano-photocatalysts was carried out by different 4 methods. Then, the resulting catalysts were used as photocatalysts in paraquat degradation.

Method 1 In this method, 20 mL of tetrabutyl titanate and 4 mL of acetic acid were added into 26 mL of absolute ethanol under continuous stirring condition to obtain the solution, named solution A. 8 mL of deionized water, 12 mL of absolute ethanol and 12 mL of acetic acid were mixed together to obtain the another solution; named solution B. Then, solution B was added drop wise into solution A under stirring. The obtained solution was sealed and stirred continuously for another 30 min at room temperature. The resultant gel was aged at room temperature for 24 h and dried in an oven at 100 °C for 36 h. After grinding, the gel was heat-treated in a furnace at 300 °C for 3 h and white crystalline TiO₂ nanoparticles were obtained at the end of the process.

Method 2 In this method, 10 g of CaCO₃ templates was dispersed into a solution containing 300 mL of Ethanol, 36 mL of water, and 30 mL of 25.0 wt% ammonia solution. After 10 min ultrasonic treatment, the uniform CaCO₃ suspension was immediately transferred to a 25 °C thermostatic water bath. Thereafter, 8 mL of TEOS was dropped in under vigorous stirring. After 3 h, the reaction was terminated by the addition of excess amount of ethanol. Particles were filtrated and washed with ethanol for several times and then dried under vacuum at 100 °C for overnight. The well dried powder was re-dispersed into 3 M HCl and stirred for 2 h to remove CaCO₃ templates. Finally, the obtained TiO₂ particles were washed with distilled water for several times, and dried under vacuum at 100 °C for overnight.

Method 3 In this method, 1.5 mL TBOT and 1 g of ammonium acetate were dissolved in 20 mL and 15 mL absolute ethanol, respectively. After vigorously stirred for 10 min, the transparent mixed solution was diluted with 30 mL of absolute ethanol, transferred into an autoclave and remained at 200 °C for 2 h.. After the cooled to ambient temperature, the precipitate was followed by washing with absolute ethanol and dried under vacuum at 60 °C for 8 h.

Method 4 In this method, 10 ml of TTIP was dissolved in 100 ml of isopropanol and then 0.15 ml of water and a few drops of about 1.0 ml of 1 M HCl were added. In fact, in order to synthesize the TiO₂ as a powder form, the stoichiometric amount of water needed is 2.5 ml for 10 ml of TTIP. The mixture was heated up in an autoclave to 200 °C at a rate of 5 °C/min, and then the temperature was kept constant for 1 h.

3.3.2 Preparation of pineapple leaf fibers (PF)

Raw pineapple leaf fibers were prepared by alkaline treatment. The pineapple leaf were immersed and stirred continuously in 20 %wt NaOH solution. The mixture was then boiled for 2 h at 90 °C. Next, the mixture was neutralized by slow adding of 5 %wt acetic acid solution, and it was washed by tap water for several times until no alkalinity detected in washed water. Finally, it was washed by distilled water. The fibers were filtered and then dried in an oven at 70 °C for 24 h. The fibers were then obtained.

3.3.3 Preparation of TiO₂ deposited on pineapple fibers

The TiO₂ loading to pineapple fibers were prepared by mix pineapple leaf fibers (PF) and TTIP in optimum method which previously study. The preparation detail was immersed and stirred continuously in the mixed solution of TTIP in different ratio 1:5, 1:1, 1:2 and 2:1 of TiO₂:PF in isopropanol solution and then 0.15 ml water and a few drops of about 1.0 ml of 1 M HCl were added to allow the TiO₂ formation occur. The mixture was heated up in an autoclave to 200 °C at a rate of 5 °C/min, and then the temperature was kept constant for 1 h. to remove the excess of solvent and complete the TiO₂ formation.

3.3.4 Preparation of crosslink on pineapple fibers

Samples of washed PF were immersed in an aqueous solution of the succinic acid (SA) as cross-link agent (6% w/w) in the presence of NaH₂PO₂ as inducer

(4%, w/w) for 1 h. Cured PF was dried in an oven at 85 °C for 3 min and then the process was applied for 2 min at 180 °C. A TiO₂ suspension was sonicated for 30 min.

3.3.5 Calibration curve

MB was dissolved in distilled water at different concentration. The MB solution was adjusted as 0, 1, 3, 5, 7, 10, 13 and 15 mg/L. The standard MB concentrations were measured using spectrophotometer at λ_{\max} 664 nm. The calibration curve were done by plotting of MB concentration (mg/L) versus absorbance.

3.4 Activity test

3.4.1 Paraquat degradation activity

The photodegradation of paraquat was tested in the homemade batch reactor at room temperature under uv lamp. The standard paraquat solution was purchased and was diluted to 1000 ppm. It was then diluted to 400 ppm and the amount of 10 ml was loaded to the reactor. The starting pH of paraquat solution was maintained at 7.0 by added either HCl or NaOH. The reaction was started after the catalyst was loaded to the paraquat solution. The mixture was stirred for 2 hour and then about 10 ml of mixture was sampling. The reaction was stopped by the separation of the solid catalyst from the solution by centrifuged at 3500 rpm for 30 min and then the transparent was obtained. The transparent was then analysed the paraquat concentration by voltammetry technique with using glassy-carbon working electrode (autolab PGSTAT204; metrohm).

3.4.2 Methylene blue degradation activity

The photodegradation of MB was tested in the homemade batch reactor at room temperature under uv lamp. The standard MB solution was diluted to 10 ppm and the amount of 10 ml was loaded to the reactor. The reaction was started after the catalyst was loaded to the MB solution. The mixture was stirred for 2 hour and then about 10 ml of mixture was sampling. The reaction was stopped by the separation of the solid catalyst from the solution by filtered solid and then the transparent was obtained. The

transparent was then analysed the MB concentration by uv-vis spectrometer by the absorbance peak at 664 nm.

3.5 Analytical methods

After uv radiation, the PQ and MB concentrations was calculated from the calibration curve. The photodegradation efficiency of PQ and MB was calculated by

$$\text{follows \%MBremoval} = \left(\frac{C_{\text{initial}} - C_{\text{residual}}}{C_{\text{initial}}} \right) \times 100$$

3.6 Characterization of catalyst

3.6.1 Fourier transform infrared spectroscopy (FTIR)

To study the surface properties of all catalyst prepared under various conditions, the functional groups of the catalysts were characterized by Attenuated Total Reflection-Fourier Transform Infrared (ATR-FTIR) spectroscopy (Spectrum GX-1, Perkin Elmer). The scan was conducted in the range of 4000-650 cm^{-1} at resolution of 4 cm^{-1} . The number of scans was set to 32.

3.6.2 Scanning electron microscopy (SEM)

The surface morphological characterization of all catalyst were performed by scanning electron microscope (SEM) (JEOL; JSM- 6460LV, Tokyo, Japan) operated with an accelerating voltage of 15 kV. The BFs were sputter-coated with gold for enhanced surface conductivity.

3.6.3 BET Surface area analysis (BET)

The BET surface area and porous structure were calculated using an Autosorb-1 Gas Sorption system (Quantachrome Corporation) with BET and BJH equation. All the samples were heated at 150 $^{\circ}\text{C}$ for 2 h before the surface analysis. The adsorption/desorption isotherms were also obtained to estimate the type and volume of porous in the catalyst (microporous, mesoporous and macroporous).

3.6.4 X-ray diffraction spectroscopy (XRD)

The X-ray diffraction profile (XRD) was also studied to obtain the crystallinity of the catalysts by using a D8 Advance: Bruker BioSpin AG with 2θ between 20-80°.

3.6.5 Diffuse reflectance UV-vis spectroscopy

Diffuse reflectance UV-vis spectra of the catalysts were recorded in air at 200-800 nm using UV-vis-NIR scanning spectrophotometer (Shimadzu/UV-3101PC model) to evaluate the band gap energy of the catalysts.

3.6.6 Thermogravimetric analysis (TGA)

Thermal decomposition behaviors of catalysts were determined by thermogravimetric analyzer (TGA) module was a TA Instruments/SDT Q600. The 2 - 5 mg of sample was heated at the heating rate of 20 °C/min under nitrogen flow.

3.6.7 Inductively Coupled Plasma-Optical Emission Spectrometer (ICP-OES)

The amount of TiO₂ coated on PF detected by Inductively Coupled Plasma-Optical Emission Spectrometer (ICP-OES) module was a Perkin Elmer/Optima 7300DV.

3.7 Data analysis

- The Photocatalytic activity results in MB removal were carried out at least triplicate (n = 3).
- The data was expressed contained means and standard deviation (S.D.).
- Equation were used to calculate the amount of MB concentration as follows $y = 0.1757x + 0.0239$ (calibration curve) respectively.

CHAPTER 4

RESULTS AND DISCUSSION

4.1 TiO₂ catalyst preparation

Preparation of TiO₂ nano-photocatalysts was carried out by 4 methods, sol-gel (method 1), precipitation over CaCO₃ (method 2), hydrothermal (method 3) and hydrolysis with autoclave annealing (method 4). After obtain the catalyst, all the catalyst was studied the photocatalytic activity and catalyst properties. The information was explained as following part.

4.1.1 Characterizations

4.1.1.1 X-Ray diffraction analysis

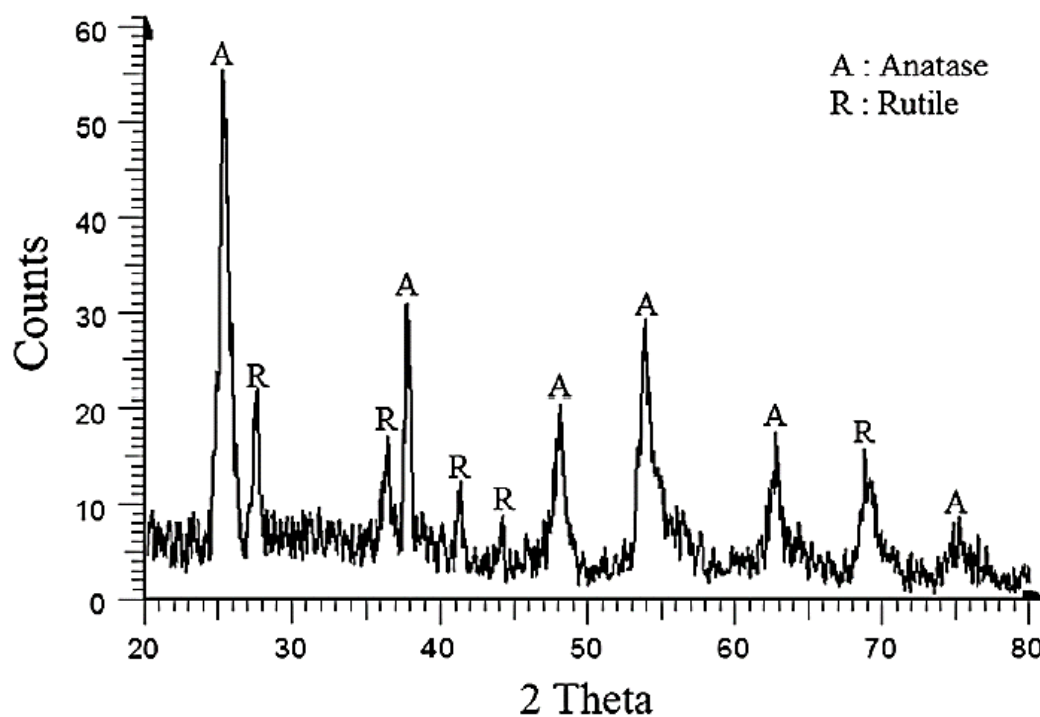


Figure 8 XRD pattern of TiO₂ powder used in geometries calcined at 450°C for 2 h. which contains both anatase and rutile phase.

XRD pattern of TiO₂ which expresses both anatase and rutile phase is shown in Fig. 8. This spectrum belongs to TiO₂ particles calcined at 450°C. The XRD pattern shows a crystalline structure of the anatase phase due to the existence of the distinguished peaks at 2θ of about 25.4°, 37.8°, 48.0°, and 53.7°, which correspond to the indices of (101), (103), (200), and (105) diffraction planes of the anatase TiO₂, respectively. Also, the existence of the distinguished peaks at 2θ of about 27.5°, 36.1°, 49.2°, and 44.0°, which correspond to the indices of (110), (101), (111), and (210) diffraction planes respectively, indicates the formation of the rutile TiO₂ [95].

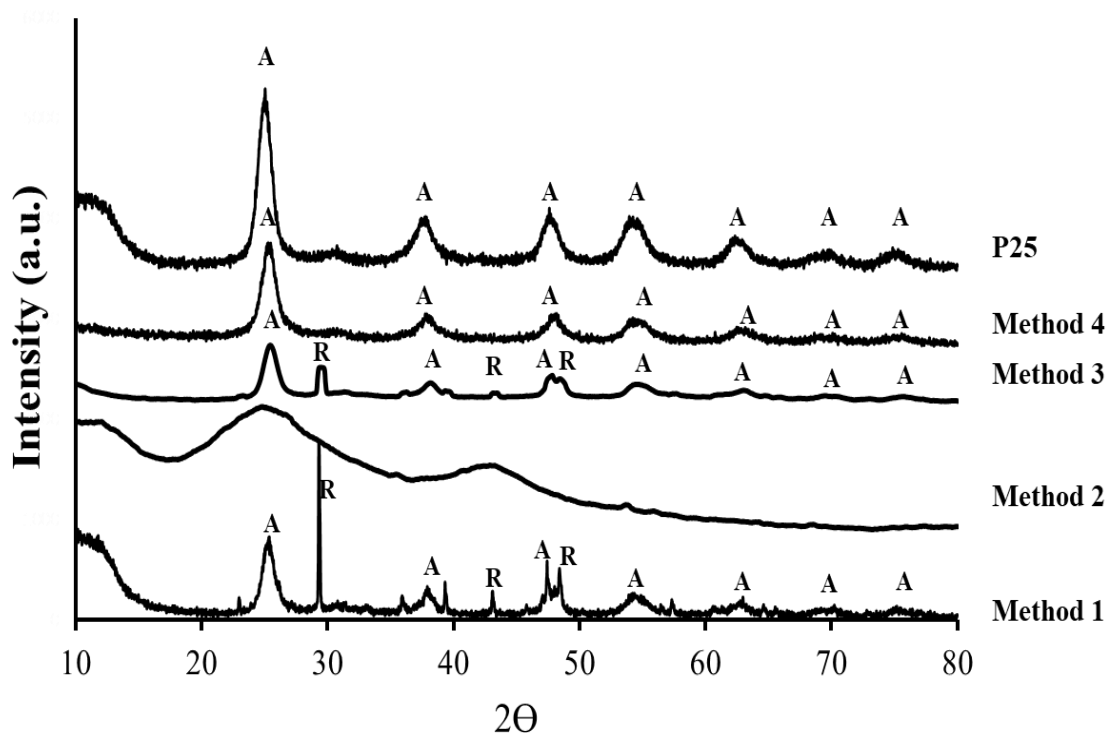


Figure 9 The XRD pattern of P25 and TiO₂ with different 4 methods.

The X-ray diffraction technique was used to study the phase composition and grain size of the samples. Figure 9 shows the X-ray diffraction pattern of the prepared powder synthesized by different 4 methods and compare with commercial TiO₂ (P25). The XRD pattern reveals that the P25 and TiO₂ synthesized by method 4 clearly exhibit anatase phase. The characteristic diffraction peaks exhibited the major anatase phase. The characteristic diffraction peaks of anatase are 25.4°, 38.0°, 48.0°, 54.7°, 63.1. The peak intensities and positions agree well with the expected literature values [31,63,96]. The TiO₂ synthesized by method NO. 1 and 3 shows a crystalline structure of the rutile

phase at 27.5° , 44.0° , 49.2° and also the peak of anatase at 200°C . Therefore, the sample synthesized by methods 1 and 3 consists of both anatase and rutile phases.

Interestingly, the broad peaks of the sample synthesized by methods 2 was found that powder sample existed in an amorphous state. It has to be further identifying that it contains only TiO_2 or TiO_2 based compound.

4.1.1.2 Surface morphological analysis

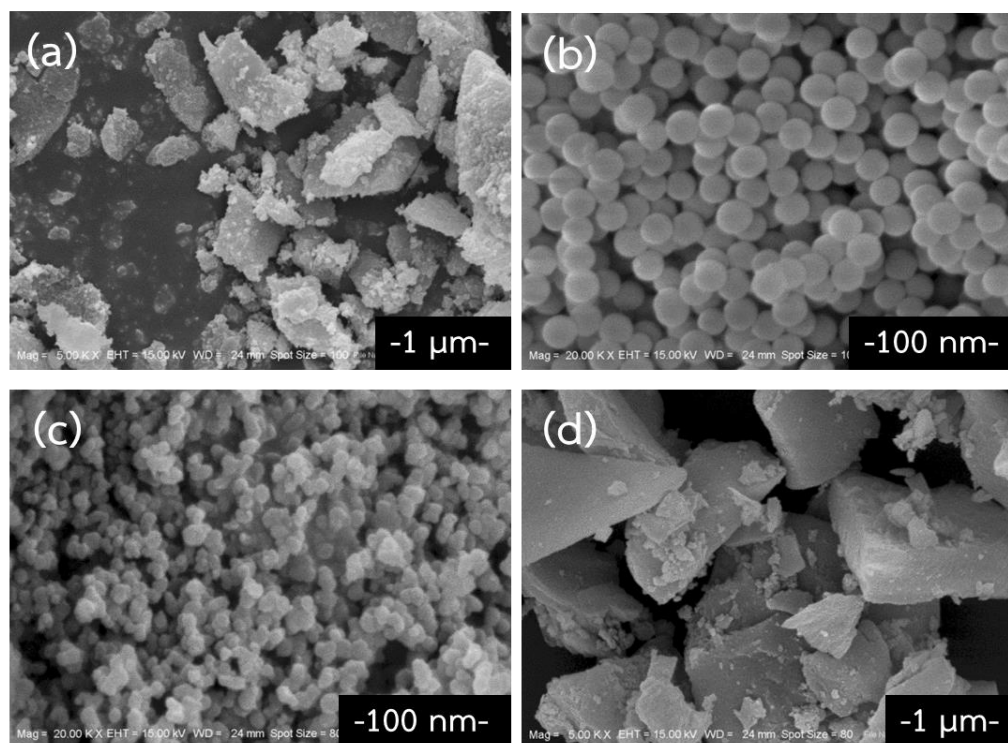


Figure 10 The surface morphological of various TiO_2 powder prepare from 4 different methods, (a) method 1, (b) method 2, (c) method 3 and (d) method 4.

Inspection of the morphology of TiO_2 powder synthesized by different 4 methods was carried out using SEM. The shape of TiO_2 powder synthesized by method 2 (Fig.10 (b)) was good spherical in shape, which is quite abnormal for TiO_2 compound. However, the investigation of the composition will be studied by XPS in the next part. The morphology of TiO_2 prepared by method 3 (Fig.4.3 (c)) consists of aggregated spherical particles originating clusters of TiO_2 particles as found in work of Totka

Bakalova and co-worker, 2016 [132-134]. Catalysts sample prepared by methods 1 and 4 shows in Figure 4.3 (a) and 4.3 (d) had irregular morphology of block or flake with smooth surface, which possess block or flake of TiO₂ particles as found in work of Ritu Vershney and co-worker, 2018 [42,66,67].

4.1.1.3 Surface area analysis

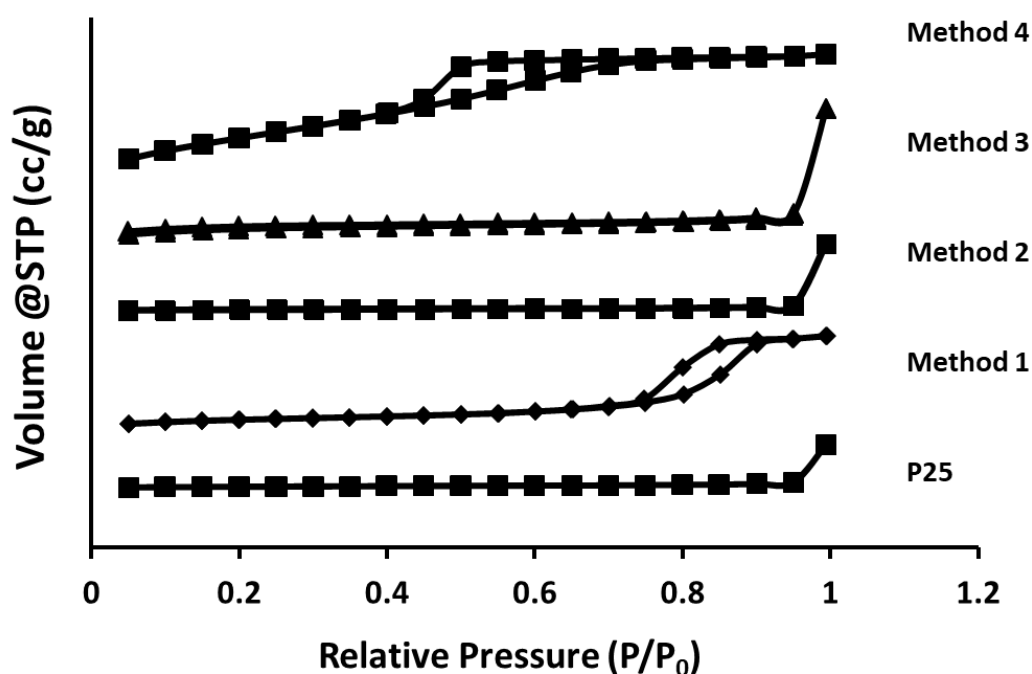


Figure 11 Nitrogen adsorption-desorption isotherm of P25 and TiO₂ with 4 different methods.

The nitrogen adsorption-desorption isotherms of pure TiO₂ (P25) and TiO₂ powder catalysts synthesized with 4 different methods were compared in Figure 11. The hysteresis loops were obtained which indicated the microporous materials. The BET surface area of the commercial TiO₂ (P25) and TiO₂ powder synthesized with different 4 methods was clearly shows the TiO₂ powder synthesized by 4 methods exhibited the specific surface area higher than P25 (3.5 m²/g). It is interesting that the specific surface of the TiO₂ powder synthesized by method 4 increased up to 338.8 m²/g, showed very high surface area when compared with others methods (exhibited specific surface 100.8, 6.1 and 16.9 m²/g, respectively, for method 1, 2 and 3).

4.1.1.4 Functional group analysis

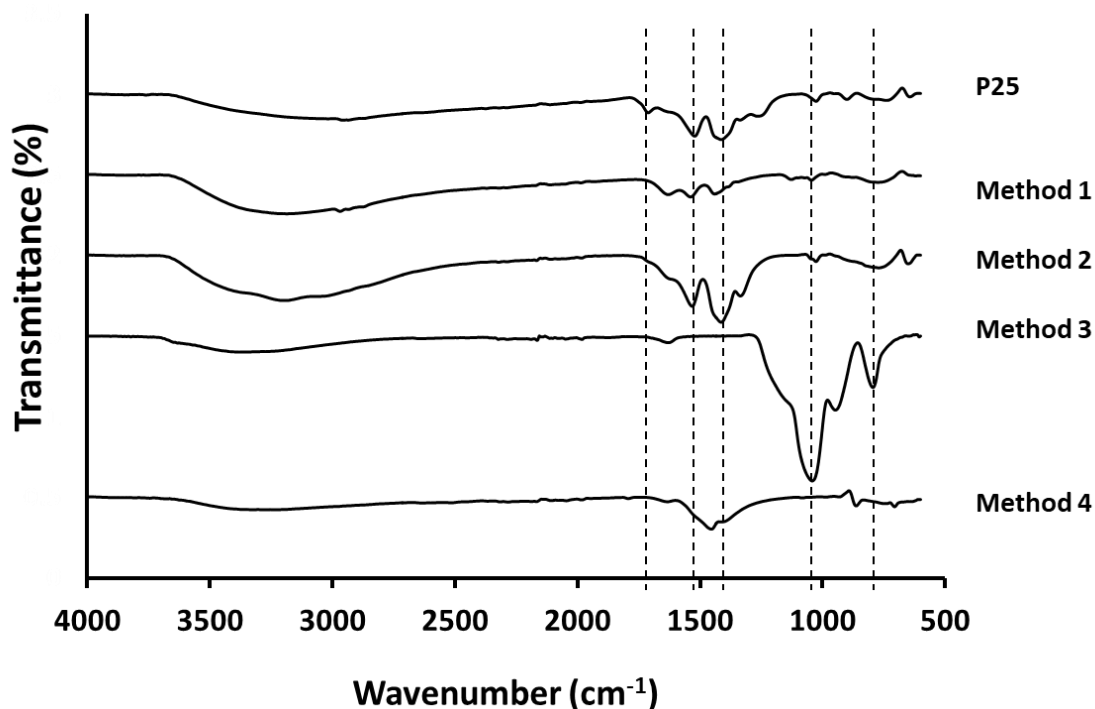


Figure 12 The FTIR spectra of P25 and TiO₂ over prepared from different methods.

The FTIR spectra were recorded to identify the functional groups of the prepared catalysts. Figure 12 shows the ATR-FTIR spectra of P25 and TiO₂ powder prepared with 4 different methods. The characteristic absorption bands of the TiO₂ spectra of all sample correspond to the vibration of C-OH groups situated around 3,000–3,500 cm⁻¹, O-H bond of hydroxyl group at 1,500-1,600, C-OH stretching at around 1,300-1,370 cm⁻¹ and stretching vibration of C-O groups at 1050 cm⁻¹ but not found in sample from method 4. The C=O carbonyl groups at 1720 cm⁻¹ was found in P25 sample only [10,65,96,97]. The ATR spectra of bare TiO₂ show a common characteristic band, typical peak of the TiO₂ material corresponding to Ti-O-Ti bonds at 800-950 cm⁻¹ [65]. It is interesting to note that the intensity of the peak in the sample from method 3 which associated to stretching vibration of C-O groups significant higher than other samples.

4.1.1.5 Band gap energy analysis

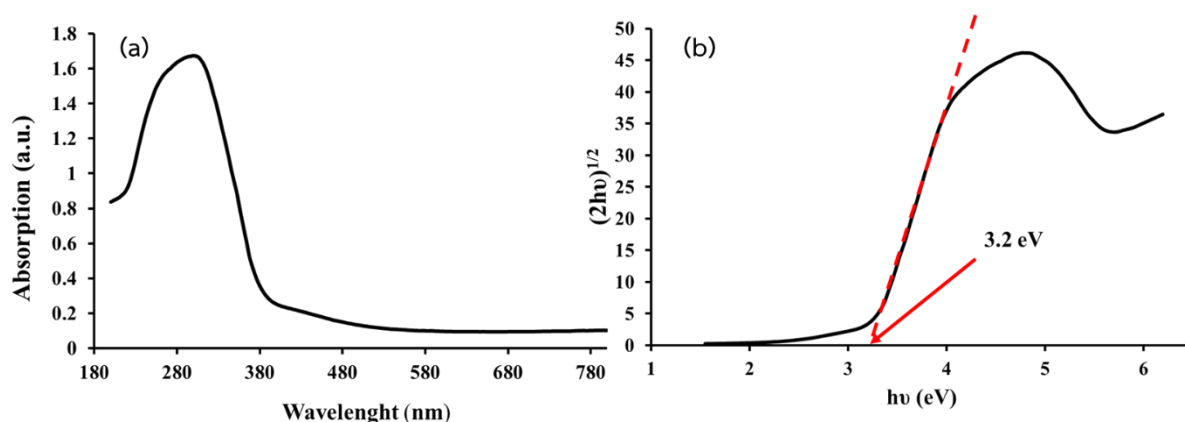


Figure 13 a) UV-vis diffuse reflectance spectrum b) spectrum curves of Kubelka-Munk function as the vertical axis and plotted against the photo energy of TiO_2 synthesized from method 4.

Figure 13 a) showed UV-vis diffuse reflectance spectrum, the absorption spectrum clearly indicates that the optical absorbance of TiO_2 synthesized from method 4 is in the ultraviolet region. Figure (b) shown spectrum curves of Kubelka-Munk function as the vertical axis and plotted against the photo energy of TiO_2 powder in method 4. The calculated band gap energy of pure TiO_2 is 3.2 eV, it is close with TiO_2 commercial (P25) had estimated band gaps of 3.25 eV [135, 136]. It can be seen that TiO_2 synthesized from method 4 was strong absorptions in the ultraviolet region. Which is normal property of pore TiO_2 [67,68].

4.1.1.6 XPS analysis

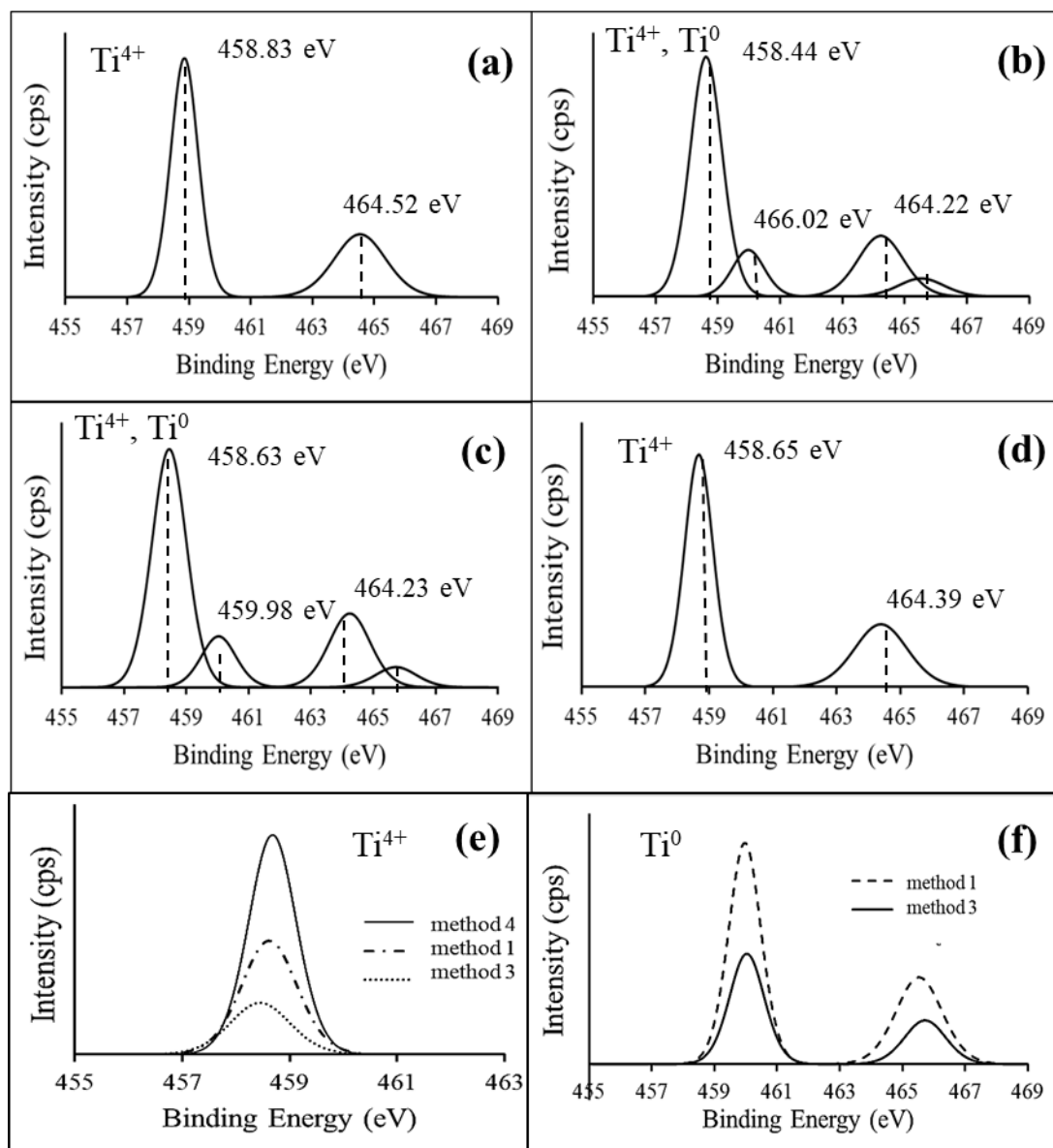


Figure 14 XPS spectra of Ti element on various TiO_2 powder prepared from different methods, (a) P25, (b) method 1, (c) method 3, (d) method 4 and (e) and (f) intensity of Ti^{4+} and Ti^0 in various materials, respectively.

The surface element of powder sample prepared from different method 1, 3 and 4 were identified by XPS spectra. The analysis of metal Ti oxidation state in the various catalysts was shown in Figure 14 (a) - (d). The XPS results exhibited clearly that Ti elements appear in the TiO_2 synthesized from method 1, 3 and 4 but not found in

method 2. The Ti 2p spectrum shows at region about 457-467 eV. Figure 14 (a) - (d) shows the XPS core level of Ti 2p composed of Ti 2p_{3/2} centered appeared at about 458 eV and Ti 2p_{1/2} appeared at about 464 eV in P25, method 1, 3 and 4, respectively [69]. These peaks attribute to the Ti⁴⁺ presence. Figure 14 (b) and (c) show XPS peak of TiO₂ catalyst from method 1 and 3, respectively. The amount of Ti⁴⁺ regarded to the peak area and the comparison of Ti⁴⁺ amount in each sample was exhibited in Figure 14 (e). Comparing the peak area of Ti⁴⁺ between TiO₂ from method 1, 3 and 4 as shows in figure 14 (e). The peak area of method 4 higher than method 1 and 3, respectively, which means that the Ti⁴⁺ level present in method 4 sample higher than method 1 and 3 sample. These peak appeared at about 460 eV with assigned to the present of Ti⁰. For the comparing the peak area of Ti⁰ between TiO₂ from method 1 and 3 as shows in figure 14 (f). It showed that sample from method 1 exhibited more Ti⁰ amount than sample from method 3.

However, the surface element of powder prepared from methods 2 exhibited the absent of Ti elements. In contrast, the XPS signal shows the spectrum at region 102.80 eV which related to Si 2p of SiO₂ this could be come from then the Tetraethyl orthosilicate (TEOS) which used as the reactant in method 2. It is corresponding with the good spherical in shape of SiO₂ from SEM result in figure 10 (b) in the previous part. It could be concluded that the TiO₂ could not be formed by method 2 whereas SiO₂ was form instead. Therefore, in the part of photo activity this powder was excluded.

4.1.2 Catalytic activity

4.1.2.1 Paraquat degradation

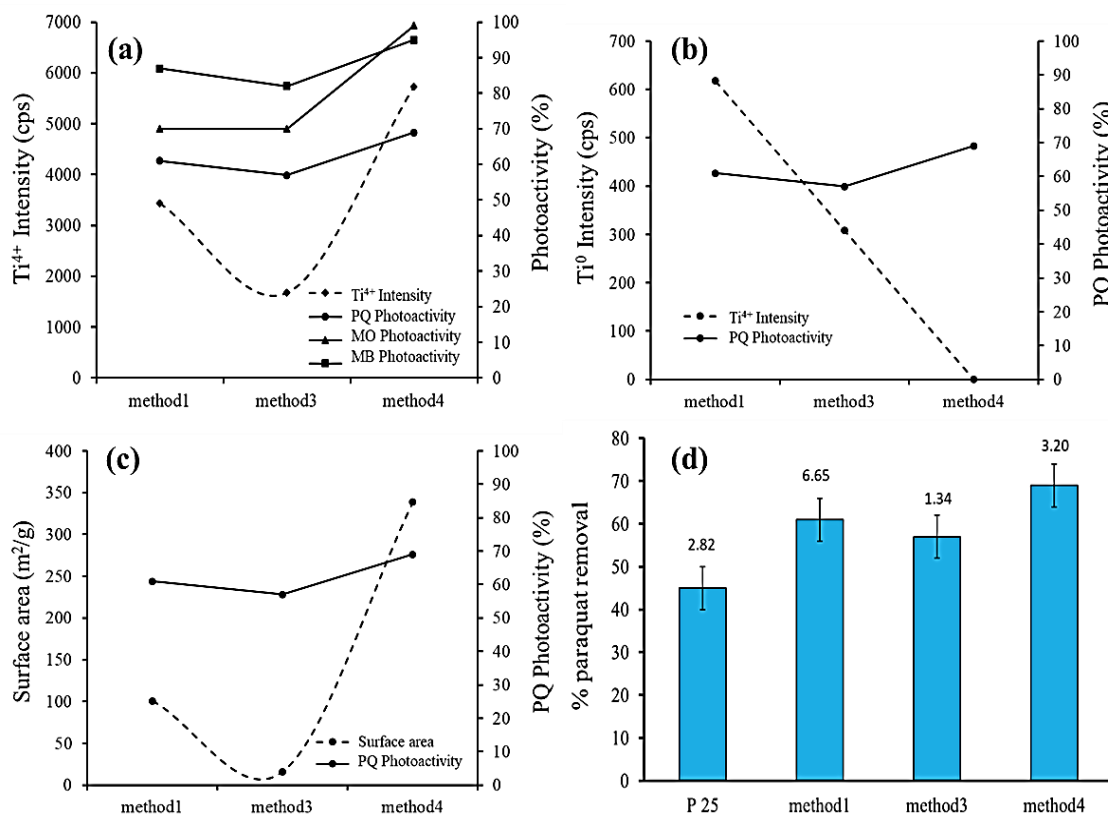


Figure 15 (a) Effect of maximum intensity of Ti^{4+} on PQ photoactivity, (b) Effect of maximum intensity of Ti^0 on PQ photoactivity, (c) Effect of surface area on PQ photoactivity and (d) The photo PQ degradation under UV irradiation using various TiO_2 powder prepared from different 4 methods.

Figure 15 (a), (b) and (c) shows the trend of the photoactivity, amount of Ti^{4+} , Ti^0 and surface area found in each sample, respectively. From the results shows that the % PQ removal increased when the maximum intensity of Ti^{4+} and surface area of samples increased. It should be mentioned that the trend of Ti^0 and the PQ activity was not correlated as shown in figure 4.8 (b). It is clearly that Ti^0 is not the factor to express the activity like the amount of Ti^{4+} . From figure 4.8 it can be concluded that the amount of Ti^{4+} and surface area was the key factor to own the photo-activity of catalysts. TiO_2 catalyst from method 4 shows both of the highest maximum intensity of Ti^{4+} , surface

area and %PQ removal. However, the sample from method 2 was not compared here because the sample is SiO_2 compound confirmed from XRD and SEM result.

All the prepared catalysts were then used as the catalyst in the degradation of paraquat and the residual of paraquat was monitored using voltammetry technique. Figure 15 (c) shows the % removal of paraquat over various TiO_2 compound compared with commercial TiO_2 P25 (using catalyst content at 2 g/l and the reaction time was 2 hours to ensure the maximum catalyst performance was achieved). The result showed clearly that the TiO_2 synthesized from method 4 exhibited the highest photoactivity in paraquat degradation. The order of photoactivity related to the order of surface area and the Ti^{4+} content. To investigate that which parameter between surface area and Ti^{4+} content played more effect to the expressed activity, the figure 15 (a) and (b) was plotted.

4.1.2.3 Methylene blue degradation

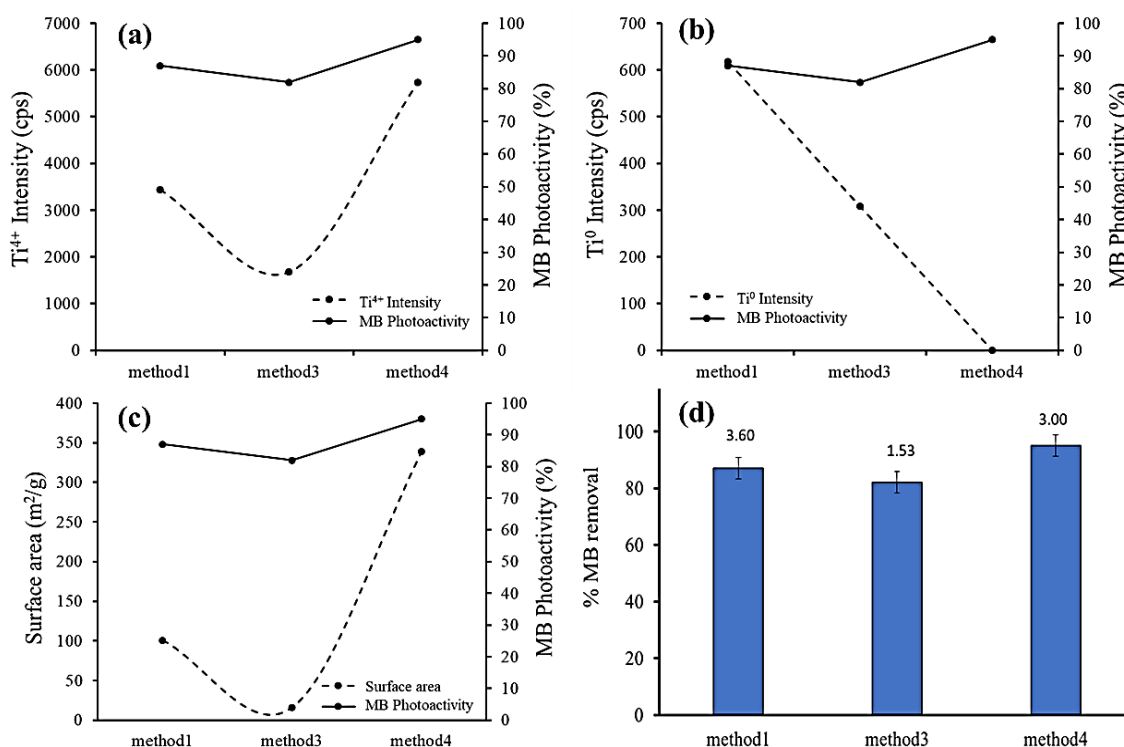


Figure 16 (a) Effect of maximum intensity of Ti⁴⁺ on MB photoactivity, (a) Effect of maximum intensity of Ti⁰ on MB photoactivity, (c) Effect of surface area on MB photoactivity and (d) The photo MB degradation under UV irradiation using various TiO₂ powder prepare from different 4 methods.

Figure 16 (a), (b) and (c) shows the trend of the photoactivity, amount of Ti⁴⁺, Ti⁰ and surface area found in each sample, respectively. From the results shows that the % MB removal increased when the maximum intensity of Ti⁴⁺ and surface area of samples increased, indicated that the trend of Ti⁰ and the MB activity was not correlated as show in figure 16 (b). It clearly that the Ti⁰ is not the factor to express the activity but Ti⁴⁺ and surface area was the key factor to own the photo-activity of catalysts. TiO₂ catalyst from mehod 4 shows both of the highest maximum intensity of Ti⁴⁺, surface area and %MB removal.

For the methylene blue (MB) degradation of TiO₂ powder preparation from difference 4 methods compared with commercial TiO₂ P25 showed in Figure 16. This process operated by using catalyst content at 2 g/l and the reaction time was 2 hours.

The residual of MB was monitored using UV-Vis spectrometer technique at 664 nm. The result showed clearly that the TiO₂ particle synthesized from method 4 exhibited highest photoactivity of MB degradation compared with other methods in the same as result of PQ degradation.

4.1.2.5 Methyl orange degradation

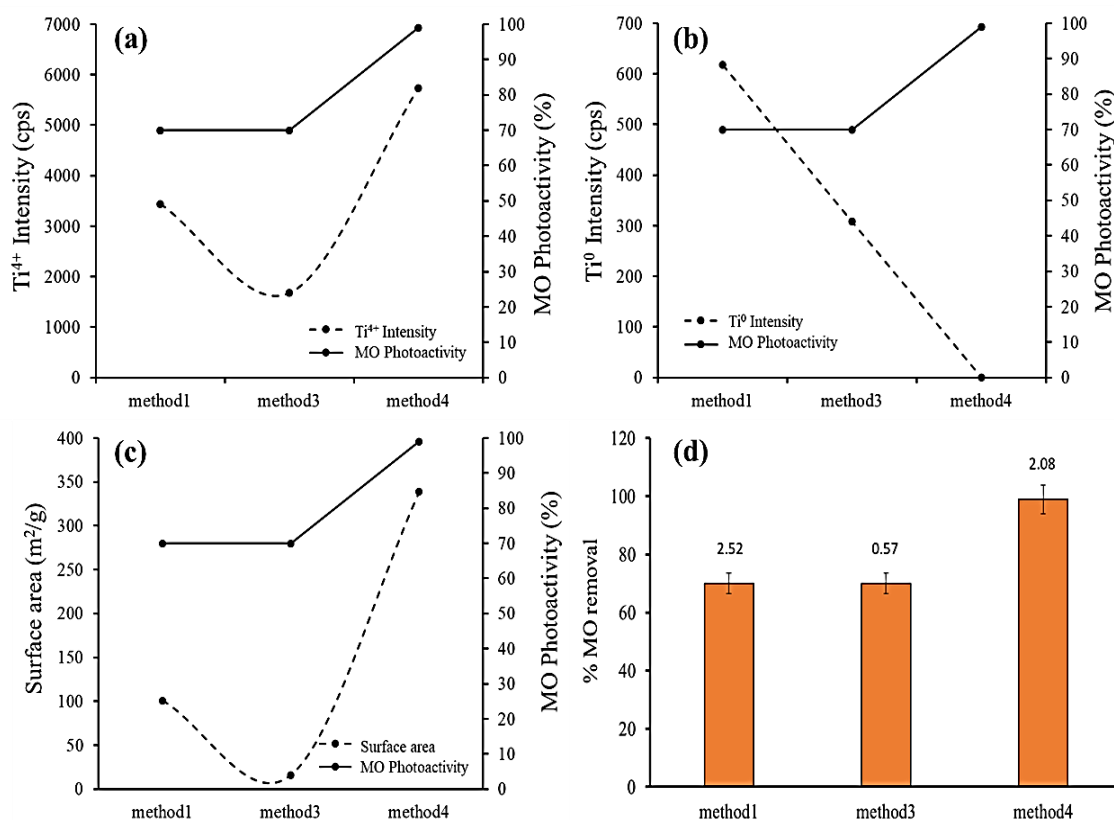


Figure 17 (a) Effect of maximum intensity of Ti⁴⁺ on MO photoactivity, (b) Effect of maximum intensity of Ti⁰ on MO photoactivity, (c) Effect of surface area on MB photoactivity and (d) The photo MO degradation under UV irradiation using various TiO₂ powder prepared from different 4 methods.

Figure 17 (a), (b) and (c) shows the trend of the photoactivity, amount of Ti⁴⁺, Ti⁰ and surface area found in each sample, respectively. From the results shows that the % MO removal increased when the maximum intensity of Ti⁴⁺ and surface area of samples increased. It should be mentioned that the trend of Ti⁰ and the MO activity was not correlated as shown in figure 17 (b). It is clearly that Ti⁰ is not the factor to express the activity like the amount of Ti⁴⁺. From figure 4.10 it can be concluded that the amount

of Ti^{4+} and surface area was the key factor to own the photo-activity of catalysts. TiO_2 catalyst from method 4 shows both of the highest maximum intensity of Ti^{4+} , surface area and %MO removal.

For the methyl orange (MO) degradation of TiO_2 powder preparation from different 4 methods compared with commercial TiO_2 P25 show in Figure 17. This process operated by using catalyst content at 2 g/l and the reaction time was 2 hours under UV irradiation to ensure the maximum catalyst performance was achieved. The residual of MO was monitored using UV-Vis spectrometer technique at 464 nm. The result shows clearly that the TiO_2 particles synthesized from method 4 exhibit the highest photo activity of MO degradation compared with other methods in the same as PQ and MB degradation.

4.1.2.7 Photo degradation

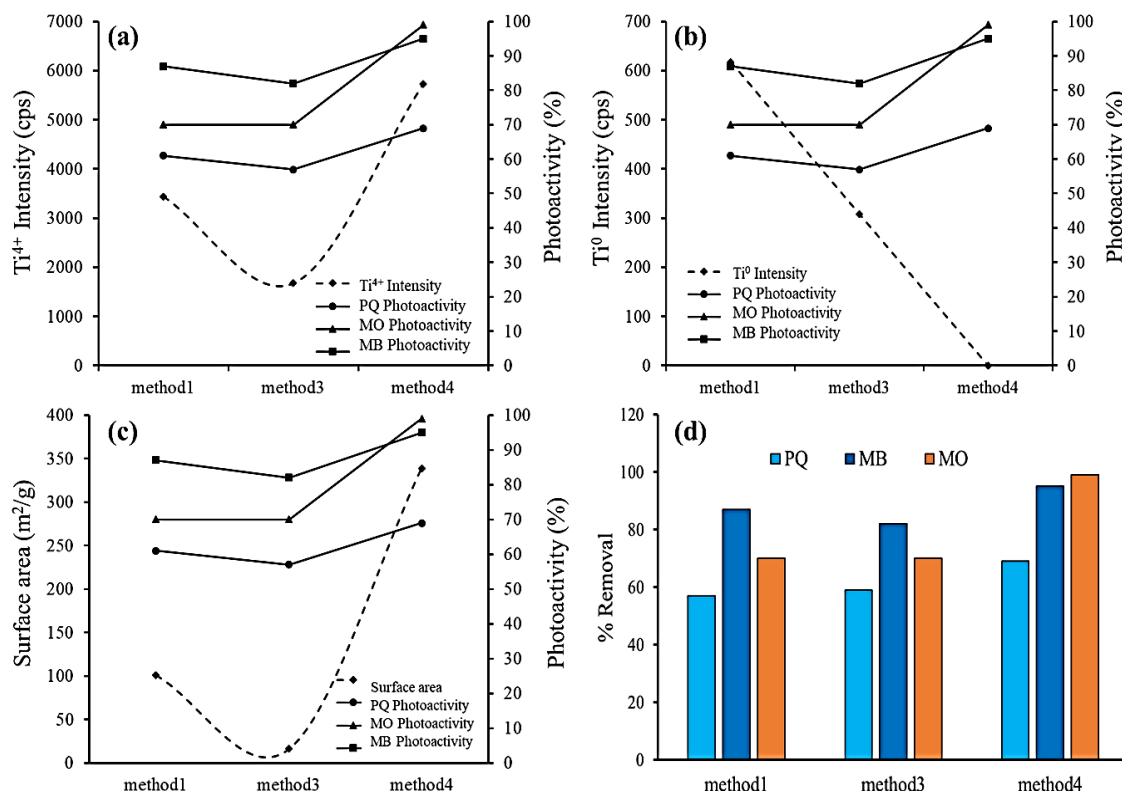


Figure 18 (a) Effect of maximum intensity of Ti^{4+} on photoactivity, (b) Effect of maximum intensity of Ti^0 on photoactivity, (c) Effect of surface area on photoactivity and (d) The photo degradation under UV irradiation using various TiO_2 powder prepare from different 4 methods.

Figure 18 shows the trend of the photoactivity, surface area and amount of Ti^{4+} found in each sample. From the results shows that the % organic compound removal (PQ, MB and MO) tend to increased when the maximum intensity of Ti^{4+} and surface area increased.

Normally, the photoactivity of catalyst is corresponding with the high of surface area of catalyst as shows in figure 12. It is indicated that the surface area was the factor to own the photo-activity of catalysts. However, the photo-activity of catalyst increase not significant related to the surface area increased in the same negativity. From the result of XPS analysis in figure 18, the amount of Ti^{4+} also was the factor own the photo-activity of catalysts. Therefore, the surface area and Ti^{4+} level were the factor own the photoactivity.

For the photodegradation of paraquat (PQ), methylene blue (MB) and methyl orange (MO) using TiO₂ powder preparation from difference 4 methods compared with commercial TiO₂ P25 under UV irradiation 2 h. show that in Figure 18. The result showed clearly that the TiO₂ particle synthesise from method 4 exhibited highest photo activity of organic solution as PQ, MB and MO degradation when compared with P25 and other methods. The best photoactivity confirm that the highest specific surface area at 338.8 m²/g of method 4. The result seen that TiO₂ synthesized from method 4 can be used degradation of other organic compounds due to around surface of catalyst have various active site in nature due to MB and PQ is cationic dye and MO is anionic dye. Moreover, TiO₂ catalyst from method 4 can capture the both systems. This reasons confirm that TiO₂ catalyst from method 4 is good catalyst because it is can adsorb both of cationic and anionic compound.

4.2 Application of TiO₂ deposited on pineapple fibers (PF)

The TiO₂ loading to pineapple fibers were prepared by mix PF and TTIP in optimum method from the previous part. The ratio of TiO₂: PF was 1:10, 1:5, 1:1 and 2:1.

4.2.1 Characterizations

4.2.1.1 X-Ray diffraction analysis

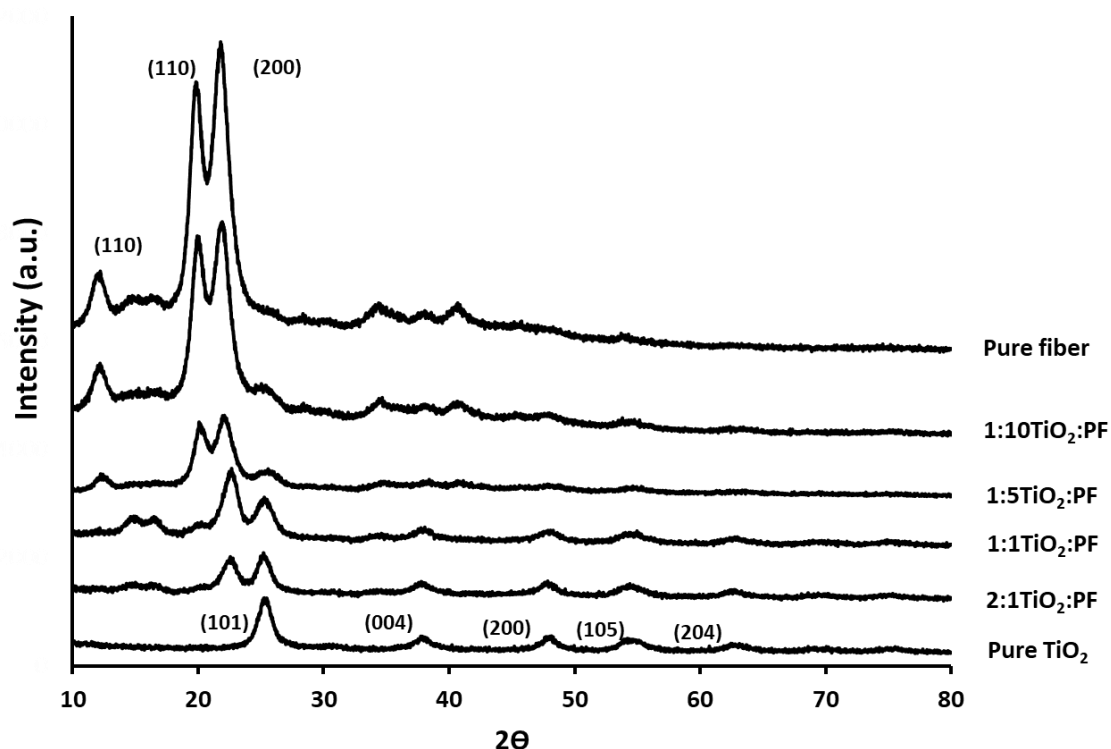


Figure 19 The XRD pattern of pure TiO₂ and TiO₂:PF with difference ratio.

Figure 19 showed the XRD patterns of the pure fiber, pure TiO₂ and the TiO₂ composited on fibers with difference ratio of TiO₂:PF as 1:10, 1:5, 1:1 and 2:1. The peaks at $2\theta = 12.1, 20.3, \text{ and } 21.8^\circ$ are corresponding to the (110), (110), and (200) which are the planes of cellulose crystalline, respectively [113]. The peaks at $2\theta = 25.4^\circ, 38.0^\circ, 48.0^\circ, 54.7^\circ, 63.1^\circ$ are corresponding to the (101), (004), (200), (105) and (204) which are the planes of anatase phase of TiO₂, respectively [33,45,67]. For the TiO₂ composited on fibers, to study the crystalline structure of absorbed nano TiO₂ on fibers, the XRD pattern of pure nano TiO₂ and nano TiO₂-treated sample were recorded. It can

be observed that the major peak of the spectrum of pure nano TiO₂ is anatase. The anatase phase for the sample increase when the amount of TiO₂ loading increased, reaching to the interesting of peak at 25.4°.

4.2.1.2 Surface morphological analysis

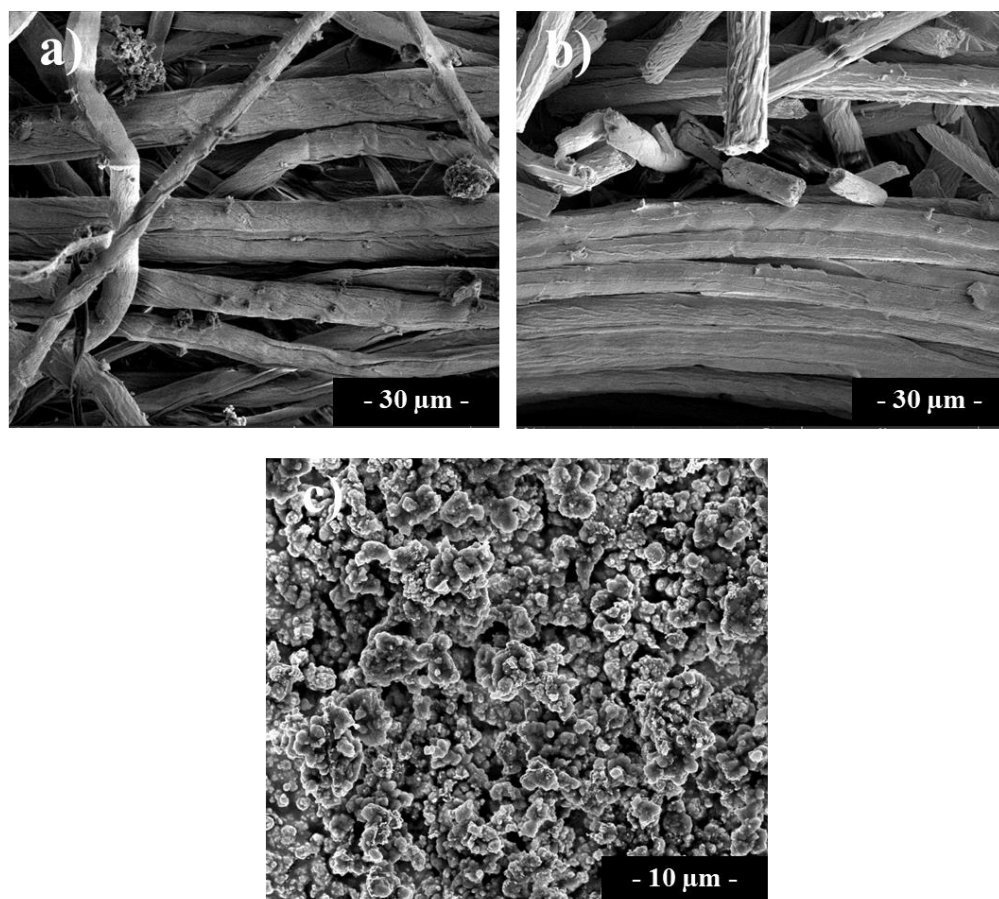


Figure 20 The SEM image of a) virgin fiber, b) fibers after calcination and c) pure TiO₂.

Figure 20 illustrates the SEM image of pure TiO₂ and pure fibers before and after calcination. From the figure 20 a) and 20 b) are comparison between virgin fiber and calcined fiber, respectively, indicated that the sample of virgin fiber destroyed by calcination and after calcination the surface of fiber smoother than before calcination. Figure 20 c) show the morphology of pure TiO₂ synthesized from method 4 consisted of aggregated spherical particles originating cluster of TiO₂ particles.

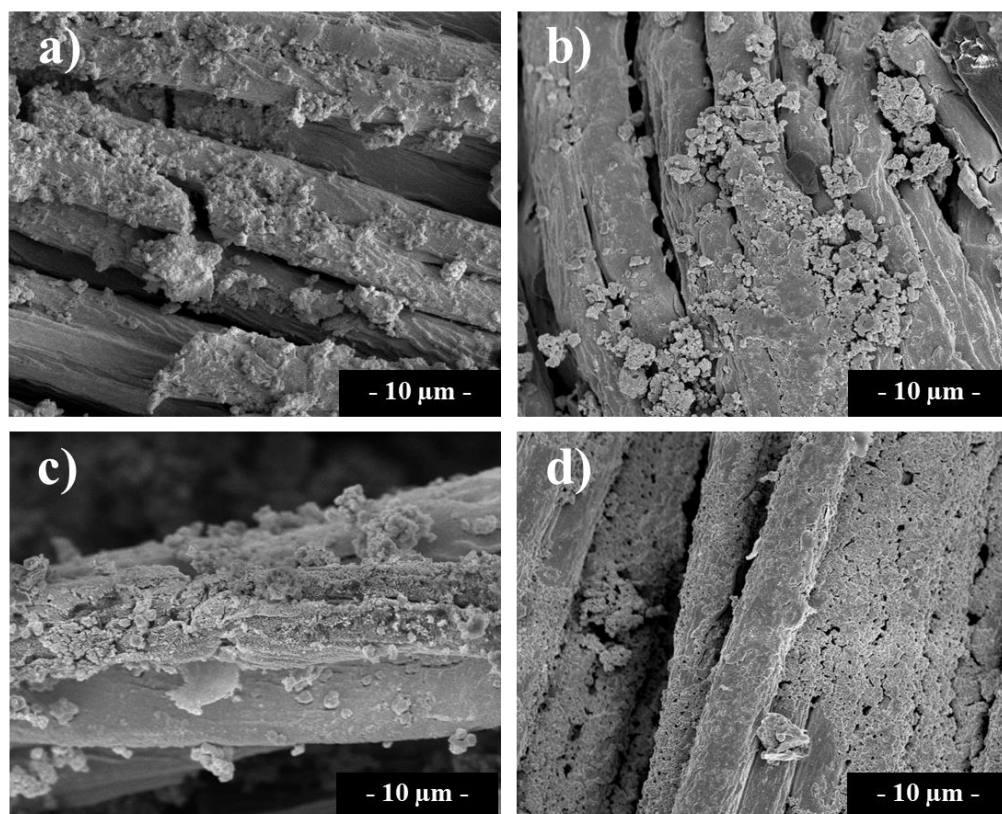


Figure 21 The SEM image of TiO_2 :PF with different ratio a) 1:10, b) 1:5, c) 1:1, d) 2:1.

Figure 21 shows the SEM images of TiO_2 composited on fibers with difference ratio of TiO_2 :PF as 1:10, 1:5, 1:1 and 2:1. These all sample images show that nano TiO_2 particles were applied on fiber by the dipping process, but their distribution on fiber surface was not quite even, which is due to the aggregation of some nano TiO_2 particles. For the sample prepared ratio 2:1 TiO_2 :PF demonstrated TiO_2 particles coated on the fiber more than other ratio of TiO_2 :PF.

4.2.1.3 SEM EDX analysis

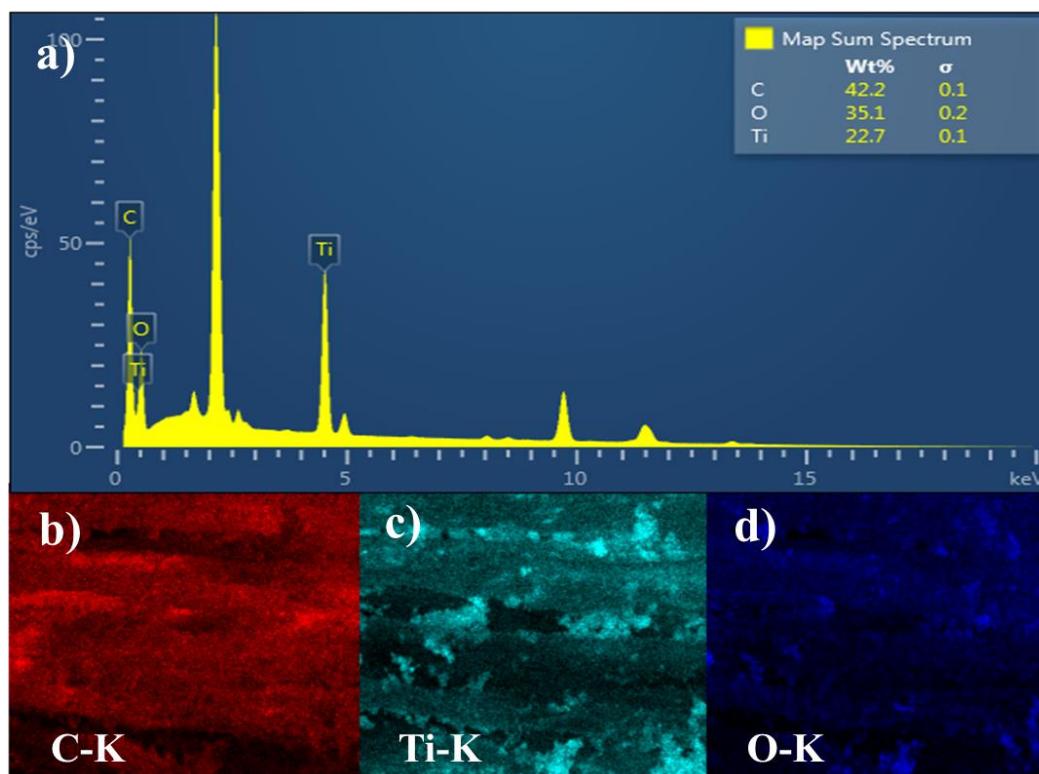


Figure 22 SEM-EDX of 2:1 TiO₂:PF.

Energy dispersive X-ray (EDX) analysis of the 2:1 TiO₂:PF showed in Fig. 22. The EDX spectrum (Fig. 22a) indicated prominent signals of C, O and Ti elements. The C signal should be from the carbon fiber on cellulose fibers. For the Ti and O signal should be from the TiO₂ powder deposited on cellulose fibers. These confirmed two elements of O and Ti are detected on the surface. The element distribution in the TiO₂ on fibers was further certified by the elemental mapping recorded from Figure 22 b) – d). The elemental mappings showed in Figure 4.16 b) – d) reveal the distributions of C, Ti and O in the TiO₂:PF.

4.2.1.4 Surface area analysis

Table 5 Physicochemical properties of catalysts.

Catalyst	Calcination temperature (°C)	BET surface area (m ² /g)	Pore volume (mL/g)	Average pore size (Å)
Pure PF	200	0.113	0.007	1204.543
1:10 TiO ₂ :PF	200	1.792	0.009	28.140
1:5 TiO ₂ :PF	200	32.765	0.080	19.140
1:1 TiO ₂ :PF	200	60.490	0.125	19.123
2:1 TiO ₂ :PF	200	51.152	0.108	19.095
Pure TiO ₂	200	259.556	0.330	17.097

Table 5 showed specific surface area, pore volume and average pore size of pure FB, pure TiO₂ and TiO₂:PF with difference ratio. From the results, it can be seen that the surface area of samples tend to increase when increase amount of TiO₂ loading on fibers. The TiO₂:PF in ratio 1:1 and 2:1 indicated that the surface area of both sample not difference. The pure TiO₂ showed highest surface area of sample when compared with TiO₂:PF sample. The pore size distribution of TiO₂:PF was not different. The adsorption average pore volume and diameter of the TiO₂:PF in ratio 1:1 and 2:1 was not different.

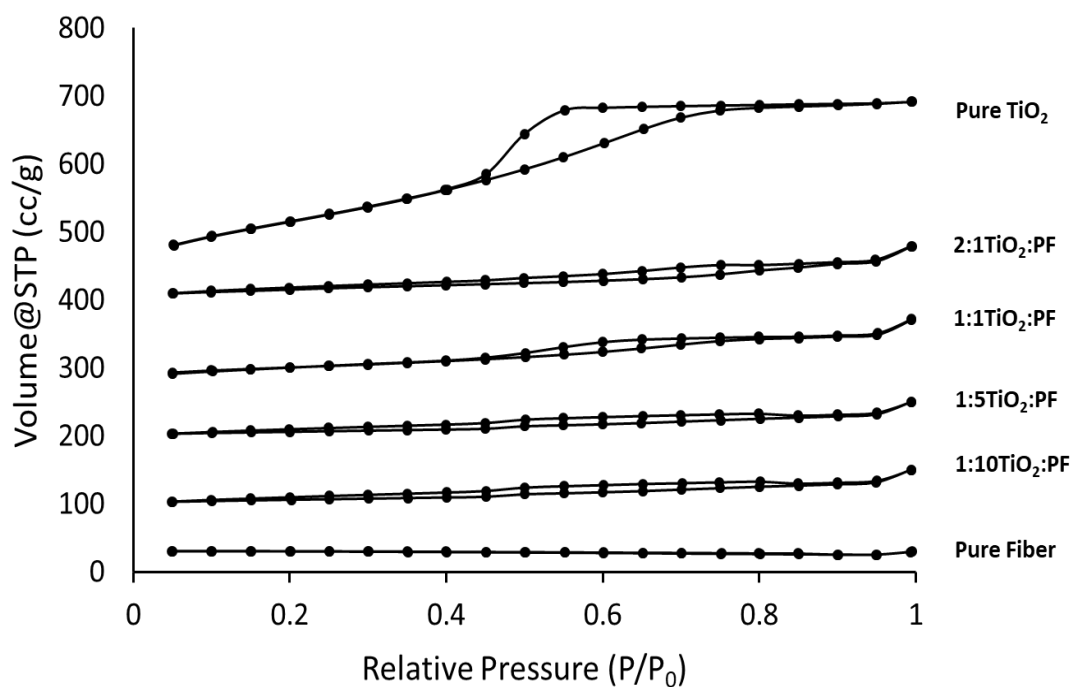


Figure 23 Nitrogen adsorption-desorption isotherm of pure TiO₂ and TiO₂:PF with different ratio.

The nitrogen adsorption-desorption isotherms of pure TiO₂ and TiO₂:PF catalysts synthesized with methods 4 in different ratio of TiO₂:PF were compared in Figure 23. The hysteresis loops were obtained which suggested the microporous materials of TiO₂ composite. Moreover, the similar shape of the isotherm was established with in agreement to the similar surface area of TiO₂ composited. The result from the isotherm confirmed the surface area of pure TiO₂ was higher than TiO₂:PF and the ratio 1:1 and 2:1 is not difference.

4.2.1.5 Functional group analysis

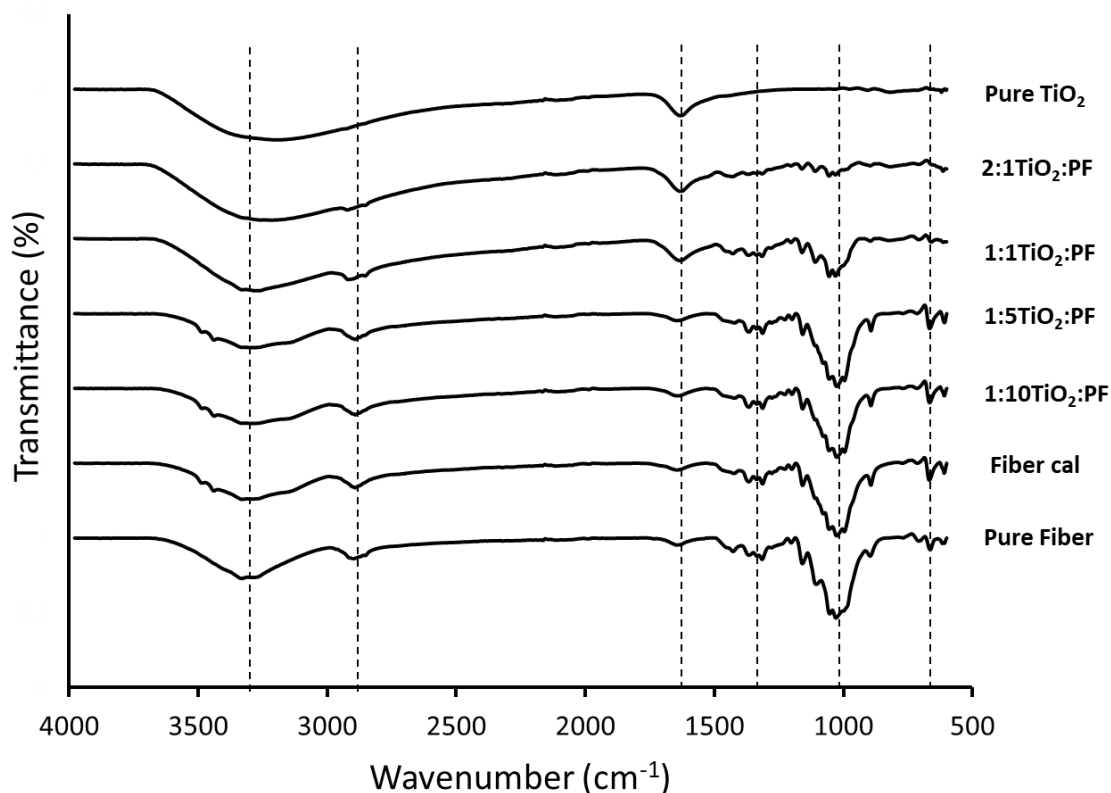


Figure 24 The FTIR of pure FB, pure TiO₂ and TiO₂:PF with different ratio.

Figure 24 shows the ATR-FTIR spectra of pure TiO₂, pure fiber and TiO₂:PF. From the spectra indicated that peak at wave number about 800 cm⁻¹ is Ti-O bond of TiO₂ [69]. The peak at wave number about 1,000 cm⁻¹ is C-O stretching and at wave number about 1,300 cm⁻¹ and 2,700 cm⁻¹ are peak of C-H stretching of fibers, at wave number about 3,000 cm⁻¹ - 3,500 cm⁻¹ indicate that the hydroxyl group [72,73]. For the 1:1 and 2:1 ratio samples showed the peak of -OH broader than other samples.

4.2.1.6 Band gap energy analysis

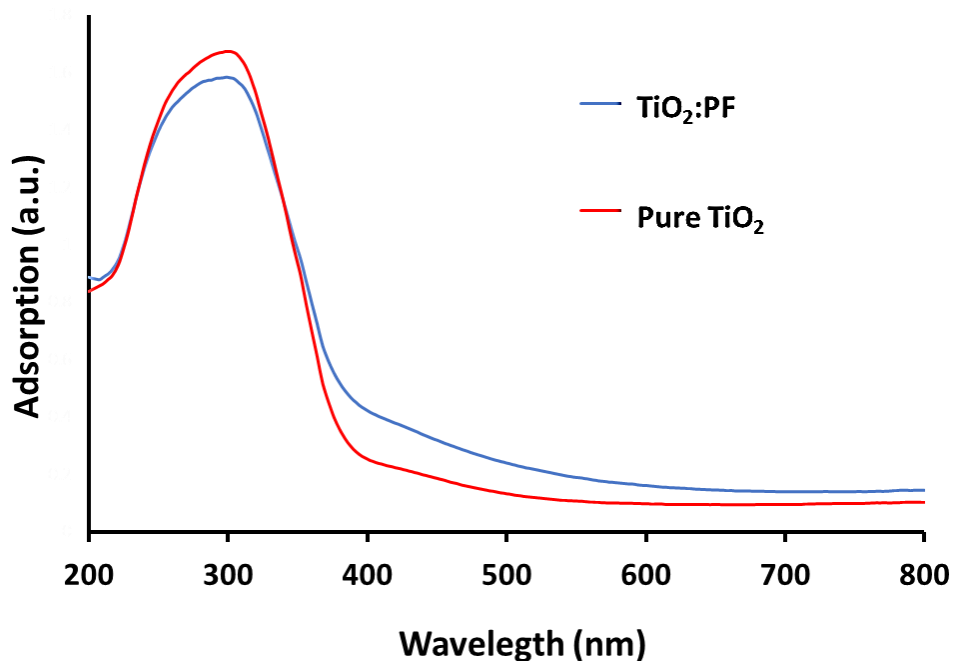


Figure 25 UV-vis diffuse reflectance spectra of pure TiO₂ and 2:1 TiO₂:PF.

Figure 25 showed UV-Vis diffuse reflectance spectra of pure TiO₂ compared TiO₂ composite as ratio 2:1 TiO₂:PF. This spectra indicated that pure TiO₂ is photoactive in UV region which is less than 400 nm. For TiO₂:PF presented significant increase of absorption in Vis spectra range above 400 nm. The absorption spectra clearly indicated that the optical absorbance of TiO₂ composited on fibers in Vis-light region was markedly enhanced, compared to pure TiO₂ [44].

4.2.1.7 Thermogravimetric analysis

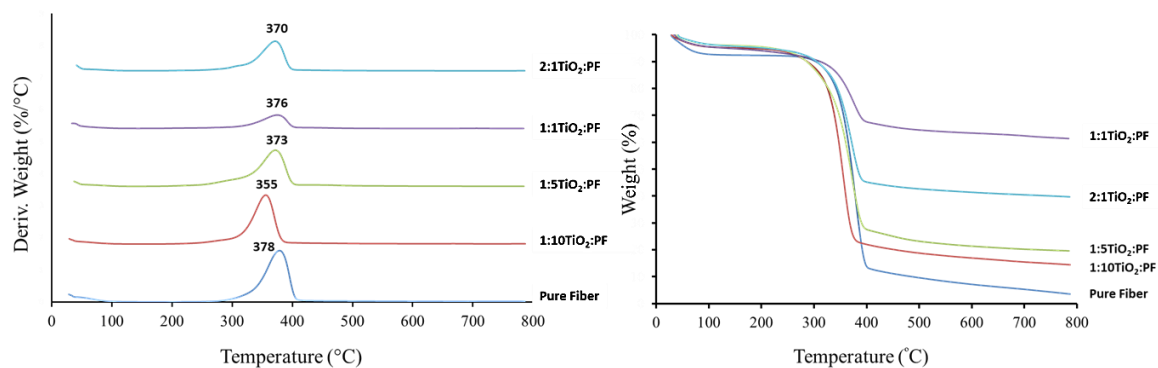


Figure 26 DTG and TG curves of pure FB and TiO₂:PF with different ratio.

The thermal decomposition of pure fiber and TiO₂:PF with different ratio there are 1:10, 1:5, 1:1 and 2:1 TiO₂:PF as showed in figure 26. The results showed all samples of pure fiber and TiO₂:PF with different ratio exhibited a single step of decomposition weightless at 378°C, 355°C, 373°C, 376°C and 370°C, respectively. It can be concluded that, the temperature of maximum decomposition of all samples was not difference. From the results indicated that % weight loss of pure fibers tend to decrease when added amount of TiO₂ on fibers. The TG results suggested that TiO₂ powder increased thermal stability of cellulose fiber.

4.2.2 Catalytic activity

4.2.2.1 Methylene blue removal

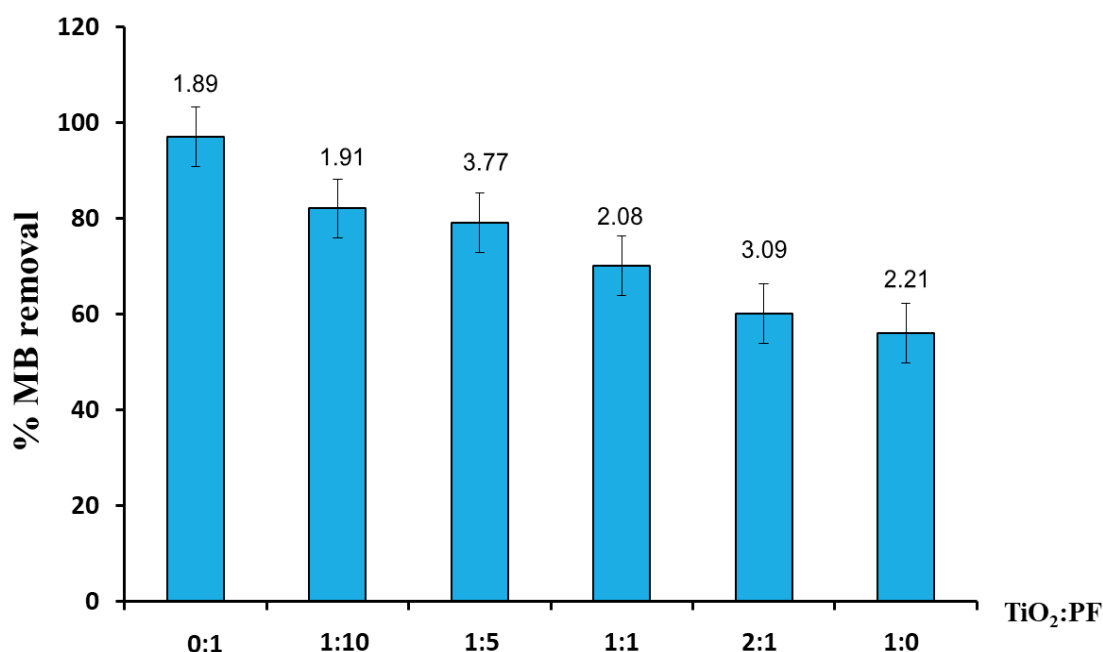


Figure 27 The total MB removal under UV irradiation using pure TiO₂ and different ratio of TiO₂:PF.

The MB total removal of catalysts was occurred by photodegradation and adsorption process. Total MB removal of TiO₂:PF with difference rather were 1:10, 1:5, 1:1 and 2:1 under UV light irradiation for 2 hour are showed in Figure 27. The loaded amount of TiO₂ has a significant effect on the total MB removal of the composite fibers. The results showed that the % of total MB removal decrease when amount of TiO₂ loading increase, because TiO₂ decrease surface adsorption of the fiber as refer to results of BET surface area characterization.

4.2.2.2 Methylene blue adsorption study

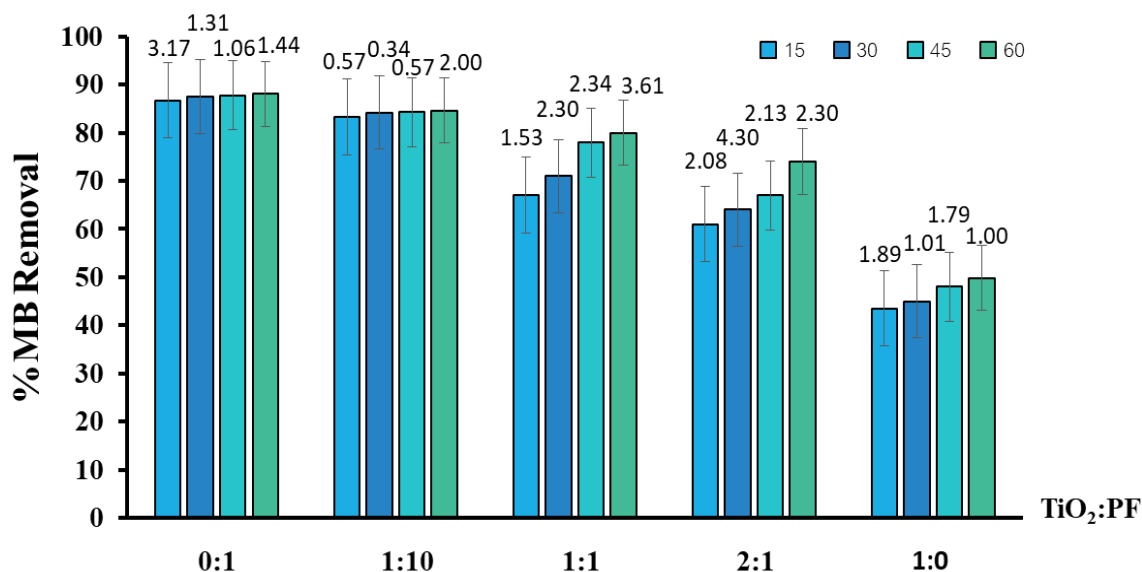


Figure 28 MB adsorption under dark reaction for 60 minute using pure TiO₂ and different ratio of TiO₂:PF.

Figure 28 exhibit the influence of MB removal by adsorption method, this process operated sampling every 15 minute by using pure fiber and TiO₂ composited on fiber with different ratio under dark condition, only. From the result showed that MB removal using pure FB and 1:10 TiO₂:PF is quite stable since 15 minute under testing. For others catalysts system, the % MB removal was increasing from 15 – 60 minutes under reaction and seem reached equilibrium at 60 minute.

After the MB concentration at 60 minutes was calculated for each catalyst, it was named as C_0 is the initial MB concentration before photodegradation step. These C_0 values used to study the photodegradation efficiency as shown in figure 28.

4.2.2.3 Methylene blue photodegradation study

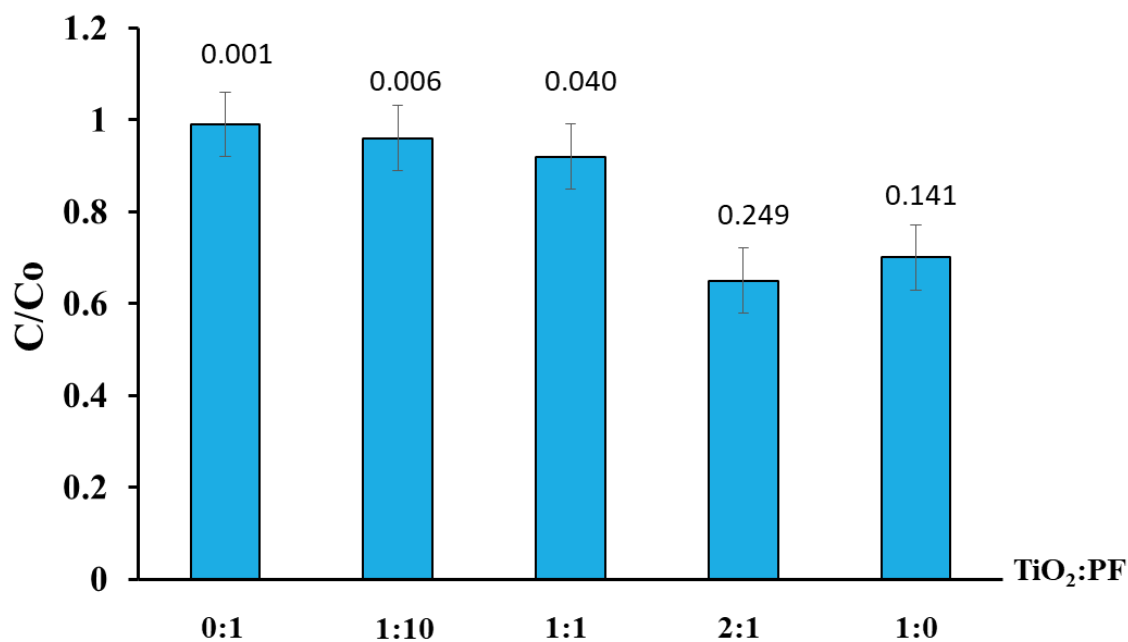


Figure 29 MB degradation under UV irradiation for 2 hour using pure TiO₂ and different ratio of TiO₂:PF.

The result from figure 29 showed experiment performed after the reaction in figure 4.19. The reaction is continues under the process of MB removal on photodegradation. When C₀ is residual MB concentration under dark reaction after 60 minute and C is residual MB concentration after 2 hour UV irradiation. The photocatyticactivity showed in C/C₀ pattern by the low of C/C₀ is means high of MB removal. From the result showed the TiO₂ over fiber with 2:1 ratio showed highest MB removal efficiency by photodegradation process. It could be seen that 2:1 ratio is the best component for MB removal for photo degradation. From the result confirmed that, this catalyst possibility to be recycle.

4.3 Application of crosslink molecule on TiO₂ composite on pineapple fibers

The loaded TiO₂ on pineapple fibers were prepared by mixed FB and TTIP in optimum method for preparation TiO₂ powder (method 4) with ratio of 2:1 TiO₂:PF. The TiO₂ composited with fibers using non crosslink named as TiO₂:PF catalyst, TiO₂ composited with fibers using succinic acid as across-link named as TiO₂:PF+SA were synthesis. Moreover, the sodium hydrogen phosphite (NaH₂PO₂) was added during preparation of TiO₂:PF+SA, thus this catalyst was named as TiO₂:PF+SA+Na as the enhancement of succinic acid efficiency in the preparation.

4.3.1 Characterizations

4.3.1.1 X-Ray diffraction analysis

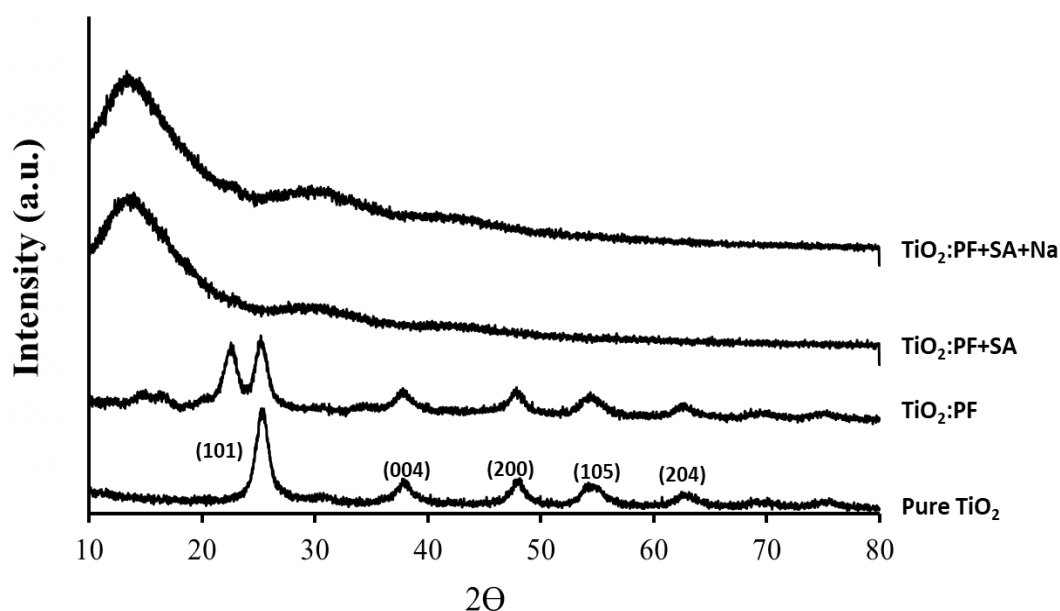


Figure 30 XRD pattern of various TiO₂:PF.

Figure 30 illustrates the X-ray patterns of pure TiO₂ and TiO₂ composited on fibers which are TiO₂:PF, TiO₂:PF+SA and TiO₂:PF+SA+Na. The XRD peaks found that pure TiO₂ and TiO₂ composited on fibers indicated the formation of only anatase crystalline phase. The diffraction spot ring could be index to (101), (004), (200), (105) and (204) crystal planes of anatase TiO₂ [84,98]. For the TiO₂:PF+SA+Na, it suggested that the TiO₂ nanoparticles in the composite fibers existed in an almost amorphous state.

4.3.1.2 Surface morphological analysis

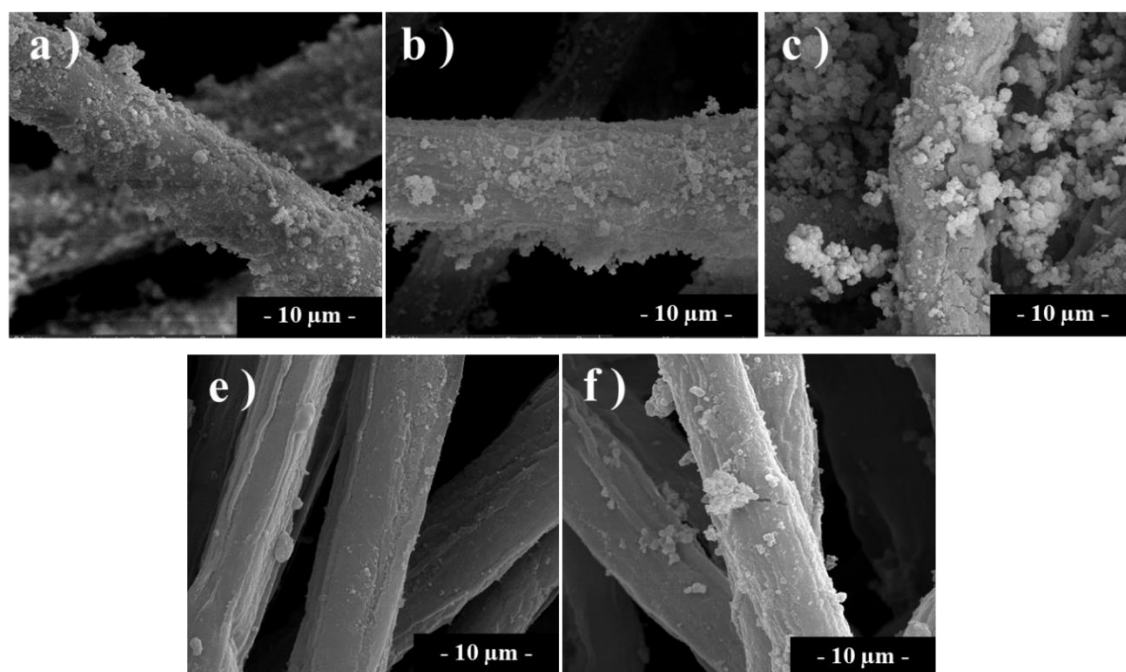


Figure 31 The SEM image of a) $\text{TiO}_2\text{:PF}$, b) $\text{TiO}_2\text{:PF+SA}$, c) $\text{TiO}_2\text{:PF+SA+Na}$ e) $\text{TiO}_2\text{:PF}$ after recycle and f) $\text{TiO}_2\text{:PF+SA+Na}$ after recycle.

Figure 31 (a-c) illustrated the SEM image of TiO_2 composited on fibers a) $\text{TiO}_2\text{:PF}$, b) $\text{TiO}_2\text{:PF+SA}$ and c) $\text{TiO}_2\text{:PF+SA+Na}$. The morphology of $\text{TiO}_2\text{:PF}$ indicated that TiO_2 particles distribution on fiber surface as show in figure a). The morphological of SA-treated sample showed that, the surface of the SA-treated sample has a higher number of nano TiO_2 particles than sample $\text{TiO}_2\text{:PF}$ sample. This could be due the fact that more carboxylic acid groups of SA can hold more particles of nano TiO_2 . Moreover, these images show that the surface of the $\text{TiO}_2\text{:PF+SA+Na}$ showed the most of nano TiO_2 particles deposited on fiber surface, when compared with the $\text{TiO}_2\text{:PF+SA}$ samples.

For figure 31 e) and f) showed the $\text{TiO}_2\text{:PF}$ and $\text{TiO}_2\text{:PF+SA+Na}$ after recycle for 3 cycles, respectively. From the results, it was found that the TiO_2 particles was fall out from the fiber. From the figure 31 e) and f) indicated that, the $\text{TiO}_2\text{:PF+SA+Na}$ sample showed the more TiO_2 deposition over FB surface than $\text{TiO}_2\text{:PF}$. This result confirmed that succinic acid improved the interaction of TiO_2 deposited on fibers.

4.3.1.3 Functional group analysis

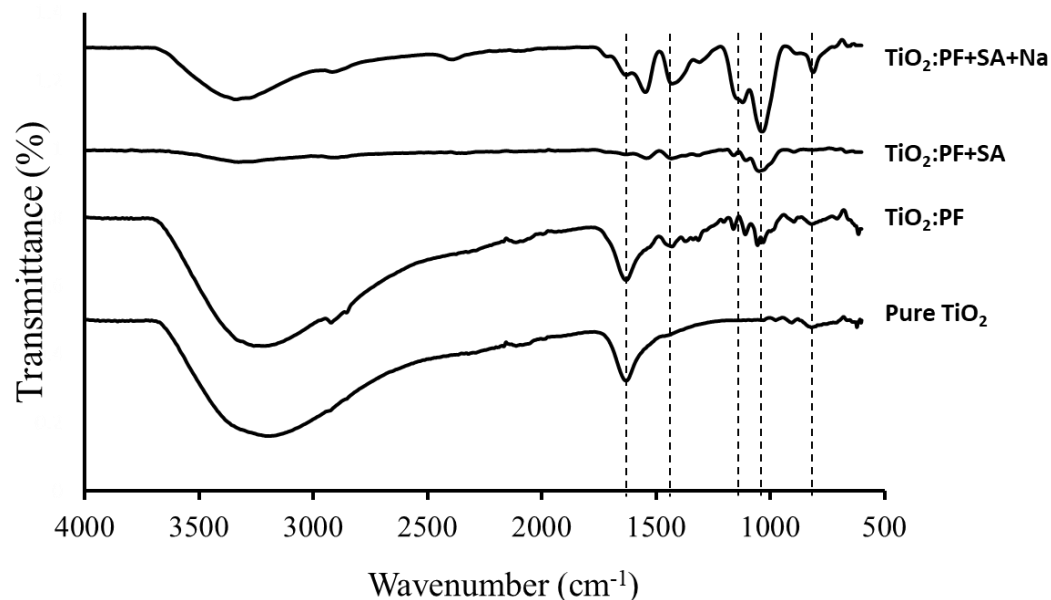


Figure 32 ATR-FTIR spectrum of various $\text{TiO}_2\text{:PF}$.

Figure 32 showed the ATR-FTIR spectra of pure TiO_2 , and TiO_2 composited on fibers which are $\text{TiO}_2\text{:PF}$, $\text{TiO}_2\text{:PF+SA}$ and $\text{TiO}_2\text{:PF+SA+Na}$. From the spectra, it can be seen that the peak at wave number about 800 cm^{-1} is Ti-O bond of TiO_2 [116]. The peak at $1,000\text{ cm}^{-1}$ is C-O stretching and at $1,300\text{ cm}^{-1}$ is peak of C-H stretching of fibers, at $3,000\text{ cm}^{-1} - 3,500\text{ cm}^{-1}$ indicated that the hydroxyl group [(15,99)]. For the $\text{TiO}_2\text{:PF+SA}$ catalyst showed the broader peak of $-\text{OH}$ when compared to the other catalysts. The C=O carbonyl groups at 1720 cm^{-1} was found in pure TiO_2 and $\text{TiO}_2\text{:PF}$ only.

4.3.1.4 Thermogravimetric analysis

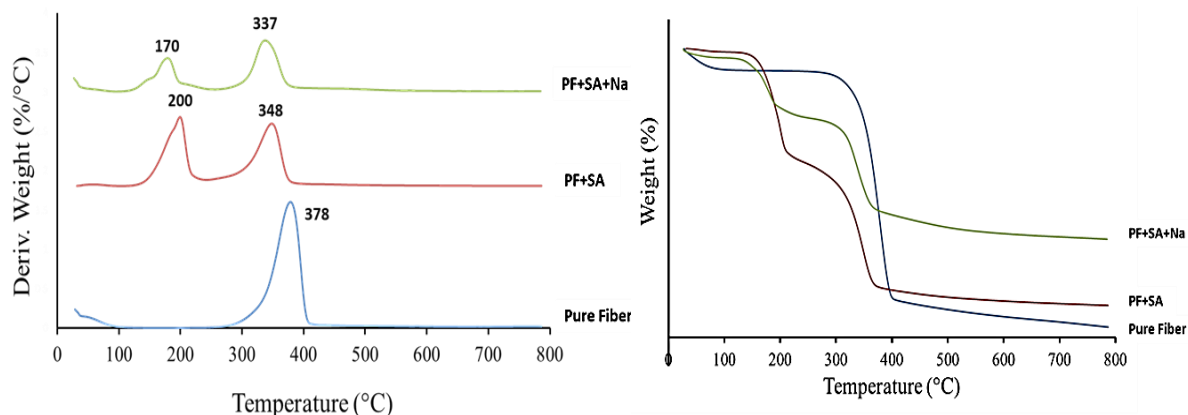


Figure 33 DTG and TG curves of various materials.

The thermal decomposition of pure fiber, fiber coated succinic acid as a crosslink (PF+SA), for fiber coated succinic acid used NaH_2PO_2 as the promoter (PF+SA+Na). The pure fiber exhibited a single step of maximum decomposition weight at 378°C of cellulose fibers. While both the PF+SA and PF+SA+Na exhibited two-step maximum decompositions weight of succinic acid and cellulose fiber at 170°C, 348°C and 200°C, 348°C respectively. From the results indicated that % weight loss of pure fibers tend to decrease when add succinic acid and NaH_2PO_2 . The TG results suggested that succinic acid and NaH_2PO_2 increase thermal stability of cellulose fiber.

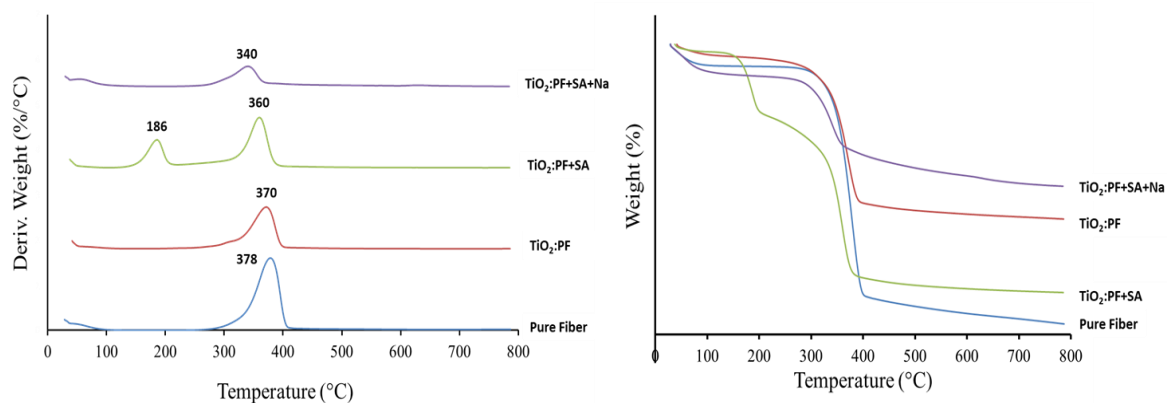


Figure 34 DTG and TG curves of various materials.

The thermal decomposition of pure TiO₂, and TiO₂ composited on fibers which are TiO₂:PF, TiO₂:PF+SA and TiO₂:PF+SA+Na. The pure fiber and TiO₂:PF exhibited a single step of maximum decomposition weight at 378°C and 370°C, respectively. For the TiO₂:PF+SA exhibited two-step decompositions weightless of succinic acid and cellulose fiber at 186°C, 360°C respectively. It is interesting that, the TiO₂:PF+SA+Na exhibited a single step of maximum decomposition weight at 340°C which is decomposition of fiber. This sample the peaks of decomposition of SA was not appear because carboxyl group of SA is occur interaction with TiO₂ molecules can examined from scheme 1. From the results indicated that % weight loss of TiO₂:PF+SA+Na decrease when compared with other samples. The TG results suggested that succinic acid and NaH₂PO₂ increase thermal stability of PF.

4.3.1.4 XPS analysis

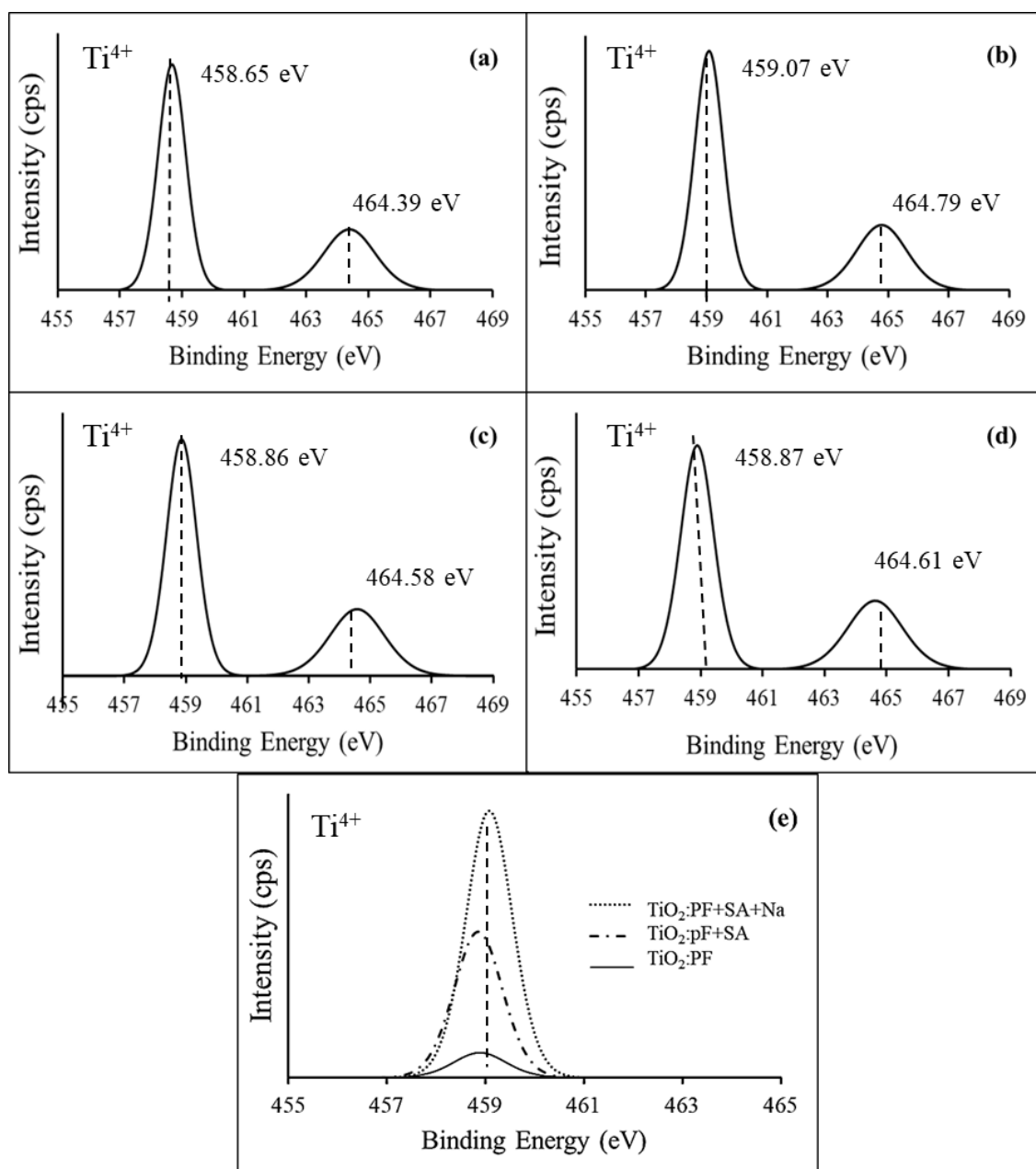


Figure 35 XPS spectra of Ti element on various TiO_2 , (a) pure TiO_2 , (b) $\text{TiO}_2:\text{PF}$, (c) $\text{TiO}_2:\text{PF}+\text{SA}$ (d) $\text{TiO}_2:\text{PF}+\text{SA}+\text{Na}$ and (e) intensity of Ti^{4+} in various materials.

The surface element of pure TiO_2 , and TiO_2 composited on fibers which are $\text{TiO}_2:\text{PF}$, $\text{TiO}_2:\text{PF}+\text{SA}$ and $\text{TiO}_2:\text{PF}+\text{SA}+\text{Na}$ were identified by XPS spectra. The analysis of metal Ti oxidation state in the various catalysts was showed in Figure 35 (a)

- (d). The XPS results exhibited clearly that Ti elements appear in the pure TiO₂, and TiO₂ composited on fibers. The Ti 2p spectrum shows at region about 457-467 eV. Figure 35 (a) - (d) shows the XPS core level of Ti 2p composed of Ti 2p_{3/2} centered appeared at about 458 eV and Ti 2p_{1/2} appeared at about 464 eV in all samples [30]. These peaks attributes to the Ti⁴⁺ presence. Indicating that the loading TiO₂ on PF and used crosslink, the oxidation state of TiO₂ synthesized from method 4 not different. In term of the amount of Ti⁴⁺ regarded to the peak area, the labeled of Ti in the catalyst name was related to the amount of Ti⁴⁺ appeared (Figure 35 (e)). Comparing the peak area of Ti⁴⁺ between TiO₂:PF, TiO₂:PF+SA and TiO₂:PF+SA+Na as shows in figure 35 (e). The highest peak area as shows in TiO₂:PF+SA+Na sample, which means that the higher Ti⁴⁺ level present in TiO₂:PF+SA+Na sample than TiO₂:PF and TiO₂:PF+SA sample.

4.3.2 Catalytic activity

4.3.2.1 Methylene blue removal

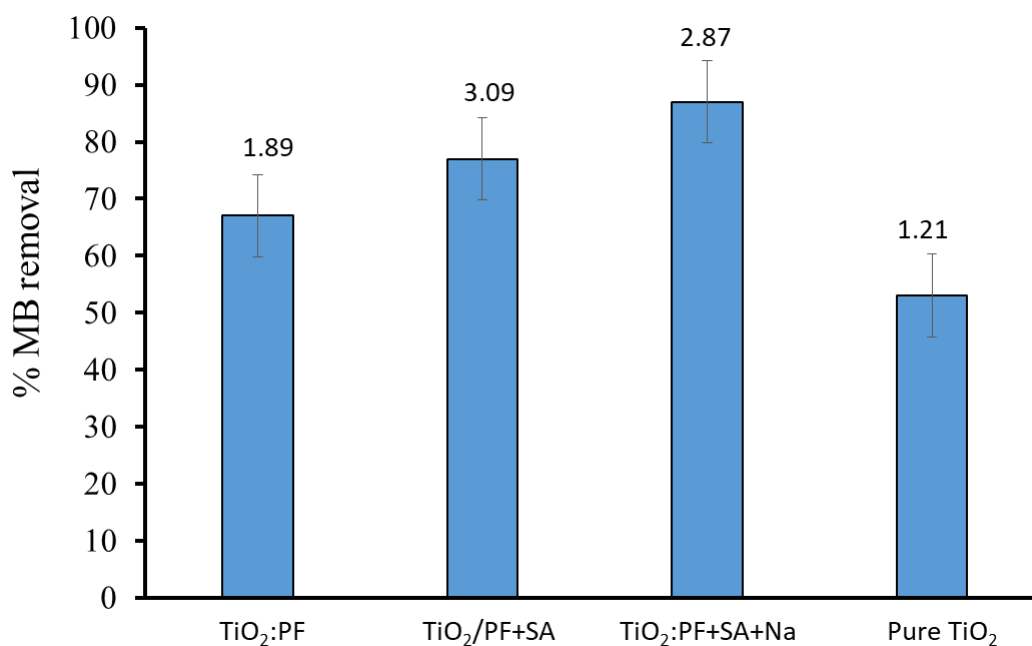


Figure 36 Effect of total MB removal (first hr. in dark and another hrs. under UV irradiation) using various TiO₂:PF.

The MB total removal of catalysts was occurred by photodegradation and adsorption process. Total MB removal of pure TiO₂, TiO₂:PF, TiO₂:PF+SA and TiO₂:PF+SA+Na under UV light irradiation for 2 hour are shown in Figure 4.26. The results showed that the TiO₂:PF+SA+Na show highest activities for total MB removal. This result confirmed that succinic acid improved interaction of TiO₂ deposited on fibers as showed in SEM results in figure 36.

4.3.2.2 Methylene blue adsorption study

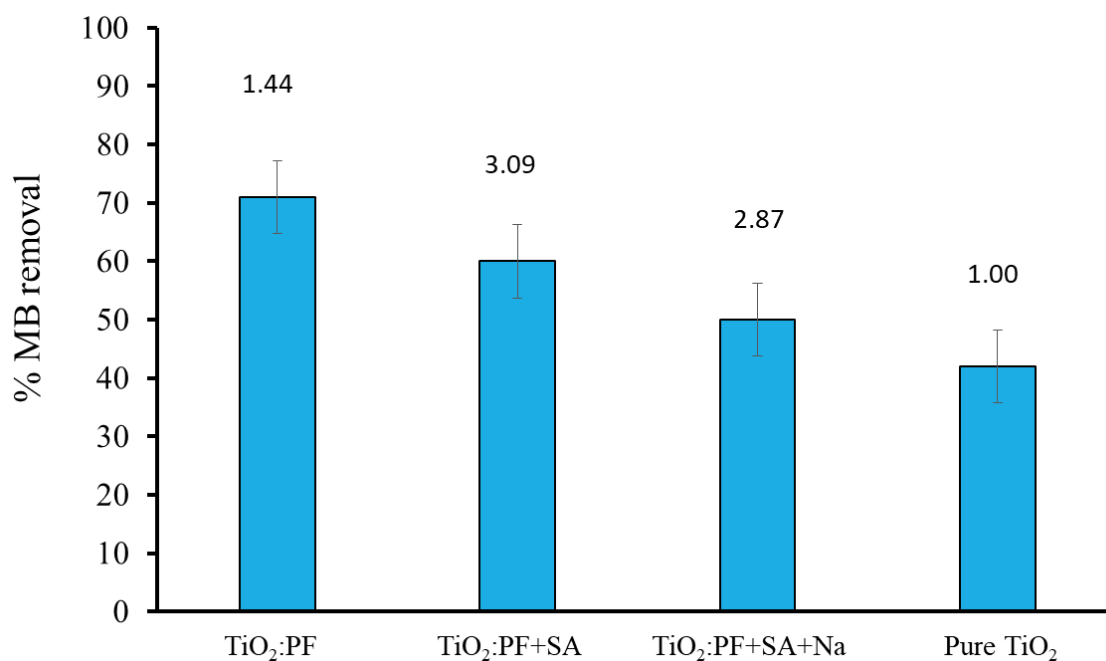


Figure 37 MB adsorption under dark reaction for 60 minute using various TiO₂:PF.

Figure 37 exhibit the influence of MB removal by adsorption method. This process operating by using pure TiO₂, TiO₂:PF, TiO₂:PF+SA and TiO₂:PF+SA+Na under dark condition for 1 hour. From the result, it was seen that MB removal of TiO₂:PF showed highest activities for MB adsorption. After the MB concentration at 60 minutes was calculated for each catalyst, it was named as C₀ is the initial MB concentration before photodegradation step. These C₀ values used to study the photodegradation efficiency as shown in figure 37.

4.3.2.3 Methylene blue photo degradation

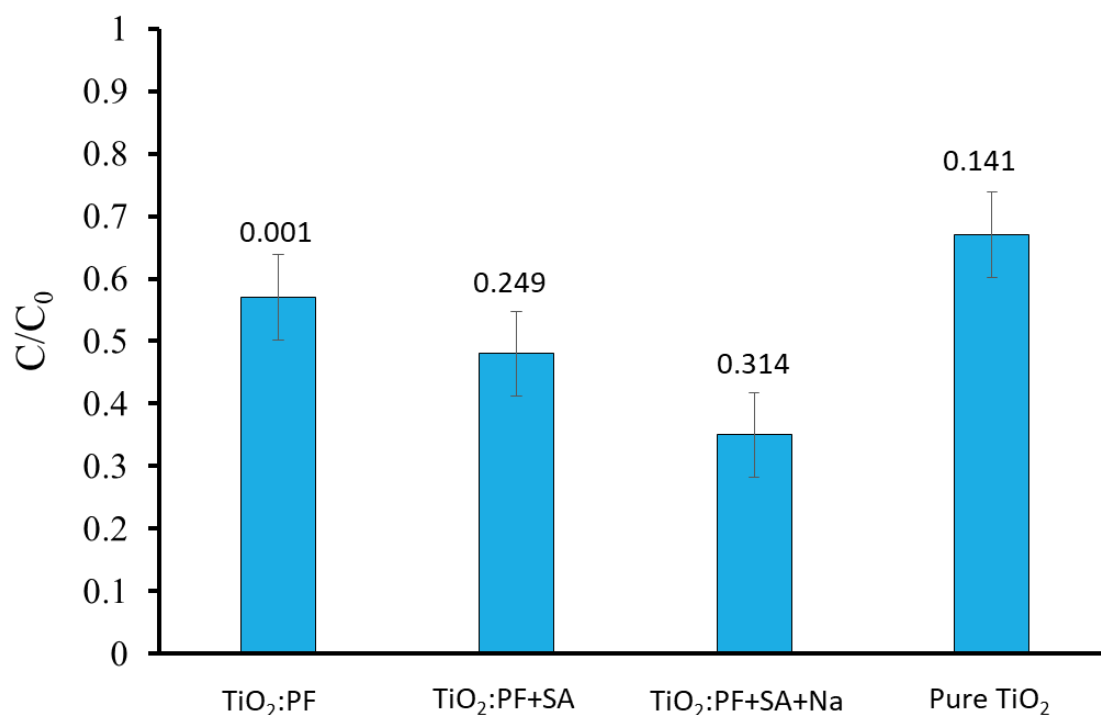


Figure 38 Effect of MB degradation under UV irradiation of various TiO₂:PF.

The result from figure 36 showed experiment performed after the reaction in figure 37. The reaction is continues under the process of MB removal on photodegradation. When C_0 is residual MB concentration under dark reaction after 60 min and C is residual MB concentration after 2 h UV irradiation. The photocatyticactivity showed in C/C_0 pattern by the low of C/C_0 is means high of MB removal. From the result showed the TiO₂:PF+SA+Na showed highest MB removal efficiency by photodegradation process. It could be seen that TiO₂:PF+SA+Na is the best component for MB removal for photodegradation. From the result confirmed that, this catalyst possibility to be recycle.

This results can be indicated that the photodegradation efficiency of catalyst corresponding to amount of TiO₂ deposited on the fiber. This results confirmed TiO₂:PF+SA+Na showed the succinic acid improved interaction of TiO₂ deposited on fibers as showed in SEM results in figure 22 e) and f) and confirm with amount of % Ti on catalyst with ICP-OES technique in table 6.

4.3.1.4 XPS analysis and Activity of catalyst

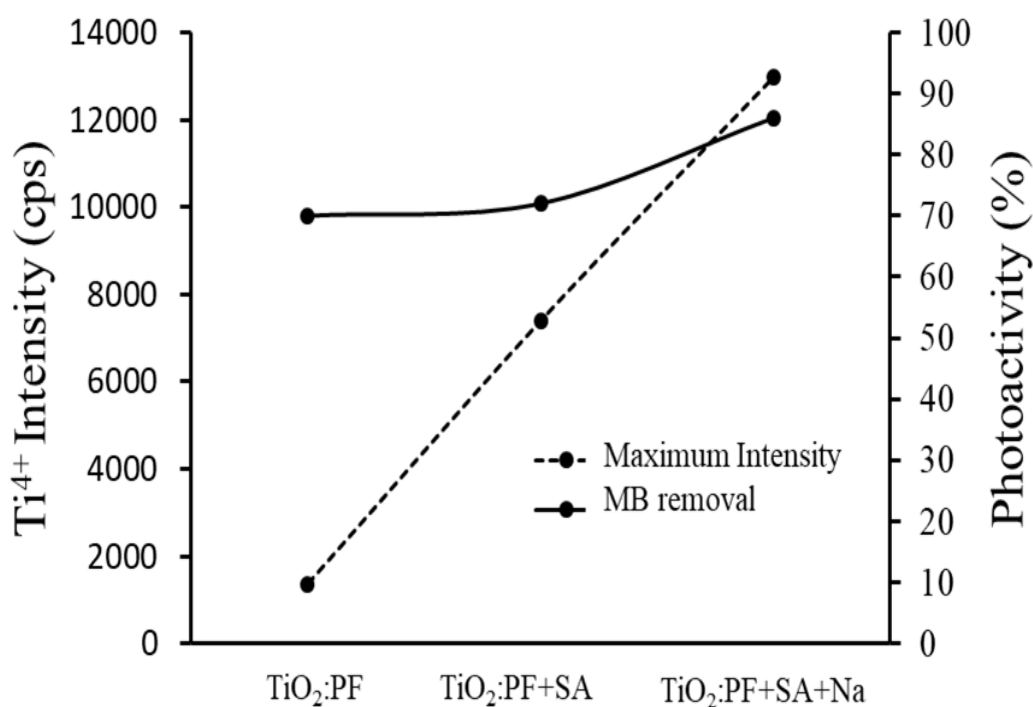


Figure 39 Effect of maximum intensity of Ti^{4+} on photo-activity using various TiO_2 materials.

Figure 39 shows compared the maximum intensity of Ti^{4+} with photo-activity of TiO_2 :PF, TiO_2 :PF+SA and TiO_2 :PF+SA+Na using MB degradation. From the results shows that the %MB removal increased when the maximum intensity of Ti^{4+} increased, indicated that the amount of Ti^{4+} effected with photo-activity of catalysts. TiO_2 catalyst from TiO_2 :PF+SA+Na shows both of the highest maximum intensity of Ti^{4+} and %MB removal. From the results seen that ehe used of succinic acid can improve the TiO_2 immobilized on fiber.

4.3.2.4 Recycle ability

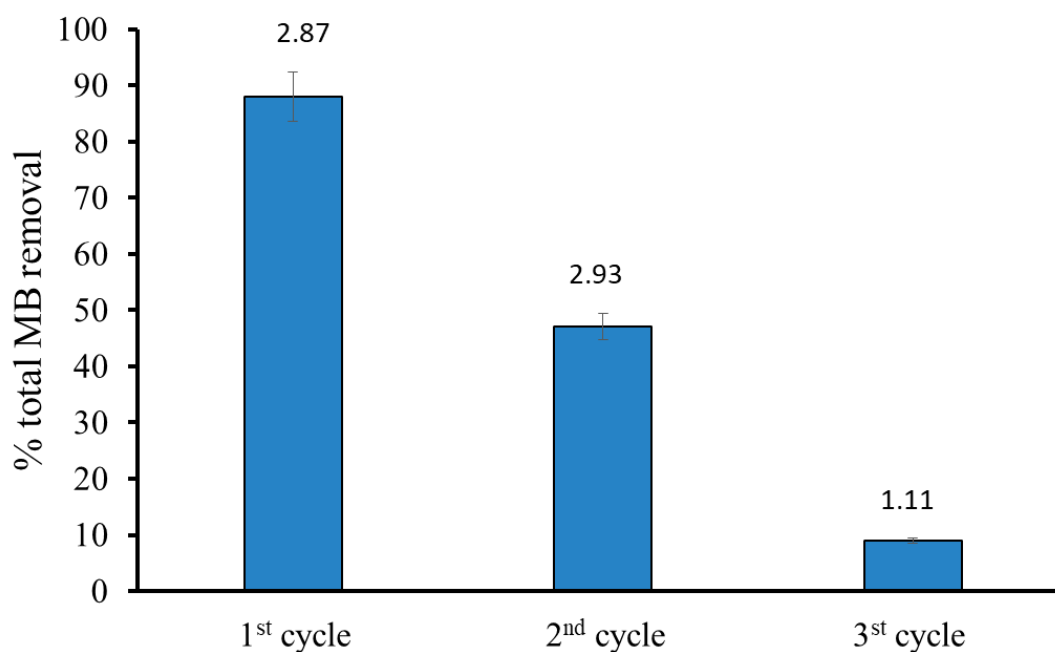


Figure 40 Effect of recycling on the photocatalytic degradation with 3 cycle using $\text{TiO}_2\text{:PF+SA+Na}$.

The recycling used of the $\text{TiO}_2\text{:PF+SA+Na}$. The photocatalyst up to the 3rd cycle leading to total MB removal is showed below in Figure 40. The activity was detected by the photocatalyst during its recycling after 3 time as showed in $\text{TiO}_2\text{:PF+SA+Na}$. For $\text{TiO}_2\text{:PF+SA+Na}$ showed the loss in the percentage of total MB removal was less than 50% and 10 % even after the twice and third cycle respectively. From the result was found that activity of catalyst decrease corresponding to the loss in the percentage of Ti from catalysts confirmed by ICP-OES results in table 6.

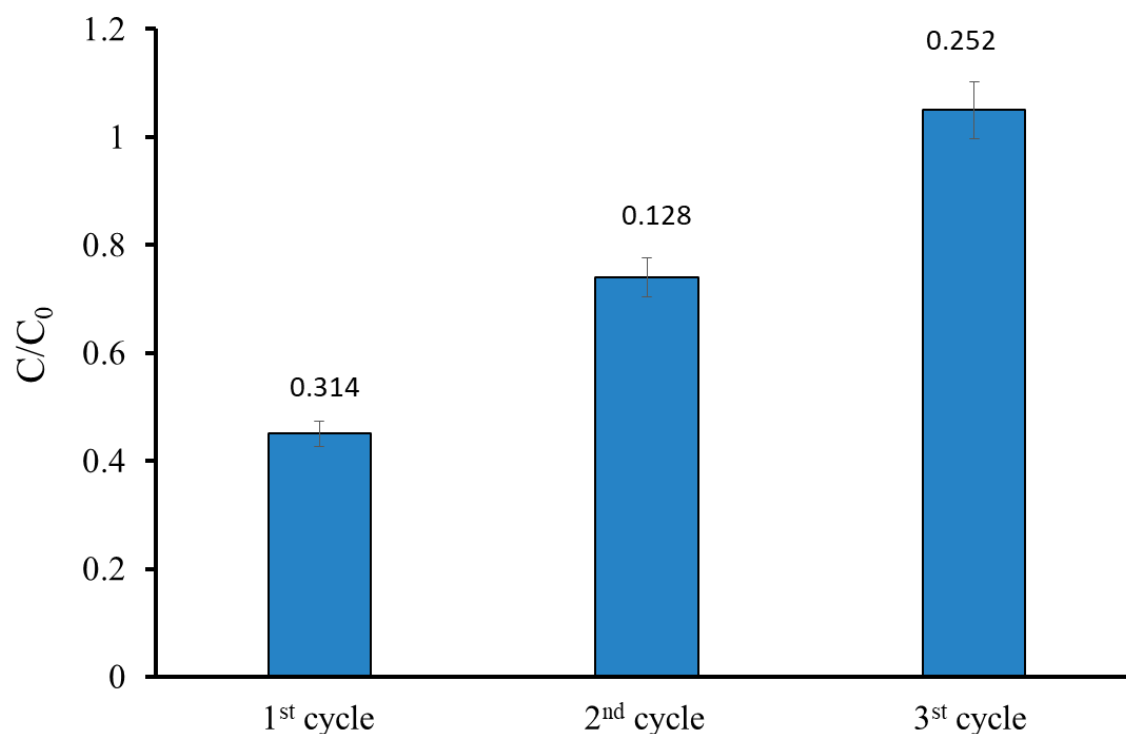


Figure 41 Effect of recycling on the photocatalytic degradation with 3 cycle using $\text{TiO}_2\text{:PF+SA+Na}$.

The recycling used of the $\text{TiO}_2\text{:PF+SA+Na}$. The photocatalyst up to the 3rd cycle leading to photo MB degradation is shown in Figure 41. The activity of $\text{TiO}_2\text{:PF+SA+Na}$ showed the loss in total photocatalytic degradation after third cycle. This result confirmed that the succinic acid improved interaction of TiO_2 deposited on fibers as showed in SEM results in figure 22 e) and f). Although the succinic acid as a crosslink can improved interaction of TiO_2 deposited on fibers but can't improve catalysts for recycles ability confirm with amount of % loss of Ti on catalyst with ICP-OES technique in table 6.

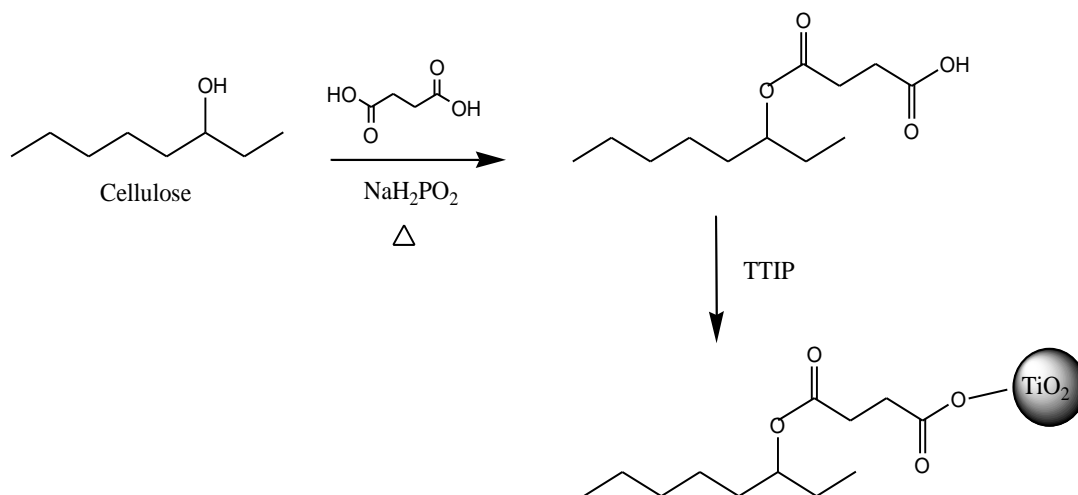
4.3.2.5 Determination of TiO₂ deposited on catalyst analysis

Table 6 Results of Ti incatalyst analyses by ICP-OES.

Catalyst	Recycle	% Recovery
TiO ₂ :PF	fresh	18.30
TiO ₂ :PF	1 st	8
TiO ₂ :PF	3 rd	0
TiO ₂ :PF+SA+Na	fresh	69.90
TiO ₂ :PF+SA+Na	1 st	11
TiO ₂ :PF+SA+Na	3 rd	0

The determination of Ti over fiber of each catalyst which analyze by ICP-OES. The recycling use of the TiO₂:PF compared to TiO₂:PF+SA+Na was also in attaches. The Ti deposited on fibers in 1st the 3rd cycle leading to total MB removal was showed above in Table 6. The %Recovery of fresh the TiO₂:PF compared with the fresh TiO₂:PF+SA+Na are 18.30 % and 69.90 %, respectively. After 1st cycle, the %recovery of TiO₂:PF and TiO₂:PF+SA+Na sample decrease to 8 and 11%, respectively. This results showed that the loss in the percentage of Ti in crosslink sample sytem was less than the sample which did not used crosslink even after the twice cycle. For after 3rd cycle, it did not found Ti deposited on fibers in both catalyst system. The use of succinic acid can improve the TiO₂ immobilized on fiber after reaction.

4.3.2.6 Connection of succinic acid to cellulose and TiO₂



Scheme 1. Connection of succinic acid to cellulose fibers using NaH₂PO₂ as a inducer and TiO₂ through using the cross-link method.

The reaction modes of cellulose with succinic acid at 180°C in the presence of NaH₂PO₂ imparts wet strength up after brief thermal curing. It was found that the effectiveness of such carboxylic acids increased with their functionality in the order succinic acid. These structurally carboxylic acids were chosen based upon their ability to form highly reactive cyclic anhydrides under the thermal reaction conditions of the curing process. The greatly increased reactivity of the in situ generated anhydride moiety over the parent poly functional carboxylic acids in the reaction with the cellulosic hydroxyl groups permits high conversion of the carboxylic acid moieties into ester linkages at moderate reaction temperatures and short curing times. We view the excellent wet-strengthening properties of succinic acid as a reflection of their ability to form multiple anhydrides during the curing reaction either directly. The cross-link agent (succinic acid) needs to have at least two free carboxylic groups to be able to bind both cotton and TiO₂. The cross-link agent will be introduced by the formation of a covalent ester bond. This implies esterification of one carboxylic group of the cross-link agent by a hydroxyl group of cellulose. The second cross-link agent carboxylic group is meant to attach TiO₂ by an electrostatic interaction (Scheme 1) [93,100].

CHAPTER 5

CONCLUSIONS

Part1

Preparation of TiO₂ nano-photocatalysts was carried out by 4 methods, sol-gel (method 1), precipitation over CaCO₃ (method 2), hydrothermal (method 3) and hydrolysis with autoclave annealing (method 4). After obtain the catalyst, all the catalyst was studied the photocatalytic activity and catalyst properties. The TiO₂ particle synthesize from method 4 exhibited highest photo activity of organic solution as PQ, MB and MO degradation when compared with P25 and other methods. The best photoactivity confirm that the highest specific surface area at 338.8 m²/g of method 4. The result seen that TiO₂ synthesized from method 4 can be used degradation of other organic compounds.

Part2

The TiO₂ loading to pineapple fibers were prepared by mix PF and TTIP in optimum method from the previous part. The ratio of TiO₂: PF was 1:10, 1:5, 1:1 and 2:1. The TiO₂ over fiber with 2:1 ratio showed highest MB removal efficiency by photodegradation process. It could be seen that 2:1 ratio is the best component for MB removal for photo degradation.

Part3

The effect of crosslink addition to TiO₂ deposited over PF was studied. Moreover, the sodium hydrogen phosphite (NaH₂PO₂) was added during preparation of TiO₂:PF+SA as the enhancement of succinic acid efficiency in the preparation. From the results showed that the TiO₂/FB+SA+Na showed highest activities for total MB removal. The result confirmed that the succinic acid improved interaction of TiO₂ deposited on fibers indicated by the photodegradation efficiency of catalyst corresponding to amount of TiO₂ deposited on the fiber as showed in SEM results in figure 4.22 and confirm with amount of % Ti on catalyst with ICP-OES technique.

REFERENCES

Bibliography

1. Llorent-Martínez EJ, Ortega-Barrales P, Fernández-de Córdoba ML, Ruiz-Medina A. Trends in flow-based analytical methods applied to pesticide detection: A review. *Anal Chim Acta*. 2011;684(1–2):30–9.
2. Xu J, Ao Y, Fu D, Yuan C. Low-temperature preparation of anatase titania-coated magnetite. *J Phys Chem Solids*. 2008;69(8):1980–4.
3. Hegde MS, Nagaveni K RS. Synthesis structure and photocatalytic activity of nano TiO₂ and nano Ti_{1-x}M_xO_{2-δ} (M = Cu, Fe, Pt, Pd, V, W, Ce, Zr). *J Phys*. 2005;65:614–45.
4. Hoffmann MR, Martin ST, Choi W, Bahnemann DW. Environmental Applications of Semiconductor Photocatalysis. *Chem Rev*. 1995;95(1):69–96.
5. Yu JC, Zhang L, Zheng Z, Zhao J. Synthesis and characterization of phosphated mesoporous titanium dioxide with high photocatalytic activity. *Chem Mater*. 2003;15(11):2280–6.
6. Shiraishi Y, Saito N, Hirai T. Adsorption-driven photocatalytic activity of mesoporous titanium dioxide. *J Am Chem Soc*. 2005;127(37):12820–2.
7. Zhang R, Elzatahry AA, Al-Deyab SS, Zhao D. Mesoporous titania: From synthesis to application. *Nano Today* [Internet]. 2012;7(4):344–6. Available from: <http://dx.doi.org/10.1016/j.nantod.2012.06.012>
8. Antonelli DM, Ying JY. Synthesis of Hexagonally Packed Mesoporous TiO₂ by a Modified Sol–Gel Method. *Angew Chemie Int Ed English*. 1995;34(18):2014–7.
9. Wang H-W, Kuo C-H, Lin H-C, Kuo I-T, Cheng C-F. Rapid Formation of Active Mesoporous TiO₂ Photocatalysts via Micelle in a Microwave Hydrothermal Process. *J Am Ceram Soc* [Internet]. 2006;89(11):3388–92. Available from: <http://doi.wiley.com/10.1111/j.1551-2916.2006.01251.x>
10. C. Yu J, Zhang L, Yu J. Rapid synthesis of mesoporous TiO₂ with high photocatalytic activity by ultrasound-induced agglomeration. *New J Chem* [Internet]. 2002;26(4):416–20. Available from: <http://xlink.rsc.org/?DOI=b109173e>
11. Smarsly B, Grosso D, Brezesinski T, Pinna N. Highly crystalline cubic mesoporous TiO₂ with 10-nm pore diameter made with a new block copolymer template.pdf. 2004;(4):2948–52.
12. Simonsen ME, Jensen H, Li Z, Søgaard EG. Surface properties and photocatalytic activity of nanocrystalline titania films. *J Photochem Photobiol A*

- Chem. 2008;200(2–3):192–200.
13. Yu J, Zhou M, Cheng B, Yu H, Zhao X. Ultrasonic preparation of mesoporous titanium dioxide nanocrystalline photocatalysts and evaluation of photocatalytic activity. *J Mol Catal A Chem.* 2005;227(1–2):75–80.
 14. Zhang Q, Chakraborty AK, Lee WI. Preparation of titania nanotape array and its photocatalytic property. *J Phys Chem Solids.* 2008;69(5–6):1450–3.
 15. Bozzi A, Yuranova T, Guasaquillo I, Laub D, Kiwi J. Self-cleaning of modified cotton textiles by TiO₂ at low temperatures under daylight irradiation. *J Photochem Photobiol A Chem.* 2005;174(2):156–64.
 16. Wahi RK, Yu WW, Liu Y, Mejia ML, Falkner JC, Nolte W, et al. Photodegradation of Congo Red catalyzed by nanosized TiO₂. *J Mol Catal A Chem.* 2005;242(1–2):48–56.
 17. Pei J, Ma W, Li R, Li Y, Du H. Preparation and Photocatalytic Properties of TiO₂-Al₂O₃ Composite Loaded Catalysts. *J Chem [Internet].* 2015;2015(1):1–7. Available from: <http://www.scopus.com/inward/record.url?eid=2-s2.0-84924308733&partnerID=tZOtx3y1>
 18. Wu X, Wei Q, Zhaohua J. Influence of Fe³⁺ ions on the photocatalytic activity of TiO₂ films prepared by micro-plasma oxidation method. *Thin Solid Films.* 2006;496(2):288–92.
 19. Langlet M, Kim A, Audier M, Guillard C, Herrmann JM. Transparent photocatalytic films deposited on polymer substrates from sol-gel processed titania sols. *Thin Solid Films.* 2003;429(1–2):13–21.
 20. Amin SA, Pazouki M, Hosseinnia A. Synthesis of TiO₂-Ag nanocomposite with sol-gel method and investigation of its antibacterial activity against *E. coli*. *Powder Technol [Internet].* 2009;196(3):241–5. Available from: <http://dx.doi.org/10.1016/j.powtec.2009.07.021>
 21. Yang FC, Wu KH, Huang JW, Horng DN, Liang CF, Hu MK. Preparation and characterization of functional fabrics from bamboo charcoal/silver and titanium dioxide/silver composite powders and evaluation of their antibacterial efficacy. *Mater Sci Eng C [Internet].* 2012;32(5):1062–7. Available from: <http://dx.doi.org/10.1016/j.msec.2009.11.016>
 22. Nishimoto S, Kubo A, Zhang X, Liu Z, Taneichi N, Okui T, et al. Novel hydrophobic/hydrophilic patterning process by photocatalytic Ag nucleation on TiO₂ thin film and electroless Cu deposition. *Appl Surf Sci.* 2008;254(18):5891–4.

23. Goncalves G, Marques PAAP, Pinto RJB, Trindade T, Neto CP. Surface modification of cellulosic fibres for multi-purpose TiO₂ based nanocomposites. *Compos Sci Technol* [Internet]. 2009;69(7–8):1051–6. Available from: <http://dx.doi.org/10.1016/j.compscitech.2009.01.020>
24. Chong MN, Jin B, Chow CWK, Saint C. Recent developments in photocatalytic water treatment technology: A review. *Water Res* [Internet]. 2010;44(10):2997–3027. Available from: <http://dx.doi.org/10.1016/j.watres.2010.02.039>
25. M F. Photocatalytic Oxidation of Organic Substances. In: Kluwer (ed.) *Photocatalysis and Environment: Trends and Applications*. 1988. 445–467 p.
26. Gaya UI, Abdullah AH. Heterogeneous photocatalytic degradation of organic contaminants over titanium dioxide: A review of fundamentals, progress and problems. *J Photochem Photobiol C Photochem Rev*. 2008;9(1):1–12.
27. Tang WZ, An H. Photocatalytic degradation kinetics and mechanism of acid blue 40 by TiO₂/UV in aqueous solution. *Chemosphere*. 1995;31(9):4171–83.
28. Van Gerven T, Mul G, Moulijn J, Stankiewicz A. A review of intensification of photocatalytic processes. *Chem Eng Process Process Intensif*. 2007;46(9 SPEC. ISS.):781–9.
29. Rauf MA, Ashraf SS. Fundamental principles and application of heterogeneous photocatalytic degradation of dyes in solution. *Chem Eng J*. 2009;151(1–3):10–8.
30. Mills A, Le Hunte S. An overview of semiconductor photocatalysis. *J Photochem Photobiol A Chem*. 1997;108(1):1–35.
31. Diebold U. The surface science of titanium dioxide. *Surf Sci Rep* [Internet]. 2003;48(5–8):53–229. Available from: <http://linkinghub.elsevier.com/retrieve/pii/S0167572902001000>
32. Rajeshwar K IJ. *Environmental Electrochemistry, Fundamentals and Applications in Pollution Abatement*. 1997.
33. Fujishima A, Rao TN, Tryk DA. Titanium dioxide photocatalysis. *J Photochem Photobiol C Photochem Rev*. 2000;1(1):1–21.
34. Fujishima A, Honda K. Electrochemical photolysis of water at a semiconductor electrode. *Nature*. 1972;238(5358):37–8.
35. Carp O, Huisman CL, Reller A. Photoinduced reactivity of titanium dioxide. *Prog Solid State Chem*. 2004;32(1–2):33–177.
36. Abu Tariq M, Faisal M, Saquib M, Muneer M. Heterogeneous photocatalytic

- degradation of an anthraquinone and a triphenylmethane dye derivative in aqueous suspensions of semiconductor. *Dye Pigment*. 2008;76(2):358–65.
37. Akpan UG, Hameed BH. Parameters affecting the photocatalytic degradation of dyes using TiO₂-based photocatalysts: A review. *J Hazard Mater*. 2009;170(2–3):520–9.
 38. Marlina Samsudin E, Nee Goh S, Yeong TW, Tong Ling T, Bee Abd Hamid S, Ching Juan J. Evaluation on the Photocatalytic Degradation Activity of Reactive Blue 4 using Pure Anatase Nano-TiO₂ (Penilaian pada Aktiviti Degradasi Fotopemangkinan daripada Reaktif Blue 4 menggunakan Anatase Nano-TiO₂ Tulen). *Sains Malaysiana* [Internet]. 2015;44(7):1011–9. Available from: http://journalarticle.ukm.my/8987/1/13_Emy_Marlina.pdf
 39. Fox MA, Dulay MT. Heterogeneous Photocatalysis. *Chem Rev*. 1993;93(1):341–57.
 40. Phanikrishna Sharma M V., Durga Kumari V, Subrahmanyam M. Photocatalytic degradation of isoproturon herbicide over TiO₂/Al-MCM-41 composite systems using solar light. *Chemosphere*. 2008;72(4):644–51.
 41. Kim SB, Hong SC. Kinetic study for photocatalytic degradation of volatile organic compounds in air using thin film TiO₂ photocatalyst. *Appl Catal B Environ*. 2002;35(4):305–15.
 42. Legrini O, Oliveros E, Braun AM. Photochemical Processes for Water Treatment. *Chem Rev*. 1993;93(2):671–98.
 43. Sun J, Wang X, Sun J, Sun R, Sun S, Qiao L. Photocatalytic degradation and kinetics of Orange G using nano-sized Sn(IV)/TiO₂/AC photocatalyst. *J Mol Catal A Chem*. 2006;260(1–2):241–6.
 44. Chun H, Yizhong W, Hongxiao T. Preparation and characterization of surface bond-conjugated TiO₂/SiO₂ and photocatalysis for azo dyes. *Appl Catal B Environ*. 2001;30(3–4):277–85.
 45. Li Y, Li N, Tu J, Li X, Wang B, Chi Y, et al. TiO₂ supported on rod-like mesoporous silica SBA-15: Preparation, characterization and photocatalytic behaviour. *Mater Res Bull* [Internet]. 2011;46(12):2317–22. Available from: <http://dx.doi.org/10.1016/j.materresbull.2011.08.044>
 46. Teng H, Suuberg EM. Chemisorption of nitric oxide on char. 1. Reversible nitric oxide sorption. *J Phys Chem*. 1993;97(2):478–83.
 47. Meacock G, Taylor KDA, Knowles MJ, Himonides A. The improved whitening of minced cod flesh using dispersed titanium dioxide. *J Sci Food Agric*.

- 1997;73(2):221–5.
48. Muneer M, Qamar M, Saquib M, Bahnemann DW. Heterogeneous photocatalysed reaction of three selected pesticide derivatives, propham, propachlor and tebuthiuron in aqueous suspensions of titanium dioxide. *Chemosphere*. 2005;61(4):457–68.
 49. Fujishima A, Zhang X, Tryk DA. TiO₂ photocatalysis and related surface phenomena. *Surf Sci Rep*. 2008;63(12):515–82.
 50. Schiavello M, Organization NAT. Photocatalysis and environment :trends and applications. NATO ASI Ser Ser C, Math Phys Sci ; 1988;237:706.
 51. Herrmann JM, Duchamp C, Karkmaz M, Hoai BT, Lachheb H, Puzenat E, et al. Environmental green chemistry as defined by photocatalysis. *J Hazard Mater*. 2007;146(3):624–9.
 52. Banerjee S, Pillai SC, Falaras P, O'shea KE, Byrne JA, Dionysiou DD. New insights into the mechanism of visible light photocatalysis. *J Phys Chem Lett*. 2014;5(15):2543–54.
 53. Ding Z, Hu X, Yue PL, Lu GQ, Greenfield PF. Synthesis of anatase TiO₂ supported on porous solids by chemical vapor deposition. *Catal Today*. 2001;68(1–3):173–82.
 54. Xue G, Liu H, Chen Q, Hills C, Tyrer M, Innocent F. Synergy between surface adsorption and photocatalysis during degradation of humic acid on TiO₂/activated carbon composites. *J Hazard Mater [Internet]*. 2011;186(1):765–72. Available from: <http://dx.doi.org/10.1016/j.jhazmat.2010.11.063>
 55. Zhang J, Zhou P, Liu J, Yu J. New understanding of the difference of photocatalytic activity among anatase, rutile and brookite TiO₂. *Phys Chem Chem Phys [Internet]*. 2014;16(38):20382–6. Available from: <http://xlink.rsc.org/?DOI=C4CP02201G>
 56. Mattioli G, Filippone F, Alippi P, Amore Bonapasta A. *Ab initio* study of the electronic states induced by oxygen vacancies in rutile and anatase TiO_2 . *Phys Rev B [Internet]*. 2008;78(24):241201. Available from: <https://link.aps.org/doi/10.1103/PhysRevB.78.241201>
 57. Luttrell T, Halpegamage S, Tao J, Kramer A, Sutter E, Batzill M. Why is anatase a better photocatalyst than rutile? - Model studies on epitaxial TiO₂ films. *Sci Rep*. 2015;4:1–8.

58. Xu M, Gao Y, Moreno EM, Kunst M, Muhler M, Wang Y, et al. Photocatalytic activity of bulk TiO₂ anatase and rutile single crystals using infrared absorption spectroscopy. *Phys Rev Lett*. 2011;106(13):1–4.
59. Maity P, Mohammed OF, Katsiev K, Idriss H. Study of the Bulk Charge Carrier Dynamics in Anatase and Rutile TiO₂ Single Crystals by Femtosecond Time Resolved Spectroscopy. *J Phys Chem C* [Internet]. 2018;acs.jpcc.8b00256. Available from: <http://pubs.acs.org/doi/10.1021/acs.jpcc.8b00256>
60. Scanlon DO, Dunnill CW, Buckeridge J, Shevlin SA, Logsdail AJ, Woodley SM, et al. Band alignment of rutile and anatase TiO₂. *Nat Mater*. 2013;12(9):798–801.
61. Alivisatos AP. Semiconductor Clusters, Nanocrystals, and Quantum Dots. *Science* (80-) [Internet]. 1996;271(5251):933–7. Available from: <http://www.sciencemag.org/cgi/doi/10.1126/science.271.5251.933>
62. Alivisatos AP, Alivisatos AP. Perspectives on the Physical Chemistry of Semiconductor Nanocrystals Perspectives on the Physical Chemistry of Semiconductor Nanocrystals. 1996;100(August):13226–39.
63. Hines MA, Guyot-Sionnest P. Synthesis and characterization of strongly luminescing ZnS-capped CdSe nanocrystals. *J Phys Chem*. 1996;100(2):468–71.
64. Gao B, Yap PS, Lim TM, Lim TT. Adsorption-photocatalytic degradation of Acid Red 88 by supported TiO₂: Effect of activated carbon support and aqueous anions. *Chem Eng J* [Internet]. 2011;171(3):1098–107. Available from: <http://dx.doi.org/10.1016/j.cej.2011.05.006>
65. Mallakpour S, Nikkhoo E. Surface modification of nano-TiO₂ with trimellitylimido-amino acid-based diacids for preventing aggregation of nanoparticles. *Adv Powder Technol* [Internet]. 2014;25(1):348–53. Available from: <http://dx.doi.org/10.1016/j.appt.2013.05.017>
66. Paz Y. Composite Titanium Dioxide Photocatalysts and the “Adsorb & Shuttle” Approach: A Review. *Solid State Phenom* [Internet]. 2010;162:135–62. Available from: <http://www.scientific.net/SSP.162.135>
67. Li G, Bono A, Krishnaiah D, Collin JG. Preparation of titanium dioxide photocatalyst loaded onto activated carbon support using chemical vapor deposition : A review paper. 2008;157:209–19.
68. Byranvand MM, Kharat AN, Fatholahi L, Beiranvand ZM. A Review on Synthesis of Nano-TiO₂ via Different Methods. 2013;3:1–9.
69. Andersson M, Lars O. Preparation of Nanosize Anatase and Rutile TiO₂ by

- Hydrothermal Treatment of Microemulsions and Their Activity for Photocatalytic Wet Oxidation of Phenol. 2002;10674–9.
70. Castro AL, Nunes MR, Carvalho AP, Costa FM, Florêncio MH. Synthesis of anatase TiO₂ nanoparticles with high temperature stability and photocatalytic activity. *Solid State Sci.* 2008;10(5):602–6.
 71. Lee JC, Kim MS, Kim BW. Removal of paraquat dissolved in a photoreactor with TiO₂ immobilized on the glass-tubes of UV lamps. *Water Res.* 2002;36(7):1776–82.
 72. Wahi RK, Liu Y, Falkner JC, Colvin VL. Solvothermal synthesis and characterization of anatase TiO₂ nanocrystals with ultrahigh surface area. 2006;302:530–6.
 73. Wu YC, Tai YC. Effects of alcohol solvents on anatase TiO₂ nanocrystals prepared by microwave-assisted solvothermal method. *J Nanoparticle Res.* 2013;15(6).
 74. Yuan S, Shi L, Mori K, Yamashita H. Preparation of highly dispersed TiO₂ in hydrophobic mesopores by simultaneous grafting and fluorinating. *Microporous Mesoporous Mater* [Internet]. 2009;117(1–2):356–61. Available from: <http://dx.doi.org/10.1016/j.micromeso.2008.07.012>
 75. Alwash AH, Abdullah AZ, Ismail N. TiO₂-zeolite Y catalyst prepared using impregnation and ion-exchange method for sonocatalytic degradation of amaranth dye in aqueous solution. *Int J Chem Mol Nucl Mater Metall Eng.* 2013;7(6):375–83.
 76. Wang W, Yang Y, Luo H, Hu T, Wang F, Liu W. Ultrasound-assisted preparation of titania-alumina support with high surface area and large pore diameter by modified precipitation method. *J Alloys Compd* [Internet]. 2011;509(7):3430–4. Available from: <http://dx.doi.org/10.1016/j.jallcom.2010.12.119>
 77. Huang C-H, Bai H, Liu S-L, Huang Y-L, Tseng Y-H. Synthesis of neutral SiO₂/TiO₂ hydrosol and its photocatalytic degradation of nitric oxide gas. *Micro Nano Lett.* 2011;6(8):646.
 78. Montes M, Getton FP, Sermon PA, Lane K, Kingdom U. Titania on Silica . A Comparison of Sol-Gel Routes and Traditional Methods. 1997;137:131–7.
 79. Sayilkan F, Asilturk M. Characterization of TiO₂ Synthesized in Alcohol by a Sol-Gel Process: The Effects of Annealing Temperature and Acid Catalyst. *Turkish J ...* [Internet]. 2005;29(2005):697–706. Available from:

<http://link.springer.com/article/10.1007/BF03246194%5Cnhttp://journals.tubitak.gov.tr/chem/issues/kim-05-29-6/kim-29-6-14-0501-12.pdf>

80. Behnajady MA, Eskandarloo H, Modirshahla N, Shokri M. Sol-gel low-temperature synthesis of stable anatase-type TiO₂ nanoparticles under different conditions and its photocatalytic activity. *Photochem Photobiol.* 2011;87(5):1002–8.
81. Livage J, Henry M, Sanchez C. Sol-gel chemistry of transition metal oxides. *Prog Solid State Chem.* 1988;18(4):259–341.
82. Yap PS, Lim TT, Srinivasan M. Nitrogen-doped TiO₂/AC bi-functional composite prepared by two-stage calcination for enhanced synergistic removal of hydrophobic pollutant using solar irradiation. *Catal Today* [Internet]. 2011;161(1):46–52. Available from: <http://dx.doi.org/10.1016/j.cattod.2010.09.024>
83. Yagub MT, Sen TK, Afroze S, Ang HM. Dye and its removal from aqueous solution by adsorption: A review. *Adv Colloid Interface Sci* [Internet]. 2014;209:172–84. Available from: <http://dx.doi.org/10.1016/j.cis.2014.04.002>
84. Yadav A, Prasad V, Kathe AA, Raj S, Yadav D, Sundaramoorthy C, et al. Functional finishing in cotton fabrics using zinc oxide nanoparticles. *Bull Mater Sci* [Internet]. 2006;29(6):641–645. Available from: <http://link.springer.com/10.1007/s12034-006-0017-y>
85. Yuranova T, Laub D, Kiwi J. Synthesis, activity and characterization of textiles showing self-cleaning activity under daylight irradiation. *Catal Today.* 2007;122(1–2):109–17.
86. Sears KD, Jacobson R, Caulfield DF, Underwood J. Reinforcement of Engineering Thermoplastics with High Purity Wood Cellulose Fibers. *sixth Int Conf woodfiber-plastic Compos.* 2001;27–34.
87. Bozzi A, Yuranova T, Guasaquillo I, Laub D KJ. Self-cleaning of modified cotton textiles by TiO₂ at low temperatures under daylight irradiation. *J Photochem Photobiol, A.* 2005;174:156–64.
88. Yetria Rildaa*, Fadhli, Syukria, Admin Alifa, Hermansyah Aziza, Sheela Chandrenb HN, ADepartment. *Jurnal Teknologi ON COTTON TEXTILE PREPARED BY DIP-SPIN. J Teknol Eng &Science.* 2016;7:113–20.
89. Lopattananon N, Panawarangkul K, Sahakaro K, Ellis B. Performance of pineapple leaf fiber-natural rubber composites: The effect of fiber surface treatments. *J Appl Polym Sci.* 2006;102(2):1974–84.

90. Threepopnatkul P, Kaerkitcha N, Athipongarporn N. Effect of surface treatment on performance of pineapple leaf fiber-polycarbonate composites. *Compos Part B Eng* [Internet]. 2009;40(7):628–32. Available from: <http://dx.doi.org/10.1016/j.compositesb.2009.04.008>
91. Meilert KT, Laub D, Kiwi J. Photocatalytic self-cleaning of modified cotton textiles by TiO₂ clusters attached by chemical spacers. *J Mol Catal A Chem*. 2005;237(1–2):101–8.
92. Qi K, Daoud WA, Xin JH, Mak CL, Tang W, Cheung WP. Self-cleaning cotton. *J Mater Chem* [Internet]. 2006;16(47):4567. Available from: <http://xlink.rsc.org/?DOI=b610861j>
93. Karimi L, Mirjalili M, Yazdanshenas ME, Nazari A. Effect of Nano TiO₂ on Self-cleaning Property of Cross-linking Cotton Fabric with Succinic Acid Under UV Irradiation. 2010;(21):1030–7.
94. Nazari A, Montazer M, Rashidi A, Yazdanshenas M, Anary-abbasinejad M. Applied Catalysis A: General Nano TiO₂ photo-catalyst and sodium hypophosphite for cross-linking cotton with poly carboxylic acids under UV and high temperature. 2009;371:10–6.
95. Wang C, Li Y. Synthesis, characterisation and photocatalytic activity of natural zeolite supported Fe/S and Cr/S codoped nanoTiO₂ photocatalysts. *Mater Technol* [Internet]. 2014;29(6):372–6. Available from: <http://www.tandfonline.com/doi/full/10.1179/1753555714Y.0000000169>
96. Kortan AR, Hull R, Opila RL, Bawendi MG, Steigerwald ML, Carroll PJ, et al. Nucleation and Growth of CdSe on ZnS Quantum Crystallite Seeds, and Vice Verca, in Inverse Micelle Media. *J Am Chem Soc*. 1990;112(12):1327–32.
97. Preparation of visible light-activated titania photocatalyst by mechano chemical method.
98. Mao Z, Yu X, Zhang L, Zhong Y, Xu H. Novel Infrared Stealth Property of Cotton Fabrics Coated with Nano ZnO: (Al, La) Particles. *Vacuum* [Internet]. 2014; Available from: <http://dx.doi.org/10.1016/j.vacuum.2014.01.011>
99. Yuranova T, Mosteo R, Bandara J, Laub D, Kiwi J. Self-cleaning cotton textiles surfaces modified by photoactive SiO₂ / TiO₂ coating. 2006;244:160–7.
100. Alwash AH, Abdullah AZ, Ismail N. La Loaded TiO₂ Encapsulated Zeolite y Catalysts: Investigating the Characterization and Decolorization Process of Amaranth Dye. *J Eng (United States)*. 2013;2013.

BIOGRAPHY

NAME Miss Suchadee Sribenja

DATE OF BIRTH November 28, 1990

PLACE OF BIRTH Nakhonphanom, Thailand

ADDRESS 26 Samutbanhan Road, Tambon Naimaung, Amphoe Maung, Nakhonphanom 48000, Thailand

POSITION Doctor of Philosophy in Chemistry

PLACE OF WORK Mahasarakham University

EDUCATION 2012 Bachelor of Science degree in Chemistry
Mahasarakham University
2016 Master of Science degree in Chemistry
Mahasarakham University
2019 Doctor of Philosophy in Chemistry Mahasarakham University

Research grants & awards Division of research Facilitation and Dissemination
Mahasarakham University, fiscal year 2015,
Office of the Higher Education
Commission Mahasarakham University, fiscal year 2015,
Center of Excellence for Innovation in
Chemistry (PERCH-CIC)
Science achievement scholarship of
thailand (sast)